

**Green Adsorbents Based on Functional-modified Cellulose and Copolymers for  
Water Clarification**

by

Yuan Li

M. Sc. Nanjing University of Information Science and Technology, 2011

A Dissertation Submitted in Partial Fulfillment of the Requirements for the Degree of

**Doctor of Philosophy**

in the Graduate Academic Unit of Chemical Engineering

Supervisor: Huining Xiao, PhD, Department of Chemical Engineering

Examining Board: John Kershaw, PhD, Associate Dean of Graduate Studies, Chair  
Yonghao Ni, PhD, P. Eng., Department of Chemical Engineering  
William Cook, PhD, P. Eng., Department of Chemical Engineering  
Huining Xiao, PhD, P. Eng., Department of Chemical Engineering  
Fanrui Meng, PhD, P. Eng., Forestry & Environmental Management

External Examiner: Ramin Farnood, PhD, Department of Chemical Engineering and  
Applied Chemistry, University of Toronto

This dissertation is accepted by the  
Dean of Graduate Studies

THE UNIVERSITY OF NEW BRUNSWICK

June 2018

©Yuan Li, 2018

## **ABSTRACT**

Natural adsorbents for the removal of dyes and heavy metal ions have attracted tremendous research interests because of their cost-effectiveness and easy regeneration. Cellulose fibers, as the most abundant natural resource in the world, have numerous advantages, such as being renewable, inexpensive, biodegradable, environment-friendly and nontoxic. However, due to the hydroxyl groups on the polymer structure and formation of hydrogen bonds between the molecular chains, the adsorption capacity is limited and the selectivity is low when the natural cellulose is directly used as an adsorbent. To improve its adsorption properties and widen its applications, extensive studies have been carried out in the current thesis work: 1) a comprehensive review of the conventional application of cellulose-based adsorbents, the application of cellulose nanofibers (CNF) or nanocrystals (CNC), and the responsive or smart cellulose-based adsorbents was provided; 2) the cost-effective and renewable cellulose fibre beads in conjunction with alkali-treated diatomite were prepared, leading to a range of adsorbents which could remove the dyes and heavy metal ions from aqueous solutions effectively and be re-generated readily; 3) an innovative approach was used to prepare the dissolved cellulose fibre/microfibrillated cellulose (MFC) composite beads as an environmental-friendly adsorbent for the removal of dyes from aqueous solutions; 4) NIPAM (N-isopropylacrylamide), a temperature-sensitive monomer, was polymerized and grafted onto the MFC spheres through an in-situ free radical polymerization using a microwave-assisted heating technique. The synthesis of semi-interpenetrating polymer networks

composed of cellulose/MFC spheres and poly (N-isopropylacrylamide-co-acrylic acid) was further conducted.

It was found that the adsorption capability of cellulose has been improved significantly by using renewable cellulose fibre beads in conjunction with alkali-treated diatomite. The precipitated cellulose reinforced with MFC showed excellent porous properties. The polymerization could be microwave accelerated and high efficiency could be obtained via microwave-assisted polymerization. The copolymers-grafted spheres exhibited a controllable adsorption and desorption process as pH- and temperature-responsive adsorbents. The adsorption kinetics followed the pseudo-second-order and could also be well described by a three-stage intraparticle diffusion model. Adsorption isotherms were fit using Langmuir, Freundlich, and Temkin models.

## **DEDICATION**

I would like to dedicate this thesis to my beloved parents who have given me the life, the opportunity of an education and support throughout my life. They devote their entire lives to aiding my pursuit of knowledge and education. This thesis is also specially dedicated to my dear wife, who has always stood by me and given me unconditioned support and encouragement.

## ACKNOWLEDGEMENTS

It is with immense gratitude that I acknowledge the support and help of my supervisor, Professor Huining Xiao. I am very grateful to him for his insightful advice, suggestions, and guidance throughout my Ph.D. studies.

I also wish to express my gratitude to Professor Yonghao Ni, for giving me generous amount of time whenever I need some help.

I'm thankful to Professor Mindong Chen in Nanjing University of Information Science and Technology for his help and support.

I owe my deepest gratitude to my dear parents, who have always supported me throughout my life. I would also like to thank my wife, very special thanks for her endless patience, her precious love, her practical help, and emotional support.

I cannot find words to express my gratitude to all my dear friends who are always supporting me. I feel obliged to say thanks to so many people who have been doing so many good things for me.

Thanks are also given to the colleagues and staffs in our research group, Department of Chemical Engineering and Limerick Pulp & Paper Center, UNB, for their infinite help.

At last but not the least, I am thankful to the financial support from NSERC Canada.

## Table of Contents

ABSTRACT .....	ii
DEDICATION .....	iii
ACKNOWLEDGEMENTS .....	v
Table of Contents .....	vi
List of Tables.....	xii
List of Figures .....	xiii
List of Symbols, Nomenclature or Abbreviations.....	xvii
INTRODUCTION .....	1
References.....	8
Chapter 1 Literature Review .....	12
1.1    Introduction.....	12
1.2    The conventional application of cellulose-based adsorbents.....	12
1.2.1    The removal of heavy metal ions from wastewater .....	13
1.2.2    Esterification .....	14
1.2.3    Etherification.....	16
1.2.4    Graft polymerization.....	17
1.2.5    Halogenation, oxidation, etc. ....	20
1.2.6    The treatment of organic compounds from wastewater.....	23
1.2.7    The treatment of dyes in wastewater.....	27
1.3    The application of cellulose nanofibers (CNF) or nanocrystals (CNC).....	28
1.3.1    Reinforcements for biocomposites.....	29
1.3.2    Bioadsorbents for water clarification and soil remediation .....	30
1.4    Smart or responsive bioadsorbents.....	32
1.4.1    Application of thermal/pH sensitive polymers .....	33

1.4.2	Responsive and smart cellulose-based adsorbents .....	34
1.5	References .....	37
Chapter 2 Maleic anhydride-modified cellulose fibres/diatomite adsorbents for dye removal..... 46		
ABSTRACT .....		
2.1	Introduction .....	47
2.2	Experimental .....	49
2.2.1	Materials.....	49
2.2.2	Preparation of cellulose/diatomite beads (CDBs).....	49
2.2.3	Modification of CDBs.....	50
2.2.4	Sample characterization .....	51
2.3	Results and discussion .....	52
2.3.1	FT-IR spectroscopy.....	52
2.3.2	TGA .....	53
2.3.3	Brunauer–Emmett–Teller (BET) adsorption.....	54
2.3.4	Comparative experiment .....	55
2.3.5	Effects of the concentration of initial CaCO <sub>3</sub> .....	56
2.3.6	Effects of pH on dye absorption.....	57
2.3.7	Effects of temperature on adsorption .....	58
2.3.8	Influence of shaking time on dye adsorption .....	59
2.3.9	Adsorption kinetics .....	60
2.3.10	Adsorption isotherm.....	61
2.3.11	Desorption of MB and MV from MCDBs .....	65
2.4	Conclusions .....	65

2.5	References .....	66
Chapter 3 The cellulose-based hybrid beads for adsorption of lead ions in aqueous solutions. .... 66		
ABSTRACT..... 69		
3.1	Introduction .....	70
3.2	Experimental .....	72
3.2.1	Materials.....	72
3.2.2	Methods.....	73
3.2.3	Characterization .....	75
3.2.4	Batch experiments.....	76
3.3	Results and discussion .....	78
3.3.1	FTIR spectra and colloid titration .....	78
3.3.2	SEM .....	79
3.3.3	SEM morphology .....	80
3.3.4	Comparitive test .....	81
3.3.5	Effect of pH.....	82
3.3.6	Effect of temperature.....	84
3.3.7	Adsorption behaviour.....	84
3.3.8	Desorption of Pb <sup>2+</sup> from MCDBs-30 .....	89
3.4	Conclusions .....	89
3.5	References .....	90
Chapter 4 Novel composite adsorbent consisting of dissolved cellulose fibre/ microfibrillated cellulose for dye removal from aqueous solution ..... 94		
ABSTRACT..... 94		
4.1	Introduction .....	95

4.2	Experimental .....	98
4.2.1	Materials.....	98
4.2.2	Methods.....	98
4.3	Results and discussion .....	105
4.3.1	FT-IR spectra .....	105
4.3.2	Surface morphology of CMFCs and MCMFCs .....	106
4.3.3	Thermal analysis .....	108
4.3.4	Brunauer-Emmet-Teller (BET).....	110
4.3.5	Adsorption behavior.....	111
4.4	Conclusions .....	120
4.5	References .....	121
Chapter 5 Novel cellulose filaments based composite spheres: microwave-assisted synthesis, characterization, and application in water treatment .....		125
ABSTRACT.....		125
5.1	Introduction .....	126
5.2	Experimental .....	128
5.2.1	Materials.....	128
5.2.2	Experimental methods.....	129
5.2.3	Characterization of P-MCCBs .....	131
5.2.4	Adsorption of MB and Pb <sup>2+</sup> .....	132
5.2.5	Desorption of MB and Pb <sup>2+</sup> .....	133
5.3	Results and discussion .....	133
5.3.1	FTIR spectra.....	133
5.3.2	SEM images .....	134

5.3.3	TGA .....	136
5.3.4	Bulk density of the spheres .....	137
5.3.5	The effect of reaction time (microwave-assisted).....	138
5.3.6	The graft efficiency of P1-MCCBs, P2-MMCCBs, and P3-MCCBs	139
5.3.7	pH effects on the adsorption of MB and Pb <sup>2+</sup> .....	139
5.3.8	Dye and heavy metal adsorption at different temperatures.....	141
5.3.9	The MB desorption behaviors .....	145
5.3.10	Adsorption kinetics .....	147
5.3.11	The desorption kinetic models .....	148
5.4	Conclusions .....	149
5.5	References .....	150

Chapter 6 Fabrication of dual-responsive semi-IPN cellulose microfilaments Poly (N-isopropylamide-co-acrylic acid) spheres for dye removal in single and binary system

ABSTRACT.....	153
6.1 Introduction .....	154
6.2 Experimental .....	159
6.2.1 Materials.....	159
6.2.2 Experimental methods.....	159
6.2.3 Characterization .....	162
6.2.4 Adsorption of cationic dyes .....	163
6.2.5 Desorption and regeneration .....	164
6.2.6 Adsorption kinetics .....	164
6.2.7 Adsorption isotherms .....	165
6.3 Results and discussion .....	167

6.3.1	FTIR spectra.....	167
6.3.2	Scanning electron microscope (SEM).....	168
6.3.3	Thermal analysis .....	169
6.3.4	Effect of pH on adsorption capacity.....	171
6.3.5	Effect of contact time on adsorption .....	173
6.3.6	Adsorption kinetics .....	174
6.3.7	Adsorption isotherms .....	178
6.3.8	Adsorption in a binary system - Langmuir competitive model .....	181
6.3.9	The desorption and recycling of adsorbents .....	183
6.4	Conclusions .....	184
6.5	References .....	185
Chapter 7 Conclusion and Recommendation for Future Work.....		192
7.1	Summary of the maleic anhydride-modified cellulose hybrid beads (MCDBs).....	193
7.2	Summary of dissolved cellulose fibre/microfibrillated cellulose beads ..	194
7.3	Summary of responsive semi-INP adsorbents.....	195
7.4	Recommendations for future work.....	196

Curriculum Vitae

## List of Tables

Table.1.1 Cellulose modification and associated functional groups.....	22
Table.2.1 Adsorption kinetics of dyes.....	60
Table.2.2 The isotherm models for adsorption .....	63
Table.2.3 Results for adsorption of dyes by MCDBs and other materials.....	64
Table.3.1 The BET results of CDBs and MCDBs .....	81
Table.3.2 The isotherm models for Pb <sup>2+</sup> adsorption .....	87
Table.3.3 Results for adsorption of Pb <sup>2+</sup> by MCDBs and other materials .....	88
Table.3.4 The calculation of $\Delta G^\circ$ , $\Delta H^\circ$ , and $\Delta S^\circ$ .....	88
Table.4.1 Three factors with 5 levels .....	103
Table.4.2 pH, temperature, and percentages of CaCO <sub>3</sub> -Dependent variable.....	111
Table.4.3 Tests of Between-Subjects Effects-Dependent Variable .....	112
Table.4.4 The kinetic parameters for the pseudo-first, pseudo-second-order and Elovich models .....	115
Table.4.5 Comparison of dye adsorption capacity of MCMFCs with other adsorbents.....	118
Table.4.6 The calculation of $\Delta G^\circ$ , $\Delta H^\circ$ , and $\Delta S^\circ$ .....	119
Table.5.1 Kinetic model's constants and correlation coefficients (R <sup>2</sup> ).....	149
Table.6.1 Kinetics model constants and correlation coefficients (R <sup>2</sup> ).....	177
Table.6.2 Isotherm model constants and correlation coefficients (R <sup>2</sup> ) for the adsorption of MB .....	181
Table.6.3 Adsorption isotherms parameters in single and binary system.....	183

## List of Figures

Figure.2.1 The preparation of CDBs.....	50
Figure.2.2 FT-IR spectra for CDBs and MCDBs. ....	53
Figure.2.3 TGA and DTG curves of the CDBs and MCDBs.....	54
Figure.2.4 The fraction of removal on different materials: 1-filter paper; 2-alkali-treated diatomite; 3-CDBs; 4-MCDBs.....	56
Figure.2.5 Effects of $\text{CaCO}_3$ on adsorption of MB and MV (natural pH, room temperature and 2h).....	57
Figure.2.6 Effects of pH on adsorption of dye (room temperature and 2h).....	58
Figure.2.7 Effects of temperature (for MB: pH 7.0, time 2h and for MV: pH 6.5, time 2h) .....	59
Figure.2.8 Effects of contact time (for MB: pH 7.0, temperature 30 °C and for MV: pH 6.5, temperature 30 °C) .....	59
Figure.2.9 Pseudo-second-order adsorption kinetics on MCDBs adsorbent .....	61
Figure.2.10 Linear plots of Langmuir isotherm for adsorption on MCDBs at 30 °C.....	64
Figure.3.1 The solvent-free approach of preparing the cellulose hybrid beads .....	74
Figure.3.2 FTIR spectrum of CDBs before and after modification .....	79
Figure.3.3 SEM images of surface morphology (a), cross-section structure of MCDBs-10 (10% $\text{CaCO}_3$ ) (b), MCDBs-30 (30% $\text{CaCO}_3$ ) before modification (c, d, and g), MCDBs-30 (30% $\text{CaCO}_3$ ) after modification (f, h), MCDBs-40 (40% $\text{CaCO}_3$ ) (e) of regenerated cellulose beads .....	80

Figure.3.4 Fraction of removal on different materials: 1-filter paper; 2-alkali-treated diatomite; 3- CDBs-0; 4-MCDBs-0; 5-MCDBs-10; 6-MCDBs-20; 7-MCDBs-30; 8-MCDBs-40.....	82
Figure.3.5 Effect of pH on adsorption of $Pb^{2+}$ .....	83
Figure.3.6 Effect of temperature on adsorption of $Pb^{2+}$ .....	84
Figure.3.7 Effect of contact time on adsorption of $Pb^{2+}$ .....	85
Figure.3.8 Pseudo-second-order adsorption kinetics on MCDBs .....	86
Figure.3.9 Linear plots of Langmuir isotherm for adsorption on MCDBs .....	88
Figure.4.1 The Schematic of CMFCs Preparation .....	100
Figure.4.2 FT-IR spectrum for control and modified CMFCs .....	105
Figure.4.3 SEM images of cross-section of CMFCs (10% $CaCO_3$ ) (a), cross-section of CMFCs (30% $CaCO_3$ ) (b), CMFCs (10% $CaCO_3$ ) (c), CMFCs (30% $CaCO_3$ ) (d) and CMFCs-30 (30% $CaCO_3$ ) after being modified by MA (e) .....	107
Figure.4.4 The TGA and DTG curves of CMFCs and MCMFCs .....	109
Figure.4.5 The effect of contact time (a) and the linear of pseudo second order kinetic (b) .....	115
Figure.4.6 Linear plots of Langmuir, Freundlich, and Temkin isotherm for adsorption on MCMFCs .....	118
Figure.4.7 Reusability of MCMFCs for MB adsorption (at the initial concentration of 20 mg/L at 298 k).....	120
Figure.5.1 The preparation of polymer grafted precipitated cellulose/CFs composite spheres (P-MCCBs) .....	131
Figure.5.2 FTIR spectra of MCCBs, P3-MCCBs, and dye-laden MCCBs .....	134

Figure.5.3 SEM images of pure cellulose spheres and P3-MCCBs (surface and cross-section) .....	135
Figure.5.4 TG and DTG curves of pure cellulose spheres and P3-MCCBs .....	136
Figure.5.5 Bulk density of the polymer-modified spheres.....	137
Figure.5.6 The graft efficiency and weight gain versus reaction time (5, 10, 20, 30, and 40min) .....	138
Figure.5.7 The graft efficiency of P1-MCCBs, P2-MCCBs, and P3-MCCBs .....	139
Figure.5.8 MB adsorption process by using polymer-modified spheres .....	141
Figure.5.9 MB adsorption process by using polymer-modified spheres .....	143
Figure.5.10 Pb <sup>2+</sup> adsorption process by using polymer-modified spheres.....	144
Figure.5.11 MB adsorption process at different temperatures .....	144
Figure.5.12 Pb <sup>2+</sup> adsorption process at different temperatures .....	145
Figure.5.13 Dye and Pb <sup>2+</sup> desorption process at different temperatures.....	147
Figure.5.14 The linear relation of pseudo-second-order kinetic at different temperatures .....	147
Figure.6.1 The Schematic of CCS and MPNAA Preparation.....	162
Figure.6.2 The FTIR spectra of CCS and MPNAA-3.....	168
Figure.6.3 SEM images of CCS (a, b) andMPNAA-3 (c, d) .....	169
Figure.6.4 The TGA and DTG curves of CCS, MCCS, and MPNAA-3.....	171
Figure.6.5 Effect of pH on adsorption of dyes by MPNAA-1, MPNAA-2 and MPNAA-3 .....	173
Figure.6.6 Effect of contact time on adsorption.....	174

Figure.6.7 Adsorption kinetics of MB by MPNAA-1, MPNAA-2 and MPNAA-3. (a) The pseudo-first-order rate adsorption plot. (b) The pseudo-second-order rate adsorption plot. (c) The Elovich model plot. (d) The intra-particle diffusion model ..... 177

Figure.6.8 The adsorption isotherms for the adsorption of MB by by MPNAA-1, MPNAA-2 and MPNAA-3. (a-c) Langmuir model, (d-f) Freundlich model and (g-i) Temkin model (adsorbent dosage 1000 mg/L, contact time 3 h, pH 9)..... 180

Figure.6.9 The Langmuir isotherms for the adsorption of MB and MV form single and binary systems using MPNAA-3 at pH = 9 and T = 298 k..... 182

Figure.6.10 Desorption behavior of dyes by MPNAA-3 (a) and swing desorption behavior by MPNAA-1, MPNAA-2 and MPNAA-3 with temperature variation 184

## List of Symbols, Nomenclature or Abbreviations

ATRP	Atom transfer radical polymerization
BET	Brunauer-Emmett-Teller
CaCO <sub>3</sub>	Calcium carbonate
CAs	Contact angles
CCs	Cellulose microfilaments spheres
CDBs	Cellulose diatomite beads
CNF	Cellulose nanofibers
CNC	Cellulose nanocrystals
FT-IR	Fourier transform infrared spectroscopy
HCl	Hydrochloride acid
ICP-ES	Inductive Coupled Plasma Emission Spectrometer
IPN	Interpenetrating polymer networks
KPS	Potassium persulfate
LCST	Lower critical solution temperature
MA	Maleic anhydride
MB	Methylene blue
MBA	Methylenebisacrylamide
MCCBs	Carbonylated cellulose/CFs composite spheres
MFC	Microfibrillated cellulose
MV	Methyl violet
NaOH	Sodium hydroxide

Poly-NIPAM	Poly (N-isopropyl acrylamide)
PAA	Poly (acrylic acid)
P4VP	Poly (4-vinylpyridine)
Poly-DADMAC	Poly diallyl dimethyl ammonium chloride
Pb(NO <sub>3</sub> ) <sub>2</sub>	Lead nitrate
PVSK	Polyvinylsulfuric potassium
Semi-IPN	Semi-interpenetrating polymer network
SEM	Scanning electron microscopy
TGA	Thermo Gravimetric Analyzer
TEMED	N, N, N, N-tetramethylethylene diamine

## INTRODUCTION

Environmental pollution control is a major theme of the scientific research in recent years, including wastewater treatment, waste gas treatment, solid waste treatment and noise control. There are increasingly environmental problems caused by economic development, especially those related to aquatic environments [1]. Water pollution mainly includes organic pollutants and heavy metal ions.

The removal of toxic and polluting heavy metal ions from industrial effluents, water supplies, and mine waters has received much attention over the past decades. It is well known that heavy metal ions, such as Pb(II) and Cu(II) ions, released into the environment affect ecological life, owing to their tendency to accumulate in living organisms, and are highly toxic when absorbed into the body [2]. Various methods, such as adsorption, ion exchange, reverse osmosis, as well as electro-dialysis techniques, have been developed for the removal and recovery of heavy metal ions from sewage and industrial wastewater [3]. Adsorption dominates due to its benefits such as high selectivity, easy operating, lower costs, and high efficiency.

Dyes, as organic pollutants, form a major class of environmental contaminant. Organic sewage has mainly the following three kinds of hazards: 1. Aerobic hazards: water will hypoxia due to the biodegradation of organic sewage, which will cause the death of most aquatic organisms, the deterioration of water quality and environment; 2. Organic sewage not only reduces the value of water, but also affects the lives of people around water; 3. Toxicity hazards: organic wastewater contains large amounts of toxic organic compounds and will continue to accumulate in the environment, entering the body and

eventually endangering humans. Basic dyes are the most problematic classes of dye that are found in wastewater from various industries, especially textile [4], tanning, and leather [5]. The complex aromatic molecular structures and xenobiotic properties of dyes make them difficult to degrade [6].

Water treatment has always been the focus of environmental-related research; meanwhile, natural and self-made materials as adsorbents for wastewater treatment are the hotspot (especially those materials that can be modified, such as cellulose [7-9], as well as porous materials [10-11]) being studied widely for the treatment of wastewater.

The common practices to address the environmental issues rely on the preparation and modification of activated carbon through different methods [12-14]. Compared with other adsorbents, the main shortcomings of activated carbon are the high cost involved in sample preparation and difficulty for regeneration. Therefore, if it were possible for the researchers to exploit green material and techniques to achieve the competitive performance to activated carbon with less overall chemical usage, it would be more helpful to the environment.

In recent years, modified cellulose and porous inorganic materials as adsorbents have been explored extensively. Cellulose, which constitutes the most abundant natural polymer resource, is a cost-effective and green material. In addition, cellulose is a multifunctional and renewable material which can be used to replace many other non-renewable materials. However, as an adsorbent unmodified cellulose has an adsorption capacity that is limited; and the selectivity is low because of the formation of hydrogen bonds between the molecular chains. The hydroxyls in cellulose are reactive and can be easily modified via various reactions, such as esterification, halogenation, oxidation, and

etherification [15]. Such modifications improve the properties of cellulose substantially, including the adsorptive and ion exchange capability particularly [16]. Compared with conventional cellulose fibers, microfibrillated cellulose (MFC) is superior due to its advantages in structure, performance, and application. MFC is an ideal material which would provide a variety of shapes and be biocompatible and absorbable. However, little work has been reported on combining dissolved cellulose fibres reinforced with microfibrillated cellulose (MFC) as a composite type of adsorbent [17]. Diatomite, a low cost and commercially available material, has unique advantages as an adsorbent, such as high permeability, high porosity, small particle size, and large surface area [18]. However, few of these materials have been combined with green-based cellulose fibres. Recently, smart materials, including thermo- and pH-responsive materials, were studied by many researchers, and could be utilized in the fields of biotechnology and pharmaceutical. Poly (N-isopropyl acrylamide) (Poly-NIPAM), a unique polymer with the lower critical solution temperature (LCST) at 32 °C, was a typical thermo-sensitive polymer used as one of the thermo-responsive materials [19]. When the ambient temperature is below the LCST, the polymer chains swell in water; above the LCST, the polymer segments become more hydrophobic and become water-insoluble. Apart from temperature, pH is also critical in the adsorption-desorption behaviors of adsorbents. Typical pH-responsive polymers, poly (acrylic acid) (PAA) and poly(4-vinylpyridine) (P4VP), are more stable and can offer higher binding capacity compared to the low-molecular-weight types containing carboxyl or thiol [20]. Materials with both pH- and thermos-responsive properties have been studied widely by researchers [21-23]. However, the conventional polymerization reported contains disadvantages. Therefore,

it is necessary to design novel approaches to prepare responsive polymeric materials. Some researchers have reported microwave-assisted synthesis [24-26]. However, the reports on the microwave-assisted synthesis combined with cellulose-based adsorbents with both pH- and temperature- responsive properties are relatively sparse.

Thus, this dissertation mainly focused on extensive studies and applications of the biodegradable materials to enhance the adsorption abilities and porous structures of cellulose-based materials for the removal of dyes and heavy metal ions in aqueous solutions. The adsorption behaviors were also investigated along with the fitting of adsorption models to reveal the adsorption mechanisms and evaluate the potential application in various fields. The overall objectives of this dissertation were as follows:

a) to improve adsorption properties of cellulose and create the proper porous structures of the adsorbents by dissolving the cellulose fibres in selected solvents and regenerating in the presence of a pore forming agent (nano-sized calcium carbonate). A porous inorganic material, diatomite, was used as the filler. Calcium carbonate was added during the formation of cellulose/diatomite beads (CDBs) to increase pore structure under an acidic condition. The effect of adsorption conditions, such as pH and temperature, on the adsorptive capacity of the modified cellulose beads, was investigated;

b) to prepare an environmentally-friendly adsorbent. The microfibrillated cellulose (MFC), an ideal material which would provide a variety of shapes and be biocompatible and absorbable, was used in conjunction with cellulose fibres to create a novel composite absorbent in which the dissolved cellulose fibres (as matrix) were reinforced with microfibrillated cellulose;

c) to prepare a range of dual-responsive cellulose-based adsorbents and develop a novel approach for fabricating copolymer-grafted cellulose spheres for the removal of dyes from aqueous solutions. The modification of cellulose spheres with pH and thermal dual-responsive copolymers modification of was carried out by a microwave-assisted free radical polymerization. The adsorption behaviors were also investigated to evaluate their potential application in other fields.

This dissertation is composed of 7 Chapters, and the content and contributions of each chapter are briefly described as follows.

Chapter 1 presents the literature review relevant to the research, and this review has been mainly divided into three parts. The first part of the review focuses on the conventional application of cellulose-based adsorbents. The application of cellulose-based materials used in water water clarification and the modification methods of cellulose are summarized. The second part summarizes the application of cellulose nanofibers (CNF) or nanocrystals (CNC). Renewable CNF and CNC have been seriously studied in recent years. Different types of adsorbents in conjunction with CNF and CNC are also summarized in this section. In the third part, the responsive and smart cellulose-based adsorbents are to be presented. Similar to the second part, the materials, approaches and testing methods are summarized and introduced.

Chapter 2 focuses on the maleic anhydride-modified cellulose fibres/diatomite adsorbents for dye removal. In this part, the maleic anhydride-modified cellulose beads combined with alkali-treated diatomite (MCDBs) were prepared to remove basic dyes. An appropriate amount of calcium carbonate was added during the formation of MCDBs to increase pore structure under an acidic condition. The as-modified adsorbents were

characterized using FTIR, TGA, and BET. Moreover, the adsorption ability of the MCDBs towards dyes was studied by using batch model.

Chapter 3 introduces the maleic anhydride-modified cellulose fibres/diatomite adsorbents (MCDBs) for the removal of heavy metal ions. The characteristics of adsorbents were investigated by using SEM, FTIR, and BET. The effects of pH, temperature, contact time, and the concentration of  $\text{Pb}^{2+}$  on adsorption were studied in batch mode. The experimental kinetic data fit the pseudo-second order model very well. Moreover, the adsorption isotherm models were evaluated as well.

Chapter 4 is related to a novel composite absorbent based on dissolved cellulose fibres (as matrix) reinforced with microfibrillated cellulose (MFC). In this chapter, both cellulose fibres and microfibrillated cellulose were functional-modified using an organic solvent-free approach to introduce carboxyl groups onto cellulose and the surface of MFC. After modification, the morphology of composites and the adsorption properties of the adsorbents were determined. The adsorption mechanisms were systematically studied by fitting the different kinetics and isotherms models.

Chapter 5 deals with the preparation of thermal-responsive cellulose spheres and their performance towards the removal of dyes and heavy metal ions. The main purpose of this chapter was to explore the microwave-assisted polymerization technique in the synthesis of polymer grafted cellulose spheres. The corresponding results successfully indicated the development of the low-cost and green-based materials by using microwave-assisted polymerization, which helps to broaden the use of thermal-responsive materials in water clarification.

Chapter 6 focuses on the preparation of dual-responsive semi-INP cellulose microfilaments/ Poly (N-isopropylacrylamide-co-acrylic acid) spheres for dye removal in single and binary systems. To further develop the green-based smart or responsive-adsorbents, the thermal- and pH-responsive polymers were used in the preparation of dual-responsive semi-INP spheres. In the processes, NIPAM (a temperature-sensitive monomer) and AA (a pH-sensitive monomer) were copolymerized and grafted onto the cellulose spheres through a microwave-assisted in-situ free radical polymerization. Apart from developing an appropriate protocol for the synthesis of this dual-responsive semi interpenetrating polymer network (semi-IPN) spheres, the morphology, thermal properties, and adsorption behaviors were also investigated to evaluate their potential application in other fields.

Chapter 7 summarizes the results and gives recommendations for future work. In this chapter, based on the overall extensive methods, comparisons and relationships among those methods and the results were systematically analyzed.

This dissertation is presented in article-format, the format of chapters follows the requirement of each Journal. The entire experimental work was conducted by the candidate (Yuan Li). The manuscripts for publications corresponding to key chapters were also drafted by the candidate (as the first author).

## References

- [1] Zhou YM, Jin Q, Hu XY et al (2012) Heavy metal ions and organic dyes removal from water by cellulose modified with maleic anhydride. *J. Mater. Sci.* 47: 5019-5029.
- [2] Volesky B, Holan ZR (1990) Biosorption of Heavy Metals. *Biotechnol. Prog.* 11: 235-250.
- [3] Bolto BA, Pawlowski L et al (1987) *Wastewater Treatment by Ion Exchange*. Chapman and Hall, 262.
- [4] El Qada EN, Allen SJ, Walker GM (2008) Adsorption of basic dyes from aqueous solution onto activated carbons. *Chem. Eng. J.* 135: 174-184.
- [5] Edson LF, Suellen B, Marcio AM et al (2013) Adsorption of a leather dye on mesoporous struvite obtained from swine wastewater. *Chem. Eng. Commun.* 200: 1027-1038.
- [6] Parida KM, Sahu S, Reddy KH et al (2011) A Kinetic, Thermodynamic, and mechanistic approach toward adsorption of methylene blue over water-washed manganese nodule leached residues. *Ind. Eng. Chem. Res.* 50: 843-848.
- [7] Zhang XY, Tan J, Wei XH et al (2013) Removal of remazol turquoise blue G-133 from aqueous solution using modified waste newspaper fiber. *Carbohydr. Polym.* 92: 1497-1502.
- [8] El Ghali A, Baouab MHV, Roudesli MS (2013) Use of amino-modified cotton fibers loaded with copper ions for anionic dye removal under batch and fixed-bed systems: A comparative study. *Fibers Polym.* 14: 65-75.
- [9] Jiang GB, Lin ZT, Huang XY et al (2012) Potential biosorbent based on sugarcane bagasse modified with tetraethylenepentamine for removal of eosin Y. *Int. J. Biol. Micromol.* 50: 707-712.
- [10] Sayari A, Hamoudi S, Yang Y (2005) Applications of pore-expanded mesoporous silica. 1. Removal of heavy metal cations and organic pollutants from wastewater. *Chem. Mater.* 17: 212-216.
- [11] Pizarro J, Castillo X, Jara S et al (2015) Adsorption of  $\text{Cu}^{2+}$  on coal fly ash modified with functionalized mesoporous silica. *Fuel* 156: 96-102.
- [12] Khosroshahy MZ, Abbasabadi AB, Ghasemi N et al (2015) Microwave-assisted functionalization of Rosa Canina-L fruits activated carbon with tetraethylenepentamine and its adsorption behavior toward Ni(II) in aqueous solution: Kinetic, equilibrium and thermodynamic studies. *Powder Technol.* 274: 362-371.

- [13] Oladipo AA, Gazi M (2014) Microwaves initiated synthesis of activated carbon-based composite hydrogel for simultaneous removal of copper(II) ions and direct red 80 dye: A multi-component adsorption system. *J. Taiwan Inst. Chem. E.* 47: 125-136.
- [14] Sulyman M, Namiesnik J, Gierak A (2014) Utilization of new activated carbon derived from oak leaves for removal of crystal violet from aqueous solution. *Pol. J. Environ. Stud.* 23: 2223-2232.
- [15] David WO, Colin B, Thomas FO (2008) Heavy metal adsorbents prepared from the modification of cellulose: A review. *Bioresour. Technol.* 99: 6709-6724.
- [16] Pan Y, Wang F, Wei T et al (2016) Hydrophobic modification of bagasse cellulose fibers with cationic latex: Adsorption kinetics and mechanism. *Chem. Eng. J.* 302: 33-43.
- [17] Wu H, Bremner DH, Wang H et al (2017) Fabrication and investigation of a biocompatible microfilament with high mechanical performance based on regenerated bacterial cellulose and bacterial cellulose. *Mater. Sci. Eng.: C.* 79: 516-524.
- [18] Sayari A, Yang Y, Kruk M et al (1999) Expanding the pore size of MCM-41 silicas: use of amines as expanders in direct synthesis and postsynthesis procedures. *J. Phys. Chem. B* 103: 3651-3658.
- [19] Liu P, Luo Q, Guan Y et al (2010) Drug release kinetics from monolayer films of glucose-sensitive microgel. *Polymer* 512: 668-2675.
- [20] Nalam PC, Lee HS, Bhatt N et al (2017) Nanomechanics of pH-Responsive, Drug-Loaded, Bilayered Polymer Grafts. *ACS Appl. Mater. Inter.* 9: 12936-12948.
- [21] Shi Y, Ma C, Peng L et al (2015) Conductive “smart” hybrid hydrogels with PNIPAM and nanostructured conductive polymers. *Adv. Funct. Mater.* 25: 1219-1225.
- [22] Xia F, Feng L, Wang S et al (2006) Dual-Responsive Surfaces That Switch between Superhydrophilicity and Superhydrophobicity. *Adv. Mater.* 18: 432-436.
- [23] Osypova A, Magnin D, Sibret P et al. (2015) Dual stimuli-responsive coating designed through layer-by-layer assembly of PAA-b-PNIPAM block copolymers for the control of protein adsorption. *Soft matter* 11: 8154-8164.
- [24] Komorowska-Durka M, Dimitrakis G, Bogdal D et al (2015) A concise review on microwave-assisted polycondensation reactions and curing of polycondensation polymers with focus on the effect of process conditions. *Chem. Eng. J.* 264: 633-644.
- [25] Zhang C, Liao L, Gong S (2007) Recent developments in microwave-assisted polymerization with a focus on ring opening polymerization. *Green Chem.* 9: 303-314.

- [26] Singla P, Mehta R, Berek D et al (2014) Ring opening polymerization of lactide in a monomode microwave using stannous octoate and dibutyltin dimethoxide catalysts. *J. Macromol. Sci. Pure.* 51: 350-361.
- [27] Chidanandaiah, Keshri RC, Sanyal MK (2009) Effect of sodium alginate coating with preservatives on the quality of meat patties during refrigerated ( $4\pm 1^\circ\text{C}$ ) storage. *J. Muscle Foods* 20: 275-292.
- [28] Enflo H, Gällstedta M, Nilssona H (2011) Alginate as paperboard laminate for food packaging applications. 25th IAPRI Symposium on packaging.
- [29] Pérez-Pacheco E, Moo-Huchin VM, Estrada-León RJ (2014) Isolation and characterization of starch obtained from *Brosimum malicatum* Swartz Seeds. *Carbohydr. Polym.* 101: 920-927.
- [30] Meshram MW, Patil VV, Mhaske ST (2009) Graft copolymers of starch and its application in textiles. *Carbohydr. Polym.* 75: 71-78.
- [31] Shen J, Song Z, Qian X et al (2011) Carbohydrate-based fillers and pigments for papermaking: A review. *Carbohydr. Polym.* 85: 17-22.
- [32] Ghasemian A, Ghaffari M, Ashori A (2012) Strength-enhancing effect of cationic starch on mixed recycled and virgin pulps. *Carbohydr. Polym.* 87: 1269-1274.
- [33] Ziaee Z, Qian L, Guan Y (2010) Antimicrobial/antimold polymer-grafted starches for recycled cellulose fibers. *J. Biomat. Sci. Polym. E.* 21: 1359-1370.
- [34] Billmers R, Mackewicz VL, Trksak RM (2004) US6790270B1, US patent.
- [35] Guan Y, Qian L, Xiao H et al (2008) Preparation of novel antimicrobial-modified starch and its adsorption on cellulose fibers: Part I. Optimization of synthetic conditions and antimicrobial activities. *Cellulose* 15: 609-618.
- [36] Wang B, Li D, Wang L (2012) Effect of high-pressure homogenization on microstructure and rheological properties of alkali-treated high-amylose maize starch. *J. Food Eng.* 113: 61-68.
- [37] Wooton M, Ho P (1989) Alkali gelatinization of wheat starch. *Starch-Starke* 41: 261-265.
- [38] Campus-Baypoll ON, Rosas-Burgos EC, Torres-Chavez PI et al (1999) Physico-chemical changes of starch during maize tortilla production. *Starch-Starke* 51: 173-177.
- [39] Sedlarik V, Otgonzul O, Kitano T et al (2012) Effect of phase arrangement on solid state mechanical and thermal properties of polyamide 6/poly lactide based co-polyester blends. *J. Macromol. Sci. B* 51: 982-1001.

- [40] Plackett DV, Holm VK, Johansen P et al (2006) Characterization of L-poly lactide and L-poly lactide polycaprolactone co-polymer films for use in cheese packaging applications. *Packag. Technol. Sci.* 19: 1-24.
- [41] Auras RA, Singh S, Singh JJ (2005) Evaluation of oriented poly(lactide) polymers vs. existing PET and oriented PS for fresh food service containers. *Packag. Technol. Sci.* 18: 207-216.
- [42] Jonoobi M, Harun J, Mathew AP et al (2010) Mechanical properties of cellulose nanofiber (CNF) reinforced polylactic acid (PLA) prepared by twin screw extrusion. *Compos. Sci. Technol.* 70: 1742-1747.
- [43] Frone AN, Berlioz S, Chailan J et al (2011) Cellulose fiber reinforced polylactic acid. *Polym. Composite.* 32: 976-985.
- [44] Sanchez-Garcia MD, Lagaron JM (2010) On the use of plant cellulose nanowhiskers to enhance the barrier properties of polylactic acid. *Cellulose* 17: 987-1004.
- [45] Mathew AP, Oksman K, Sain M (2006) The effect of morphology and chemical characteristics of cellulose reinforcements on the crystallinity of polylactic acid. *J. Appl. Polym. Sci.* 101: 300-310.

# **Chapter 1 Literature Review**

## **1.1 Introduction**

This chapter presents the literature review relevant to the research, and this review has been mainly divided into three parts.

The first part of the review focuses on the conventional application of cellulose-based adsorbents. The application of cellulose-based materials used in water clarification and the modification methods of cellulose are summarized.

The second part summarizes the application of cellulose nanofibers (CNF) or nanocrystals (CNC). Renewable CNF and CNC have been seriously studied in recent years. Different types of adsorbents in conjunction with CNF and CNC are also summarized in this section.

Finally, in the third part, the responsive and smart cellulose-based adsorbents are to be presented. Similar to the second part, the third part summarizes and introduces the materials, approaches and testing methods.

## **1.2 The conventional application of cellulose-based adsorbents**

Cellulose, the most abundant naturally-occurring biopolymer with many hydroxyl groups along its chain, is an ideal raw material for producing nanofillers and could be extracted or derived from various living species such as plants, algae, bacteria, animals, and some amoebas [1]. In addition, cellulose is a multifunctional and renewable material which can be used to replace many other non-renewable materials [2]. It is the principle structural component in the cell walls [3], resulting in the low cost of cellulose fibers. However, the adsorption capacity is limited, and the selectivity is low when the natural

cellulose was directly used as an adsorbent. There are many hydroxyl groups on the polymer structure forming hydrogen bonds between the molecular chains [4]. But, the hydroxyls in cellulose can be easily modified to induce functional groups including -COOH, -COO-, -SO<sub>3</sub>H or -NH<sub>2</sub> groups via various derivation reactions, such as esterification, halogenation, oxidation, and etherification [5]. Such methods can be used to vary certain properties of cellulose such as its hydrophilic or hydrophobic character, elasticity, water sorbency, adsorptive or ion exchange capability [6].

### **1.2.1 The removal of heavy metal ions from wastewater**

The removal of toxic and polluting heavy metal ions from industrial effluents, water supplies, and mine waters has received much attention in recent years. Heavy metal ions, such as Pb(II) and Cu(II) ions, affect ecological life by being released into the environment, owing to their tendency to accumulate in living organisms, and are highly toxic when absorbed into the body [7]. Various methods, such as ion exchange, reverse osmosis, as well as electrodialysis techniques, have been developed for the removal and recovery of heavy metal ions from sewage and industrial wastewater [8]. Various adsorbent materials, meanwhile, have been explored for the removal of heavy metal ions from aqueous solutions. Of all the adsorbent materials, activated carbon has been widely used for the removal of heavy metal ions at trace levels [9]. However, activated carbon is costly as an adsorbent in water treatment. Therefore, the production of low-cost materials, such as cellulose, has been the hotspot of researchers. Various cellulose derivatives have been used as ion exchange or chelate resins because they are hydrophilic and advantageous for such applications. Chemical modification can be used

to vary certain properties of cellulose such as its hydrophilic or hydrophobic character, elasticity, water sorbency, adsorptive or ion exchange capability, resistance to microbiological attack and thermal resistance [10]. Cellulose is a water-insoluble linear macromolecular compound consisting of  $\beta$  bond with many glucose residues. It contains one primary hydroxyl group and two secondary hydroxyl groups, and these are in 2,3,6 three carbon atoms, respectively. But the adsorption capacity and the selectivity are low with the direct use of the natural cellulose as adsorbents. Because there are many hydroxyl groups on the polymer structure and the formation of hydrogen bonds between the molecular chains, the cellulose should be modified to achieve the expected adsorption performance. The principles and main routes of cellulose modification in the preparation of adsorbent materials are esterification, etherification, halogenation, oxidation, and graft copolymerization [11].

### **1.2.2 Esterification**

The esterification reaction of cellulose relies on the reaction between the hydroxyl group and an acid, acid anhydride and acid halide under acid catalysis. Geay et al. have synthesized the esterified sawdust bearing a carboxyl group for the adsorption of  $\text{Cu}^{2+}$  from aqueous solution. Succinic anhydride was used to modify sawdust, and the adsorption of heavy metals was achieved [12]. McSweeny et al. milled aspen wood; then the milled aspen wood was thermochemically modified with citric acid for improving the copper ( $\text{Cu}^{2+}$ ) ion sorption capacity of the wood when tested in 24-hour equilibrium batch tests. Sorption capacity ( $q_e$ ) measured with an unbuffered standard solution increased to a maximum of 7.9 mg  $\text{Cu}^{2+}$  ion/g of wood (treated) from 1.3 mg

$\text{Cu}^{2+}$  ion/g wood (untreated). When measured with a buffered standard solution, the  $q_e$  increased to a maximum of 13.8 mg  $\text{Cu}^{2+}$  ion/g of wood (treated) from 4.1 mg  $\text{Cu}^{2+}$  ion/g wood (untreated) [13]. A novel type of adsorbent (CM) was synthesized by Zhou et al. [14]. Cellulose was modified with maleic anhydride to remove heavy metal ions and organic dyes. The adsorption of Hg(II) ions as heavy metal ions by CM was examined, while the adsorption of basic fuchsin, methylene blue and crystal violet as organic dyes by CM was investigated. The maximum adsorption capacity of Hg(II) was found to be 172.5 mg  $\text{g}^{-1}$ , and the fraction of removal of those organic dyes was 88.10, 98.47 and 92.85 % under the optimum conditions, respectively. Ikhuoria and Okieimen have examined the adsorption of cadmium, copper, lead, nickel, and zinc ions on maize Zea mays stalk. The amounts of the metal ions removed from solution depended on the metal ion type and the ionic size of the metals and were enhanced by EDTA (% N = 12.05) modification of the cellulosic sorbent. The sorption on the unmodified sorbent of lead ions from solutions containing zinc ions shows that lead ions are preferentially removed from solution [15]. Low et al. [9] used heat to convert citric acid to citric acid anhydride, which can further react with the cellulosic hydroxyl groups in wood pulp to form an ester linkage. This reaction introduced carboxyl functional groups to the cellulosic wood pulp material. The esterification process increases the carboxylic content of the wood fibre surface, leading to a corresponding increase in the sorption of divalent metal ions. This modified wood pulp had Cu(II) and Pb(II) binding capacities of 24 mg  $\text{g}^{-1}$  and 83 mg  $\text{g}^{-1}$ , respectively.

### 1.2.3 Etherification

The alcoholic hydroxyl groups of the cellulose can react with the alkyl halide or other etherifying reagents under basic conditions and generate a corresponding cellulose ether. Common etherification reagents are haloalkoxy, alkyl epoxides, glycidyl, silane, and isocyanate [16]. The etherification reaction is carried out under homogeneous conditions, pyridine, sodium hydroxide, triethylamine, etc. as a catalyst in accordance with the following steps: (1) dispersing and wetting; (2) etherifying reagent was added into dispersant; (3) termination of the etherification reaction; (4) Separation and Purification.

Liu et al. [17] have prepared a modification procedure for ramie fiber using 3-chloro-2-hydroxypropyltrimethyl ammonium chloride (CHPTAC) as a cationic agent and NaOH as a catalyst. The mechanisms for the modification and dyeing of ramie fiber were analyzed, and the optimum modification conditions were determined to be the CHPTAC concentration of  $30 \text{ g L}^{-1}$ , the NaOH concentration of  $15 \text{ g L}^{-1}$ , the reaction temperature of  $50 \text{ }^\circ\text{C}$ , and the reaction time of 60 min. In another study, Saliba et al. [18] chemically modified sawdust with amidoxime groups by reacting acrylonitrile with the sawdust through an etherification reaction to add cyano groups to the cellulose structure. These cyano groups were then amidoximated by reaction with hydroxylamine. This amidoximated sawdust had a high adsorption capacity for Cu (II) of  $246 \text{ mg g}^{-1}$  and for Ni(II) of  $188 \text{ mg g}^{-1}$ . Silane treatment can reduce the quantity of the surface hydroxyl groups and the hydrophilic of cellulose. Abdelmouleh et al. [19] have done some research whereby the surface modification of cellulosic fibres was carried out using organofunctional silane coupling agents in an ethanol/water medium. A heat treatment

(curing) was applied after reaching the equilibrium adsorption of the prehydrolysed silanes onto the cellulosic substrate. The modified fibres were then characterised by diffuse reflectance infrared spectroscopy and contact angle measurements.

#### **1.2.4 Graft polymerization**

The graft copolymerization reaction of cellulose can be divided into three categories: Free radical polymerization, ionic polymerization and condensation or addition polymerization. Graft copolymerization only happens on the surface of the cellulose in the amorphous region and the crystalline region, and the length of the branched chain may be far more than the main chain. The inherent advantages of the cellulose are not destroyed and at the same time the cellulose is given new performance, such as the adsorption of heavy metals and dye.

Hashem [20] has prepared a sunflower stalk graft copolymer by the reaction of ground sunflower stalks (SFS) with acrylonitrile (AN) in aqueous solution initiated by  $\text{KMnO}_4$ -citric acid (CA) system. Amidoximation of the grafted stalks was performed by the reaction of grafted SFS with hydroxylamine hydrochloride in alkaline medium to obtain amidoximated sunflower stalks (ASFS). The study of adsorption of Cu (II) shows that the ASFS was effectively used in adsorption of Cu (II) ions from aqueous solution. The adsorption data obeyed Langmuir and Freundlich isotherms. Guclu et al. [21] investigated the effect of composition of graft chains of four types cellulose graft copolymers on the competitive removal of  $\text{Pb}^{2+}$ ,  $\text{Cu}^{2+}$ , and  $\text{Cd}^{2+}$  ions from aqueous solution. The copolymers used were (1) cellulose-g-polyacrylic acid (cellulose-g-pAA) with grafting percentages of 7, 18, and 30%; (2) cellulose-g-p(AA-NMBA) prepared by

grafting of AA onto cellulose in the presence of crosslinking agent of N,N'-methylene bisacrylamide (NMBA); (3) cellulose-g-p(AA-AASO<sub>3</sub>H) prepared by grafting of a monomer mixture of acrylic acid (AA) and 2-acrylamido-2-methyl propane sulphonic acid (AASO<sub>3</sub>H) containing 10% (in mole) AASO<sub>3</sub>H; and (4) cellulose-g-pAASO<sub>3</sub>H obtained by grafting of AASO<sub>3</sub>H onto cellulose. All types of cellulose copolymers were found to be selective for the removal of Pb<sup>2+</sup> over Cu<sup>2+</sup> and Cd<sup>2+</sup>. Tian et al. [22] prepared cellulose acetate (CA) nonwoven membrane for heavy metal ion adsorption by electrospinning and surface modification with poly (methacrylic acid) (PMAA). The adsorption of heavy metal ions Cu<sup>2+</sup>, Hg<sup>2+</sup> and Cd<sup>2+</sup> on this membrane was investigated, and it was found that the adsorption capacity increased with the increasing of initial pH value in the system. This membrane has quite high adsorption selectivity for Hg<sup>2+</sup>. The adsorbed metal ions can be easily de-adsorbed from the membrane surface by using saturated ethylenedinitrilo tetraacetic acid solution, and the membrane can be re-used for the metal ion adsorption. Li et al. [23] prepared a novel of polymer surfactant named hydroxyethyl cellulose-based copolymer via ultraviolet (UV) irradiation by copolymerizing hydroxyethyl cellulose (HEC) with hexadecyl acrylate (HDA) and comonomer styrene (St) in aqueous solution. The result showed that the grafting of HDA on the HEC was limited by the grafting of St under UV irradiation, and the graft copolymer performed excellent surface activity when the grafting was under an appropriate condition. Zhao et al. [24] prepared the adsorbent resin by grafting copolymerization of acrylic acid and acrylamide onto cellulose under microwave irradiation and applied it to adsorb copper ions from wastewater. For Cu<sup>2+</sup>, at the optimal adsorption conditions, adsorption ratio could get to 99.2% and the adsorption

capability reached 49.6 mg/g. Adsorbent resin could be regenerated using 8%  $\text{NH}_3/\text{H}_2\text{O}$ , which had good regeneration effect, and experiments showed that adsorption ratio could remain over 90% when resin was regenerated seven times. Li et al. [25] prepared cellulose microsphere (CMS) adsorbent by radiation-induced grafting of dimethylaminoethyl methacrylate (DMAEMA) onto CMS followed by a protonation process. The adsorption of Cr(VI) onto the resulting adsorbent was very fast, and a maximum Cr(VI) uptake ( $78 \text{ mg g}^{-1}$ ) was obtained as the pH was in the range of 3.0 - 6.0. The adsorption behavior of the resultant adsorbent could be described with the Langmuir mode. This adsorbent has potential application for removing heavy metal ion pollutants (e.g. Cr(VI)) from wastewater. Enshirah et al. [26] studied BA-15 functionalized with 3-aminopropyltrimethoxy-silane as a potential adsorbent for  $\text{Cd}^{2+}$ ,  $\text{Co}^{2+}$ ,  $\text{Cu}^{2+}$ ,  $\text{Zn}^{2+}$ ,  $\text{Pb}^{2+}$ ,  $\text{Ni}^{2+}$ ,  $\text{Al}^{3+}$  and  $\text{Cr}^{3+}$ . Using single-metal solutions, the adsorbent was found to have an affinity (molar basis) for metal ions in decreasing order of  $\text{Al}^{3+} > \text{Cu}^{2+} > \text{Ni}^{2+} > \text{Zn}^{2+} > \text{Co}^{2+} > \text{Cd}^{2+} > \text{Pb}^{2+} > \text{Cr}^{3+}$ . Application of this material to remove copper in tap water, river water, and electroplating wastewater was shown to be successful. Anirudhan and Radhakrishnan [27] studied the development of a new cation exchanger (SDGPMA-SP-COOH) carrying spacer (SP) group [-CONH-(CH<sub>2</sub>)<sub>2</sub>-NHCO(CH<sub>2</sub>)<sub>2</sub>-] and carboxylate functional group at the chain end. The preparation process was carried out through graft copolymerization of methacrylic acid onto sawdust, SD (a lignocellulosic residue) using ceric ammonium nitrate as an initiator. The poly (methacrylic acid) grafted SD (SDGPMA) was subsequently treated with thionyl chloride followed by ethylenediamine (transamidation) and succinic anhydride (carboxy-functionalization) treatments. Cr(III) was removed by SDGPMA-SP-COOH

up to 99.3 and 92.6% from an initial concentration of 10 and 25 mg/L, respectively. The monolayer adsorption capacity for Cr(III) removal was found to be 36.63 mg/g. Anirudhan and Sreekumari [28] prepared a novel carboxylate functionalized graft copolymer (PGTDC-COOH) based on TiO<sub>2</sub>-densified cellulose (TDC) by grafting poly (methacrylic acid) onto TDC in the presence of N, N'-methylenebisacrylamide (MBA) as a cross-linking agent and Mn(IV)-citric acid as an initiator system. The adsorption efficiency of PGTDC-COOH for uranium(VI) from aqueous solutions was examined by batch experiments. The sorption process follows the pseudo-second-order kinetic model. The adsorption equilibrium constant and maximum adsorption capacity were evaluated to be 0.074 L/mg and 99.4 mg/g, respectively.

#### **1.2.5 Halogenation, oxidation, etc.**

Halogenation represents another cellulose modification technique. Aoki et al. [29] prepared 6-Deoxy-6-mercaptocellulose and its S-substituted derivatives from 6-bromo-6-deoxycellulose and their sorption behavior for metal ions was examined. Carboxyl, amino, isothiuronium, mercapto and additional hydroxyl groups were introduced to cellulose. The first two groups were effective for the sorption of many kinds of metal ions. Ag(I) was sorbed strongly by all the derivatives studied. Many derivatives sorbed large amounts of Hg(II).

The oxidation of cellulose introduces new functional groups, such as the aldehyde group, the ketone group, the carboxyl group, or the enol group, and generates the different nature of the water-soluble or insoluble oxides named oxidized cellulose. Depending on the difference of oxidation conditions, the oxidation products of cellulose

will have an acidic effect and restore features. Hirota et al. [30] researched the surface carboxylation of porous regenerated cellulose beads by 4-acetamide-TEMPO/NaClO/NaClO<sub>2</sub> system. Carboxylate groups were formed up to 1.87 mmol/g in the beads by the oxidation of C<sub>6</sub> primary hydroxyls to carboxylates without significant weight losses or morphological changes. Cation-exchange behavior of the TEMPO-oxidized cellulose beads was compared with carboxymethylated cellulose beads, showing that the former was characteristic and superior to the latter in terms of adsorption of metal ions and cationic polymers. Especially, the TEMPO-oxidized cellulose beads had high adsorption behavior of lead ion and high-molecular-weight cationic polymers. Ma et al. [31] prepared Ultrafine cellulose nanofibers, 5-10 nm in diameter. They were prepared from oxidation of wood pulp using the (2,2,6,6-tetramethylpiperidin-1-yl) oxyl (TEMPO)/NaBr/NaClO process followed by mechanical treatment. Carboxylate groups on the surface of these nanofibers provide negative charges, which are very effective to adsorb radioactive UO<sub>2</sub><sup>2+</sup> in water. The UO<sub>2</sub><sup>2+</sup> adsorption capability of ultrafine cellulose nanofibers was about 167 mg/g, which is 2-3 times higher than those of typical adsorbents such as montmorillonite, ion imprinted polymer particles, modified silica particles/fibrous membranes, and hydrogels. Table 1 summarises methods for direct modification of cellulose leading to heavy metal adsorbent materials.

**Table.1.1 Cellulose modification and associated functional groups**

Cellulose	Modifying Chemicals	Structure	Adsorption Capacity mg/g	Isotherm Model	Reference
Wood-OH	Succinic anhydride		Cu(II) 104 Cd(II) 168 Ni(II) 97.3		[12]
Aspen wood	Citric acid		Cu(II) 13.9		[13]
Cellulose	Maleic anhydride		Hg(II) 163.9	Freundlich	[14]
Maize stalks	EDTA		Cu(II) 12.2 Cd(II) 20.5	Langmuir	[15]
Wood-OH	Citric acid		Cu(II) 23.7 Pb(II) 82.6	Langmuir	[9]
Wood sawdust Wood flour	Acrylonitrile hydroxylamine		Cu(II) 246 Ni(II) 188		[15]
Sunflower stalk	Acrylonitrile hydroxylamine hydrochloride		Cu(II) 39.4	Langmuir Freundlich	[20]
Cellulose	Acrylic acid and Ceric ammonium nitrate	Cellulose-g-pAA	Cu(II) 63.5 Pb(II) 84.8 Cd(II) 34.9		[21]
	Acrylic acid and Ceric ammonium nitrate and N, N'-methylene bisacrylamide	Cellulose-g-p(AA-NMBA)	Cu(II) 66.7 Pb(II) 90.2 Cd(II) 39.7		
	Acrylic acid and Ceric ammonium nitrate and 2-acrylamido 2-methylpropane sulphonic acid	Cellulose-g-p(AA - AASO <sub>3</sub> H)	Cu(II) 66.7 Pb(II) 91.8 Cd(II) 25.4		
Cellulose acetate	Poly (methacrylic acid)		Cu(II) 3.1 Cd(II) 2.9 Hg(II) 4.9		[22]
Cellulose	Acrylic Acid Acrylamide		Cu(II) 49.6	Freundlich	[24]

	6-Bromo-6-deoxycellulose and 2-mercaptobutanedioic acid	$\begin{array}{c} \text{Cell}-\text{CH}_2-\text{S}-\text{CH}-\text{CH}_2 \\   \quad   \\ \text{COOH} \quad \text{COOH} \end{array}$	Cu(II) 36 Pb(II) 105 Ni(II) 0.93	
Cellulose powder	Cysteine	$\begin{array}{c} \text{Cell}-\text{CH}_2-\text{S}-\text{CH}_2-\text{CH}-\text{NH}_2 \\   \\ \text{COOH} \end{array}$	Cu(II) 22 Pb(II) 28 Ni(II) 8	[29]
	$\alpha$ -Thioglycerol	$\begin{array}{c} \text{Cell}-\text{CH}_2-\text{S}-\text{CH}_2-\text{CH}-\text{CH}_2 \\   \quad   \\ \text{OH} \quad \text{OH} \end{array}$	Cu(II) 2 Pb(II) 6 Ni(II) 10	
	3-Mercaptopropionic acid	$\text{Cell}-\text{CH}_2-\text{S}-\text{CH}_2-\text{CH}_2-\text{COOH}$	Cu(II) 24 Pb(II) 20 Ni(II) 1	
	2-aminoethanethiol	$\text{Cell}-\text{CH}_2-\text{S}-\text{CH}_2-\text{CH}_2-\text{NH}_2$	Cu(II) 6 Pb(II) 81 Ni(II) 5	

---

### 1.2.6 The treatment of organic contaminants from wastewater

Organic sewage has mainly the following three kinds of hazards: aerobic hazards, the hypoxia of water due to the biodegradation of organic sewage, and the death of most aquatic organisms. With respect to the deterioration of water quality and the environment, organic sewage not only reduces the value of water, but also affects the lives of people around water; and in regards to toxicity hazards, organic wastewater contains large amounts of toxic organic compounds and will continue to accumulate in the environment.

Despite the considerable advances in the field of water treatment, the elimination of certain types of products to fulfil the standards in place still raises some problems and remains a topic of concern. In the absence of any treatment, the organic compounds, and the persistent organic pollutants (POP), like certain pesticides, accumulate in water and favour the risk of contamination of the underground sources in an irreversible way. Maatar et al. [32] prepared highly porous cellulose organogels from nanofibrillated

cellulose hydrogels and investigated their adsorption properties towards a wide range of organic pollutants. The kinetics and adsorption isotherms of several aromatic compounds, including herbicides, were investigated. It was proposed that the adsorption process is the result of the diffusion of the organic solute inside the grafted hydrocarbon chains acting as a reservoir on which the organic compounds would be accumulated. The results showed that the modified cellulose organogels could be easily regenerated and reused without any loss of the adsorption capacity, which constitutes one of the main advantages of this category of the adsorbents derived from a renewable resource. Aloulou et al. [33] have studied the removal of organic contaminant from wastewater using chemically modified cellulose fibres, and the adsorption capacities of the modified fibres towards various organic molecules were investigated. The adsorption isotherm related to different solutes follows the Langmuir model in its entire range of concentration. The main advantage of this substrate lies in its relative facile regeneration without a significant loss of its adsorption capacity. Ipek et al. [34] have investigated the efficiency of phenol removal from model phenol solution using Purolite MN 200 and Purolite MN 202 hyper crosslinked macronet polymer adsorbents by using only adsorption and adsorption-ultrafiltration hybrid processes. This study provided a solution to the discharge of phenol containing water and wastewater problem.

In order to remove the phenol from wastewater, many researchers who have studied various modified materials in recent years. Zhou et al. [35] have produced a crosslinked beta-cyclodextrin polymer by crosslinker 2,4-toluene diisocyanate (TDI). Technological parameters of removal phenol waste water were optimized by adsorption experiments, and regeneration times and adsorptive capacity were studied. The maximum amount of

polymers was 40 mg/mL. Tohru et al. [36] synthesized a chitosan-conjugated thermo-responsive polymer containing 15% chitosan, PNIPAAm-15CS and used it for the removal of different phenols in water. The polymer was synthesized by a 1-ethyl-3-(3-dimethylaminopropyl) carbodiimide-mediated condensation of poly(N-isopropylacrylamide-co-acrylic acid) in the aqueous solution. Zhang et al. [37] have prepared four kinds of amino-functionalized nano-size composite materials (NH<sub>2</sub>-NCMs) by radical co-polymerization, of which methylmethacrylate (MMA) and glycidylmethacrylate (GMA) acted as monomers and benzoyl peroxide (BPO) acted as initiator, to obtain epoxy-functionalized polymers, and the composite materials were then modified by ethanediamine (EDA), diethylenetriamine (DETA), triethylenetetramine (TETA), or tetraethylenepentamine (TEPA), named as EDA-NCMs, DETA-NCMs, TETA-NCMs and TEPA-NCMs, respectively. Effects of pH values, initial concentration of phosphate, adsorption time, adsorption temperature and type of functional amines were studied. The adsorption data of the NH<sub>2</sub>-NCMs were fit well with the Langmuir isotherm. The maximum adsorption capacity calculated from Langmuir isotherm was 142.85, 156.25, 172.41 and 196.08 mg/g for EDA-NCMs, DETA-NCMs, TETA-NCMs and TEPA-NCMs, respectively. Deng et al. [38] prepared quaternized cotton by surface-initiated atom transfer radical polymerization (ATRP) for the removal of PFOS and PFOA from aqueous solution. The sorption equilibrium of PFOA and PFOS on quaternized cotton was achieved at 4 h and 12 h, respectively. The obtained maximum sorption capacities of PFOS and PFOA on quaternized cotton at pH 5.0 were 3.3 and 3.1 mmol/g, respectively. This quaternized cotton has promising application for the removal of perfluorinated compounds from wastewater. Zhu et al. [39]

synthesized novel organo montmorillonites with high sorption capacity towards organic. Polydiallyldimethylammonium (PDADMA) and cationic surfactant cetyltrimethylammonium (CTMA) were applied simultaneously to modify montmorillonite. Results of this work showed that simultaneous intercalation of cationic polymers could be a possible method for increasing the sorption capacity of the traditional surfactant synthesized organo montmorillonites. Zhang et al. [40] successfully synthesized superhydrophobic nanoporous polydivinylbenzene materials via a novel solvothermal route. The adsorption of typical volatile organic compounds (VOC) and organic pollutants in water indicated the synthesized materials retained an excellent adsorptive property compared with activated carbon and amberlite XAD-4 resin. The nanoporous material showed a great potential in air purification, wastewater treatment, chemical accident remediation and environmental protection.

Modified material can also be used in urban sewage treatment, Vipasiri et al. [41] have done some research about treating municipal wastewater as alternative secondary and tertiary treatment for wastewater reclamation. In this study, two of the recently developed laboratory scale wastewater treatment systems, fluidised-bed reactor (FBR) using formulated clay mixture absorbents (clay-FBR adsorption) and annular slurry photoreactor (ASP) using  $\text{TiO}_2$  impregnated kaolin catalysts ( $\text{TiO}_2$ -K-ASP), were integrated as an adsorption-photocatalysis hybrid process. The  $\text{TiO}_2$ -K-ASP showed superior degradation of dissolved organic content, while the presence of inorganic ions caused a detrimental effect on its performance. The integration of the adsorption and degradation system as a hybrid treatment process resulted in a synergetic enhancement

for the chemical removal efficiency. This adsorption-photocatalysis hybrid technology can be used as a feasible alternative treatment process for wastewater reclamation.

### **1.2.7 The treatment of dyes in wastewater**

Depending upon their structure, azo- and anthraquinone dyes are the two major classes and together represent 90% of all organic colorants. Adsorption of dye molecules onto a sorbent can be an effective, low-cost method of color removal. Most of the techniques used for removal of dyes are of high production cost, and the regeneration also makes them uneconomical. There is therefore much interest in the development of cheaper and effective newer materials for use as adsorbents.

Wang et al. [42] studied porous network-like FeOOH/ carbonized bacterial cellulose (FeOOH/CBC) nanocomposite and used it as an adsorbent to remove organic dyes. The adsorption equilibrium of as-prepared FeOOH/CBC nanocomposite for methyl orange (MO) was achieved with the maximum adsorption capacity for MO reaching 107.68 mg/g. As-prepared FeOOH/CBC nanocomposite maintains high adsorption activities after four times of adsorption and desorption. He et al. [43] investigated the dynamic batch adsorption of methylene blue (MB) onto nanocrystalline cellulose (NCC) and crushed powder of carbon monolith (CM) using the pseudo-first- and -second-order kinetics. CM outperformed NCC with a maximum capacity of 127 mg/g compared to 101 mg/g for NCC. The Langmuir isotherm model was applied for describing the binding data for MB on CM and NCC, indicating the homogeneous surface of these two materials. Liu et al. [44] synthesized a high efficiency and eco-friendly porous cellulose-based bioadsorbent by grafting acrylic acid and acrylamide to remove anionic dye acid

blue 93 (AB93) and cationic dye methylene blue (MB) from single and binary dye solutions. The maximum adsorption capacities of the bioadsorbent for both AB93 and MB were  $1372 \text{ mg g}^{-1}$  at an initial concentration of  $2500 \text{ mg L}^{-1}$ . The conditions-dependent adsorption characteristics of the bioadsorbent indicated a high efficiency of dyes removal. The cellulose-based bioadsorbent can be effectively used for the removal of dyes from industrial textile wastewater. Hu et al. [45] prepared the functionalized microcrystalline cellulose (MCC) with quaternary amine groups as an adsorbent to remove Congo Red dye (CR) from aqueous solution. The ultrasonic pretreatment of MCC was investigated during its functionalization, and the batch adsorption of the functionalized MCC was studied. The adsorbent (FM-1) obtained has been shown to be a promising and efficient adsorbent for the removal of CR from an aqueous solution. Yan et al. [46] investigated the hydroxypropyl cellulose crosslinked by epichlorohydrin (EPI) and ammonia in sodium hydroxide aqueous solution. A temperature induced phase separation (TIPS) process was applied to synthesize a microporous crosslinked HPC hydrogel. The cationic HPC hydrogel showed an excellent ability to adsorb anionic dye AO7, and the maximum adsorption capacity at room temperature was found to be  $2478 \text{ (g/kg)}$  at pH 3.96. The Langmuir model agreed well with the experimental data ( $R^2 = 0.99$ ). The strong electrostatic interaction between the quaternary ammonium and dye anions could be the main driving force for adsorption.

### **1.3 The application of cellulose nanofibers (CNF) or nanocrystals (CNC)**

Renewable CNF and CNC have been seriously studied in recent years, and have different morphologies as well as varies extraction processes. CNC are usually isolated

by using strong acids hydrolysis. The first stable CNC were prepared using sulfuric acid as the agent of hydrolysis [47]. During such processes, the strong acids can attack and digest the amorphous regions of target cellulose, leading to the transformation of long fibers to short crystalline. Other chemicals such as ammonium persulfate and hydrogen peroxide have also been reported by researchers during the isolation of CNC using biomass [48]. However, CNF can be prepared via mechanical processes, such as high pressure homogenization, grinding and refining [49]. Apart from CNC or CNF, microfibrillated cellulose (MFC) is also superior due to its advantages in structure, performance, and application. MFC is an ideal material which would provide a variety of shapes and be biocompatible and absorbable [50]. Microfibrillated cellulose is an excellent environmentally friendly adsorbent due to high specific surface area. The application of MFC in the preparation of composite-type adsorbent is expected to increase the strength of the adsorbents and thermal stability significantly owing to its high bonding potential.

### **1.3.1 Reinforcements for biocomposites**

Wood is the main source of CNC or CNF, and with the development of economy, there is increased demand for low cost natural materials, such as agricultural and industrial residues. The natural cellulosic materials have many advantages compared with other inorganic reinforcements. Apart from low density, cost and energy consumption, they are renewable and have a high strength, modulus and reactive surface. Cellulose fibrils extracted from potato peel waste have been previously studied as an additive for the reinforcements of biocomposites [51]. Chen et al. [52] investigated the effectiveness of

cellulose nanocrystals, and found that the CNC can be used as a reinforcement and vapor barrier additive. The results indicated that cellulose nanocrystals can be extracted from the potato peel waste by alkali treatment and subsequently acid hydrolysis. The prepared CNC can be compared with other nanocrystals reported, for example cotton CNC [53]. Wei et al. [54] studied the thermophysical properties and biodegradation behavior of green composites prepared from polyhydroxybutyrate (PHB) and potato peel waste fermentation residue (PPW-FR) fibers. The biocomposites showed poor mechanical properties but extremely higher biodegradation rate as compared with pure PHB. Many researchers have studied the isolation of CNC and CNF from low-value materials, including chardonnay grape skins [55], sweet potato residue [56], kenaf fibers [57], kenaf stem [58], banana pseudostems [59], banana stem [60], tomato peels [61], cotton fibers [62], bamboo pulp [63], rice straw [64], grape pomace [65], bagasse [66], coconut husks [67], pennisetum sinense [68], pea hull fiber [69], cotton, flax and agriculture byproducts [70], which are also examples of natural sources for preparing CNC.

### **1.3.2 Bioadsorbents for water clarification and soil remediation**

The water clarification has always been the focus of the research by researchers. Meanwhile, natural and self-made materials as adsorbents are the hotspot, especially those biomaterials [71-72]. The bio-adsorbents are widely investigated nowadays. Agroindustry by-products are low cost and renewable, which can be used for the water clarification. Aman et al. [73] studied potato peels as a new adsorbent for removing toxic metal ion Cu(II) from water/industrial waste water. The synthesized adsorbents

had great ability to remove heavy metal ions. Mutongo et al. [74] used potato peels as an effective biosorbent for the removal of hexavalent chromium from effluent, and the results indicated that potato peels could be used as a low cost and renewable biosorbent. In addition, potato peels have been studied as bio-adsorbents for the removal of dyes and pharmaceutical effluents. Rehman et al. [75] used guava leaves and potato peels as adsorbents for removal of synthetic dye, and the results showed that potato peels were more effective for removal of amaranth dye than guava leaves. Kyzas and Deliyanni [76] studied potato peels as environmental friendly materials for the removal of two drug compounds (dorzolamide and pramipexole) from synthetic aqueous effluents. Sharma et al. [77] treated two agricultural adsorbents, potato peel and Neem bark with HCHO and H<sub>2</sub>SO<sub>4</sub> separately and the treated adsorbents were used for the removal of Direct Red-81. The results revealed that the formaldehyde treated potato peel showed significant dye removal and the adsorption process was non-spontaneous, exothermic and reversible. Furthermore, the potato peels studied as adsorbents for the removal of Brilliant Green [78] were also carried out.

The bio-sorbents can also be used for the remediation of soil and have a dramatic potential for environmental protection. Azmat et al. [79] have studied the Ecological Particulate Matter (EPM) and its remediation using potato peel surface (PPC) bio-sorbent, which produced another strategy for the application of potato peels. Co-composting eggshell with potato peels, grass clippings, and rice husks can be used as biosorbent for the removal of Pb(II) from an aqueous medium. This study showed the potential use of egg shells and potato peels as a biosorbent for lead removal from

aqueous solutions [80]. Similarly, potato peels played an important role in biosurfactant [81], co-composting of eggshell waste [82] and organic manure [83].

#### **1.4 Smart or responsive bioadsorbents**

As mentioned above, among the various conventional methods for the removal of contaminants from wastewater including ion exchange, flotation, solvent extraction, chemical precipitation, coagulation, membrane filtration, reverse osmosis, and adsorption, adsorption is promising due to its high selectivity and easy handling, lower operating costs, and high efficiency in removing very low levels of heavy metals from aqueous solutions [84-86]. Adsorbents based on naturally occurring support materials gained increasing emphasis due to their availability in large quantities, their relatively low cost, and their facile chemical modification to introduce specific functional groups for enhanced metal binding ability [87], while of the various biological adsorbents, cellulose-based materials were believed to be a potential alternative for the removal of various contaminants. Cellulose is an ideal raw material for the fabrication of adsorbents for the removal of toxic pollutants. Nevertheless, there still exist some drawbacks in the applications of these cellulose-based adsorbents. For instance, desorption of contaminants from adsorbents is difficult and usually strong acids are needed, producing new pollutants. In addition, the adsorption behavior is uncontrollable. Recently, surface graft modifications have been considered as a convenient route for introducing new chemical and physical properties to cellulose. By means of grafting, “smart” adsorbents based on cellulose with thermal-responsive can be prepared to overcome the shortcomings mentioned above.

### 1.4.1 Application of thermal/pH sensitive polymers

Most of the thermo-sensitive polymers are based on poly (N-isopropyl acrylamide) (PNIPAM). PNIPAM is insoluble and undergoes a conformational change above its lower critical solution temperature (LCST) of 32 °C, while below the LCST, the polymer chains swell in water. Above the LCST, the solvent quality changes and the polymer segments are thought to become more hydrophobic [88]. During the past decades, PNIPAM-based materials have been widely applied in fields of biotechnology and medicine [89] and plenty of relative works have been reported. For instance, Leobandung et al. synthesized a series of PNIPAM microgels using poly (ethylene glycol) 1000 methacrylate as the comonomer and poly (ethylene glycol) 400 dimethacrylate as crosslinker [90]. M. Das et al synthesized a PNIPAM microgel to deliver anti-cancer drugs to cancer cells [91]. The drug release behaviors and mechanisms from the glucose sensitive P(NIPAM-AAPBA) microgels were studied using a microgel monolayer as the platform [92].

Apart from temperature, pH is also critical in the adsorption-desorption behaviors of adsorbents. Generally, pH affects the degree of ionization and the surface charge of materials, and thus the adsorption and desorption of probes could be controlled effectively by the changes in pH if the adsorbents exhibit the pH-responsive behavior. Typical pH-responsive polymers, poly (acrylic acid) (PAA) [93] and poly(4-vinylpyridine) (P4VP) [94] are more stable and can offer higher binding capacity compared to the low-molecular-weight types containing carboxyl or thiol.

### 1.4.2 Responsive and smart cellulose-based adsorbents

Responsive and smart materials have gained much research interest in the last few decades especially for the application of drug delivery, wastewater treatment and oil purification. Cellulose, as a natural polymer resource, has been attracting significant attention in various biomedical applications including controlled drug delivery, bioengineering and tissue engineering due to its nontoxicity, biocompatibility, and biodegradability. Smart materials based on cellulose have their unique properties, and many possible applications. Cha et al. [95] used carboxylated nanocrystalline cellulose (CNCC) to prepare N-isopropyl acrylamide-based thermal/pH sensitive hydrogels. The resulting hydrogels have been improved to possess thermal/pH sensitivity. Soyeon and Kevin [96] prepared hydrogels composed of N-isopropylacrylamide (NIPAAm) and acrylic acid (AAc) by redox polymerization, with the peptide cross-linker. Poly (N-isopropylacrylamide-co-acrylic acid) [P(NIPAAm-co-AAc)] hydrogels were also prepared, and the results indicated that P(NIPAAm-co-AAc) hydrogels can be tailored to create environmentally-responsive artificial extracellular matrixes. Ekici [97] investigated poly (N-isopropyl acrylamide) (PNIPAm)–carboxymethyl cellulose (CMC) full interpenetrating polymeric networks (IPNs) by using PNIPAm and CMC. The synthesized full IPN hydrogels can be used as pH and temperature sensitive biotechnological materials for the adsorption of proteins.

Surface functionalization with stimuli-responsive materials can turn an ordinary material into a smart one that shows adaptive properties upon external stimuli. Wang et al. [98] prepared an electrospun regenerated cellulose (RC) nanofibrous membrane; subsequently, poly(N-isopropylacrylamide) (PNIPAAm), a thermo-responsive polymer,

was surface grafted to form the polymer chains/brushes on the surface of RC nanofibers via the surface-initiated atom transfer radical polymerization (SI-ATRP) method. Thereafter, the PNIPAAm-modified RC nanofibrous membrane was investigated for its temperature-responsive surface wettability at temperatures below/above the lower critical solution temperature (LCST). With the large surface area and switchable surface wettability, the as-prepared PNIPAAm-grafted nanofibrous membrane exhibits excellent properties of controllable oil/water separation and possesses great potential towards both wastewater treatment and oil purification. Hakalahti et al. [99] obtained a functional membrane template by first fabricating a water stable film from cellulose nanofibrils and subsequently surface grafting it with a thermoresponsive polymer, poly NIPAM. The behavior of the membrane template was dependent on temperature. The increment in slope of relative water permeance around the lower critical solution temperature of poly NIPAM increased from 18 to 100% upon polymer attachment. Although the membrane template essentially consisted of wood-based materials, the benefits of smart synthetic polymers were achieved.

Hydrogels are high water content materials prepared by polymer crosslinking that can release active species, such as therapeutic, antibacterial, antiperspirant and moisturising agents, and fragrances. In recent years, several hydrogel systems have been reported based on both natural and synthetic polymers. Among the natural polymers, chitosan and cellulose-derivatives have been extensively studied, due to their stimuli responsive properties (pH and temperature sensitivity, respectively) [100]. Dutta et al. [101] prepared a new set of pH, temperature, and redox responsive hydrogels from carboxymethylcellulose (CMC) and poly(N-isopropylacrylamide). Copolymeric (CP)

hydrogels were synthesized by copolymerizing N-isopropylacrylamide (NIPA) and methacrylated carboxymethylcellulose, and semi-interpenetrating network (SIPN) hydrogels were prepared by polymerizing NIPA in presence of CMC. CP hydrogels showed gradual decrease in water retention values with increase in temperature. CBA cross-linked hydrogels showed higher swelling in comparison to BIS cross-linked hydrogels. In fact, the dependence of hydrophilic/hydrophobic characteristics on temperature makes PNIPAm-grafted polymers a potential absorbent and a few works have been performed. Kanazawa et al. [102] prepared a molecular imprinted thermo-sensitive gel adsorbent composed of NIPAM as thermo-sensitive component and N-(4-vinyl) benzyl ethylenedi- amine (VBEDA) as the chelating monomer. The adsorption and desorption were performed repeatedly by temperature swing and the selective adsorption of Cu(II) ion was confirmed by comparing the adsorption amounts of Ni(II), Zn(II) and Mn(II). Additionally, they prepared a thermosensitive NIPAM microgel adsorbent by the emulsion polymerization using an anionic polymerizable surfactant and the molecular imprinted technique [103]. They found that the adsorption rate for Cu(II) ion was quicker compared to their previous study. It was revealed from this study that a metal ion in an aqueous solution was complexed with an extractant and the metal-surfactant complexes can be adsorbed onto the NIPAM gel at the temperatures above the LCST and desorbed conveniently at those under the LCST, due to the changes in hydrophilic/hydrophobic characteristics.

Apart from PNIPAM, another candidate named random copolymers of ethylene oxide and propylene oxide (PEPO) has also been reported with LCST at around body temperature. A temperature responsive thickener has been prepared by grafting amino-

terminated PEPO on the CMC skeleton. During processes, the esterification between amino groups and carboxyl groups happened successfully in acidic solution [104]. From the methods mentioned above, it is highly likely that cellulose has great potential to be used as raw materials for the preparation of smart or responsive bioadsorbents. The resulting adsorbents maintained thermal and pH dual-responsive properties in the application of water clarification. In addition, the adsorption and desorption mechanisms can be systematically investigated by using different kinetics and isotherms models.

## 1.5 References

- [1] Keijbets MJH (2008) Potato Processing for the Consumer: Developments and Future Challenges. *Potato Res.* 51: 271-281.
- [2] Jonoobi M, Oladi R, Davoudpour Y et al (2015) Different preparation methods and properties of nanostructured cellulose from various natural resources and residues: a review. *Cellulose* 22: 935-969.
- [3] Perez S, Samain D (2010) Structure and engineering of celluloses. *Adv. Carbohydr. Chem. Bi.* 64: 5-116.
- [4] Thielemans W, McAninch IM, Barron V et al (2005) Impure Carbon Nanotubes as Reinforcements for Acrylated Epoxidized Soy Oil Composites. *J. Appl. Polym. Sci.* 98: 1325-1338.
- [5] O'Connell DW, Birkinshaw C, O'Dwyer TF (2008) Heavy metal adsorbents prepared from the modification of cellulose: A review. *Bioresource Technol.* 99: 6709-6724.
- [6] Colak S, Kusefoglul SH (2007) Synthesis and Interfacial Properties of Aminosilane Derivative of Acrylated Epoxidized Soybean Oil. *J. Appl. Polym. Sci.* 104: 2244-2253.
- [7] Volesky B, Holan ZR (1990) Biosorption of Heavy Metals, *Biotechnol. Prog.* 11: 235-250.
- [8] Bolto BA, Pawlowski L (1987) *Wastewater Treatment by Ion Exchange*. Chapman and Hall, 262.

- [9] Low KS, Lee CK, Mak SM (2004) Sorption of copper and lead by citric acid modified wood. *Wood Sci. Technol.* 38: 629-640.
- [10] McDowall DJ, Gupta BS, Stannett VT (1984) Grafting of vinyl monomers to cellulose by ceric ion initiation. *Prog. Polym. Sci.* 10: 1-50.
- [11] O'Connell DW, Birkinshaw C, O'Dwyer TF (2008) Heavy metal adsorbents prepared from the modification of cellulose: A review. *Bioresource Technol.* 99: 6709-6724.
- [12] Geay M, Marchetti V, Clément A et al (2000) Decontamination of synthetic solutions containing heavy metals using chemically modified sawdusts bearing polyacrylic acid chains. *J. Wood Sci.* 46: 331-333.
- [13] McSweeney JD, Rowell RM, Min SH (2006) Effect of Citric Acid Modification of Aspen Wood on Sorption of Copper Ion. *J. Nat. Fibers* 3: 43-58.
- [14] Zhou Y, Jin Q, Hu XY et al (2012) Heavy metal ions and organic dyes removal from water by cellulose modified with maleic anhydride. *J. Mater. Sci.* 47: 5019-5029.
- [15] Ikhuoria EU, Okieimen FE (2000) Scavenging cadmium, copper, lead, nickel and zinc ions from aqueous solution by modified cellulose adsorbent. *Int. J. Environ. Studies* 57: 401-409.
- [16] Laurence L, Etienne F, Cecile G et al (2004) Cellulose microfibrils with modified surface, preparation method and use thereof: US, 6703497.
- [17] Liu Z, Yang Y, Zhang L et al (2007) Study on the cationic modification and dyeing of ramie fiber. *Cellulose* 14: 337-345.
- [18] Saliba R, Gauthier H, Gauthier R (2005) Adsorption of heavy metal ions on virgin and chemically-modified lignocellulosic materials. *Adsorpt. Sci. Technol.* 23: 313-322.
- [19] Abdelmouleh M, Boufi S, Duarte AP et al (2004) Modification of cellulosic fibres with functionalised silanes: development of surface properties. *Int. J. Adhes. Adhes.* 24: 43-54.
- [20] Hashem A (2006) Amidoximated Sunflower Stalks (ASFS) as a New Adsorbent for Removal of Cu (II) from Aqueous Solution. *Polym-Plast. Technol.* 45: 35-42.
- [21] Guclu G, Gurdag G, Ozgumus S (2003) Competitive Removal of Heavy Metal Ions by Cellulose Graft Copolymers. *J. Appl. Polym. Sci.* 90: 2034-2039.
- [22] Tian Y, Wu M, Liu R et al (2011) Electrospun membrane of cellulose acetate for heavy metal ion adsorption in water treatment. *Carbohydr. Polym.* 83: 743-748.

- [23] Li Z, Wang L, Huang Y (2007) Photoinduced graft copolymerization of polymer surfactants based on hydroxyethyl cellulose. *J. Photoch. Photobio. A* 190: 9-14.
- [24] Zhao B, Wang P, Tong Z et al (2006) Preparation and Adsorption Performance of a Cellulosic- Adsorbent Resin for Copper(II). *J. Appl. Polym. Sci.* 99: 2951-2956.
- [25] Li C, Zhang Y, Peng J et al (2012) Adsorption of Cr(VI) using cellulose microsphere-based adsorbent prepared by radiation-induced grafting. *Radiat. Phys. Chem.* 81: 967-970.
- [26] Enshirah D, Abdelhamid S (2012) Adsorption of heavy metals on amine-functionalized SBA-15 prepared by co-condensation: Applications to real water samples. *Desalination* 285: 62-67.
- [27] Anirudhan TS, Radhakrishnan PG (2007) Chromium(III) removal from water and wastewater using a carboxylate-functionalized cation exchanger prepared from a lignocellulosic residue. *J. Colloid Interf. Sci.* 316: 268-276.
- [28] Anirudhan TS, Sreekumari SS (2010) Synthesis and characterization of a functionalized graft copolymer of densified cellulose for the extraction of uranium(VI) from aqueous solutions. *Colloid. Surface. A* 361: 180-186.
- [29] Aoki N, Fukushima K, Kurakata H et al (1999) 6-Deoxy-6-mercaptocellulose and its S-substituted derivatives as sorbents for metal ions. *React. Funct. Polym.* 42: 223-233.
- [30] Hirota M, Tamura N, Saito T et al (2009) Surface carboxylation of porous regenerated cellulose beads by 4-acetamide-TEMPO/NaClO/NaClO<sub>2</sub> system. *Cellulose* 16: 841-851.
- [31] Ma HY, Hsiao BS, Hsiao S et al., 2012. Ultrafine Cellulose Nanofibers as Efficient Adsorbents for Removal of UO<sub>2</sub><sup>2+</sup> in Water. *ACS Macro. Letters* 1: 213-216.
- [32] Matar W, Alila S, Boufi S (2013) Cellulose based organogel as an adsorbent for dissolved organic compounds. *Ind. Crop. Prod.* 49: 33-42.
- [33] Aloulou F, Boufi S, Labidi J (2006) Modified cellulose fibres for adsorption of organic compound in aqueous solution. *Sep. Purif. Technol.* 52: 332-342.
- [34] Ipek IY, Kabay N, Yuksel M et al (2012) Application of adsorption-ultrafiltration hybrid method for removal of phenol from water by hypercrosslinked polymer adsorbents. *Desalination* 306: 24-28.
- [35] Zhou YQ, Huang J, Han PF et al (2012) Synthesis and Characterization of Crosslinked beta-Cyclodextrin and Their Sorption Capacities Towards Phenol from Wastewater. *Asian J. Chem.* 24: 2007-2012.

- [36] Saitoh T, Kotaro A, Hiraide M (2011) Removal of phenols in water using chitosan-conjugated thermo-responsive polymers. *J. Hazard. Mater.* 185: 1369-1373.
- [37] Zhang Y, Xi X, Xu S et al (2012) Adsorption Studies on Phosphate by Amino-functionalized Nano-size Composite Materials. *Acta Chim. Sinica* 70: 1839-1846.
- [38] Deng SB, Zheng YQ, Xu FJ et al (2012) Highly efficient sorption of perfluorooctane sulfonate and perfluorooctanoate on a quaternized cotton prepared by atom transfer radical polymerization. *Chem. Eng. J.* 193: 154-160.
- [39] Zhu JX, Wang T, Zhu R et al (2011) Novel polymer/surfactant modified montmorillonite hybrids and the implications for the treatment of hydrophobic organic compounds in wastewaters. *Appl. Clay Sci.* 51: 317-322.
- [40] Zhang YL, Wei S, Liu F et al (2009) Superhydrophobic nanoporous polymers as efficient adsorbents for organic compounds. *Nano Today* 4: 135-142.
- [41] Vimonses V, Jin B, Chow CWK et al (2010) An adsorption-photocatalysis hybrid process using multi-functional-nanoporous materials for wastewater reclamation. *Water Res.* 44: 5385-5397.
- [42] Wang ZP, Ma YJ, He H et al (2015) A novel reusable nanocomposite: FeOOH/CBC and its adsorptive property for methyl orange. *Appl. Surf. Sci.* 332: 456-462.
- [43] He XY, Male KB, Nesterenko PN et al (2013) Adsorption and Desorption of Methylene Blue on Porous Carbon Monoliths and Nanocrystalline Cellulose. *ACS Appl. Mater. Inter.* 5: 8796-8804.
- [44] Liu L, Gao ZY, Su XP et al (2015) Adsorption Removal of Dyes from Single and Binary Solutions Using a Cellulose-based Bioadsorbent. *ACS Sustain. Chem. Eng.* 3: 432-442.
- [45] Hu DY, Wang P, Li J et al (2014) Functionalization of Microcrystalline Cellulose with N, N-dimethyldodecylamine for the Removal of Congo Red Dye from an Aqueous Solution. *BioResources* 9: 5951-5962.
- [46] Yan LF, Shuai Q, Gong X et al (2009) Synthesis of Microporous Cationic Hydrogel of Hydroxypropyl Cellulose (HPC) and its Application on Anionic Dye Removal. *Clean-Soil Air Water* 37: 392-398.
- [47] Ranby BG (1951) The colloidal properties of cellulose micelles. *Discussions Faraday Soc.* 11: 158-164.
- [48] Cheng M, Qin Z, Liu Y et al (2014) Efficient extraction of carboxylated spherical cellulose nanocrystals with narrow distribution through hydrolysis of lyocell fibers by using ammonium persulfate as an oxidant. *J. Mater. Chem. A* 2: 251-258.

- [49] Wang B, Sain M, Oksman K (2007) Study of structural morphology of hemp fiber from the micro to the nanoscale. *Appl. Compos. Mater.* 14: 89-103.
- [50] Wu H, Bremner DH, Wang H et al (2017) Fabrication and investigation of a biocompatible microfilament with high mechanical performance based on regenerated bacterial cellulose and bacterial cellulose. *Mater. Sci. Eng. C* 79: 516-524.
- [51] Alain D, Danie LD, Michel RV (2000) Cellulose Microfibrils from Potato Tuber Cells: Processing and Characterization of Starch-Cellulose Microfibril Composites. *J. Appl. Polym. Sci.* 76: 2080-2092.
- [52] Chen D, Lawton D, Thompson MR et al (2012) Biocomposites reinforced with cellulose nanocrystals derived from potato peel waste. *Carbohydr. Polym.* 90: 709-716.
- [53] Rubio-López A, Hoang T, Santiuste C (2016) Constitutive model to predict the viscoplastic behaviour of natural fibres based composites. *Compos. Struct.* 155: 8-18.
- [54] Wei L, Liang S, McDonald AG (2015) Thermophysical properties and biodegradation behavior of green composites made from polyhydroxybutyrate and potato peel waste fermentation residue. *Ind. Crop. Prod.* 69: 91-103.
- [55] Lu P, Hsieh YL (2012) Cellulose isolation and core-shell nanostructures of cellulose nanocrystals from chardonnay grape skins. *Carbohydr. Polym.* 4: 2546-2553.
- [56] Lu H, Gui Y, Zheng L, Liu X (2013) Morphological, crystalline, thermal and physicochemical properties of cellulose nanocrystals obtained from sweet potato residue. *Food Res. Int.* 50: 121-128.
- [57] Zainuddin SYZ, Ahmad I, Kargarzadeh H (2013) Cassava starch biocomposites reinforced with cellulose nanocrystals from kenaf fibers. *Compos. Interfaces* 20: 189-199.
- [58] Jonoobi M, Harun J, Tahir PM et al (2011a). Physicochemical characterization of pulp and nanofibers from kenaf stem. *Mater. Lett.* 65: 1098-1100.
- [59] Pereira ALS, Nascimento DMD, Souza Filho, MDSM et al (2014) Improvement of polyvinyl alcohol properties by adding nanocrystalline cellulose isolated from banana pseudostems. *Carbohydr. Polym.* 112: 165-172.
- [60] Kasa SN, Omar MF, Nizam I (2016) Morphology, thermal and chemical properties of nanocrystalline cellulose (NCC) hydrolyzed from banana stem. *Mater. Sci. Forum* 840: 257-261.
- [61] Jiang F, Hsieh YL (2015) Cellulose nanocrystal isolation from tomato peels and assembled nanofibers. *Carbohydr. Polym.* 122: 60-68.

- [62] Sun B, Zhang M, Hou Q et al (2016) Further characterization of cellulose nanocrystal (CNC) preparation from sulfuric acid hydrolysis of cotton fibers. *Cellulose* 23: 439-450.
- [63] Hong B, Chen F, Xue G (2016) Preparation and characterization of Cellulose nanocrystals from bamboo pulp. *Cell. Chem. Technol.* 50: 225-231.
- [64] Jiang F, Kondo T, Hsieh YL (2016). Rice Straw Cellulose Nanofibrils via Aqueous Counter Collision and Differential Centrifugation and Their Self-Assembled Structures. *ACS Sustain. Chem. Eng.* 4: 1697-1706.
- [65] Xu Y, Scales A, Jordan K et al (2016) Starch nanocomposite films incorporating grape pomace extract and cellulose nanocrystal. *J. Appl. Polym. Sci.* 134: 44438-44446.
- [66] Bhattacharya D, Germinario LT, Winter WT (2008) Isolation, preparation and characterization of cellulose microfibrils obtained from bagasse. *Carbohydr. Polym.* 73: 371-377.
- [67] Nascimento DMD, Dias AF, Araújo Junior CPD et al (2016) A comprehensive approach for obtaining cellulose nanocrystal from coconut fiber. Part II: Environmental assessment of technological pathways. *Ind. Crop. Prod.* 93: 58-65.
- [68] Lu QL, Tang LR, Wang S et al (2014) An investigation on the characteristics of cellulose nanocrystals from *Pennisetum sinense*. *Biomass Bioenerg.* 70: 267-272.
- [69] Chen Y, Liu C, Chang PR et al (2009) Bionanocomposites based on pea starch and cellulose nanowhiskers hydrolyzed from pea hull fibre: effect of hydrolysis time. *Carbohydr. Polym.* 76: 607-615.
- [70] Luduen LN, Vecchio A, Stefani PM et al (2013) Extraction of cellulose nanowhiskers from natural fibers and agricultural byproducts. *Fibers Polym.* 14: 1118-1127.
- [71] Basci N, Kaocadagistan E, Kocadagistan B (2004) Biosorption of copper (II) from aqueous solutions by wheat shell. *Desalination* 164: 135-140.
- [72] Gupta VK, Ali I (2000) Utilisation of bagasse fly ash (a sugar industry waste) for the removal of copper and zinc from wastewater. *Sep. Purif. Technol.* 18: 131-140.
- [73] Aman T, Kazi AA, Sabri MU et al (2008) Potato peels as solid waste for the removal of heavy metal copper(II) from waste water/industrial effluent. *Colloid. Surface. B* 63: 116-121.
- [74] Mutongo F, Kuipa O, Kuipa PK (2014) Removal of Cr(VI) from aqueous solutions using powder of potato peelings as a low-cost sorbent. *Bioinorg. Chem. Appl.* 973153.

- [75] Rehman R, Mahmud T, Irum M (2015) Comparative sorption studies for Amaranth dye removal from water in cost-effective way using Guava leaves and potato peels. *Asian J. Chem.* 27: 2008-2014.
- [76] Kyzas GZ, Deliyanni EA (2015) Modified activated carbons from potato peels as green environmental-friendly adsorbents for the treatment of pharmaceutical effluents. *Chem. Eng. Res. Des.* 97: 135-144.
- [77] Sharma N, Tiwari DP, Singh SK (2014) Efficiency of chemically treated potato peel and neem bark for sorption of direct red-81 dye from aqueous solution. *Rasayan J. Chem.* 7: 339-409.
- [78] Rehman R, Mahmud T, Irum M (2015) Brilliant Green Dye Elimination from Water Using Psidium guajava Leaves and Solanum tuberosum Peels as Adsorbents in Environmentally Benign Way. *J. Chem-NY* 126036.
- [79] Azmat R, Moin S, Saleem A (2016) Remediation of Cu metal-induced accelerated Fenton reaction by potato peels bio-sorbent. *Environ. Monit. Assess.* 188: 674-687.
- [80] Soares MAR, Marto S, Quina MJ et al (2016) Evaluation of Eggshell-Rich Compost as Biosorbent for Removal of Pb(II) from Aqueous Solutions. *Water Air Soil Poll.* 227: 150-165.
- [81] Das K, Mukherjee AK (2007) Comparison of lipopeptide biosurfactants production by *Bacillus subtilis* strains in submerged and solid-state fermentation systems using a cheap carbon source: Some industrial applications of biosurfactants. *Process Biochem.* 42: 1191-1199.
- [82] Soares MAR, Quina MMJ, Quinta-Ferreira RM (2013) Co-composting of eggshell waste in self-heating reactors: Monitoring and end-product quality. *Bioresource Technol.* 148: 293-301.
- [83] Priyanga K, Reji A, Bhagat JK et al (2016) Production of organic manure from potato peel waste. *Int. J. Chem. Tech. Res.* 9: 845-847.
- [84] Xu J, Song XC, Zhang Q et al (2011) Characterization of metal removal of immobilized *Bacillus* strain CR-7 biomass from aqueous solutions. *J. Hazard. Mater.* 187: 450-458.
- [85] Fu F, Wang Q (2011) Removal of heavy metal ions from wastewaters: A review. *J. Environ. Manage.* 92: 407-418.
- [86] Mouni L, Merabet D, Bouzaza A et al (2011) Adsorption of Pb (II) from aqueous solutions using activated carbon developed from Apricot stone. *Desalination* 276: 148-153.

- [87] Kang H, Liu R, Huang Y (2015) Graft modification of cellulose: methods, properties and applications. *Polymer* 70: 1-16.
- [88] Plunkett KN, Zhu X, Moore JS et al (2006) PNIPAM chain collapse depends on the molecular weight and grafting density. *Langmuir* 22: 4259-4266.
- [89] Ogawa K, Wang B, Kokufuta E (2001) Enzyme-regulated microgel collapse for controlled membrane permeability. *Langmuir* 17: 4704-4707.
- [90] Leobandung W, Ichikawa H, Fukumori Y et al (2002) Preparation of stable insulin-loaded nanospheres of poly (ethylene glycol) macromers and N-isopropyl acrylamide. *J. control. release* 80: 357-363.
- [91] Das M, Mardiyani S, Chan WC et al (2006) Biofunctionalized pH-Responsive Microgels for Cancer Cell Targeting: Rational Design. *Adv. Mater.* 18: 80-83.
- [92] Liu P, Luo Q, Guan Y et al (2010) Drug release kinetics from monolayer films of glucose-sensitive microgel. *Polymer* 51: 2668-2675.
- [93] Nalam PC, Lee HS, Bhatt N et al (2017) Nanomechanics of pH-Responsive, Drug-Loaded, Bilayered Polymer Grafts. *ACS Appl. Mater. Inter.* 9: 12936-12948.
- [94] Behbahani M, Bide Y, Bagheri S et al (2016) A pH responsive nanogel composed of magnetite, silica and poly (4-vinylpyridine) for extraction of Cd (II), Cu (II), Ni (II) and Pb (II). *Microchim. Acta* 183: 111-121.
- [95] Cha R, He Z, Ni Y (2012) Preparation and characterization of thermal/pH-sensitive hydrogel from carboxylated nanocrystalline cellulose. *Carbohydr. Polym.* 88: 713-718.
- [96] Kim S, Healy KE (2003) Synthesis and Characterization of Injectable Poly (N-isopropylacrylamide-co-acrylic acid) Hydrogels with Proteolytically Degradable Cross-Links. *Biomacromolecules* 4: 1214-1223.
- [97] Ekici S (2011) Intelligent poly(N-isopropylacrylamide)-carboxymethyl cellulose full interpenetrating polymeric networks for protein adsorption studies. *J. Mater. Sci.* 46: 2843-2850.
- [98] Wang Y, Lai C, Hu H et al (2015) Temperature-responsive nanofibers for controllable oil/water separation. *RSC Adv.* 5: 51078-51085.
- [99] Hakalahti M, Mautner A, Johansson LS et al (2016) Direct Interfacial Modification of Nanocellulose Films for Thermoresponsive Membrane Templates. *ACS Appl. Mater. Inter.* 8: 2923-2927.
- [100] Barros SC, Silva AA, Costa DB et al (2015) Thermal-mechanical behaviour of chitosan-cellulose derivative thermoreversible hydrogel films. *Cellulose* 22: 1911-1929.

[101] Yadollahi M, Gholamali I, Namazi H et al (2015) Synthesis and characterization of antibacterial carboxymethyl cellulose/ZnO nanocomposite hydrogels. *Int. J. Biol. Macromol.* 74: 136-141.

[102] Kanazawa R, Yoshida T, Gotoh T et al (2004) Preparation of molecular imprinted thermosensitive gel adsorbents and adsorption/desorption properties of heavy metal ions by temperature swing. *J. Chem. Eng. JPN* 37: 59-66.

[103] Kanazawa R, Mori K, Tokuyama H et al (2004). Preparation of thermosensitive microgel adsorbent for quick adsorption of heavy metal ions by a temperature change. *J. Chem. Eng. JPN* 37: 804-807.

[104] Karakasyan C, Lack S, Brunel F et al (2008) Synthesis and rheological properties of responsive thickeners based on polysaccharide architectures. *Biomacromolecules* 9: 2419-2429.

## **Chapter 2 Maleic anhydride-modified cellulose fibres/diatomite adsorbents for dye removal<sup>1</sup>**

### **ABSTRACT**

An adsorbent consisting of the maleic anhydride-modified cellulose beads combined with alkali-treated diatomite (MCDBs) was prepared in an attempt to remove basic dyes. An appropriate amount of calcium carbonate was added during the formation of MCDBs to increase pore structure under an acidic condition. The synthesized MCDBs were characterized with FT-IR, TGA and BET. The degree of carboxylation of MCDBs was quantified using a polyelectrolyte titration method. The removal of basic dyes such as methylene blue (MB) and methyl violet (MV) from aqueous solution were systematically investigated. The influence of pH, shaking time, and temperature on the removal process was identified. The results indicated that the MCDBs had a strong adsorption capacity toward basic dyes. The adsorption capacity increased from 51.6 to 116.6 mg/g for methylene blue, depending on the initial concentration of the dye. A similar trend was also found for methyl violet, i.e., adsorption increased from 30.5 to 61.1mg/g. The experimental data fitted two kinetic models; the results demonstrated that the adsorption of MB and MV onto the MCDBs fit the pseudo-second order model very well. The removal efficiencies of the basic dyes under the optimal conditions were up to 97.5%. The adsorption data was also fitted using Langmuir, Freundlich and Temkin isotherms, respectively. It was found that the adsorption process for basic dyes was

---

<sup>1</sup> This chapter has been published on Journal of Materials Science, the format follows the requirements of Journal. “Yuan Li, Mindong Chen, Huining Xiao, Zhaoping Song, Yi Zhao. Adsorbents based on maleic anhydride-modified cellulose fibres/diatomite for dye removal. Journal of Materials Science (2014), 49: 6696-6704.”

better described by the Langmuir isotherm model.

**Keywords:** Green absorbents, Cellulose beads, Diatomite, Dye removal, Adsorption

## 2.1 Introduction

Environmental pollution control is a major theme of scientific research in recent years. There are increasingly environmental problems caused by economic development, especially those related to aquatic environments [1]. Water pollution mainly includes organic pollutants and heavy metals. Dyes, as organic pollutant, form a major class of environmental contaminant. Basic dyes are the most problematic classes of dye. Basic dyes are found in wastewater from various industries, especially textile [2], tanning, and leather [3]. The complex aromatic molecular structures and xenobiotic properties of dyes make them difficult to degrade [4].

A variety of adsorbent materials have been researched for dye removal from aqueous solutions. Of all the adsorbent materials, activated carbon, which has good capacity of removing pollutants, is the one widely used [5]. A successful adsorbent must possess advantages, such as low cost and high capacity of adsorption. Compared with other adsorbents, the main shortcomings of activated carbon are the high cost involved in sample preparation and difficulty for regeneration [6]. Therefore, natural adsorbents for dye removal are the hotspot of research because of their low price and easy regeneration. In recent years, modified cellulose and diatomite have been investigated widely. Cellulose, which constitutes the most abundant natural polymer resource, is a cost-effective and green material. The hydroxyls in cellulose, primary hydroxyl in cellulose unit, are reactive and can be easily modified via various reactions, such as esterification,

halogenation, oxidation, and etherification [7]. Wang et al. modified cellulose from flax shive by quaternary ammonium groups to facilitate removal of C.I. Reactive Red 228 (RR228) dye from aqueous media [8]. Silva et al. modified cellulose with aminoethanethiol to remove red reactive anionic dye in an aqueous medium [9]. Nada et al. modified bagasse fibers using three different chemical methods to adsorb heavy metal ions [10]. However, limited research has been reported on the combination of modified fibres with porous fillers, such as diatomite.

Diatomite, a low cost and commercially available material, has unique advantages as an adsorbent, such as high permeability, high porosity, small particle size, and large surface area [11]. Al-Qodah et al. have treated diatomite with acid and heat to improve its performance to absorb methylene blue [12]. Lin et al. modified the diatomite, fly ash, and bentonite by heat or acid treatment to remove dyes from colored wastewater [13]. However, few of these materials have been combined with green-based cellulose fibres. The key objective of this work was to study cost-effective and renewable cellulose fibre beads in conjunction with alkali-treated diatomite, thus leading to a range of adsorbents which could remove the dyes from aqueous solutions effectively and be re-generated readily. The modified fibers with proper pore structures and functional groups on the surfaces not only act as supports for diatomite but also generate the synergetic effect with diatomite for dye adsorption. To enhance the absorption capacity of fibres, the fibres were dissolved and regenerated in the presence of maleic anhydride. Calcium carbonate was added during the formation of CDBs to increase pore structure under an acidic condition. The effect of reaction conditions, such as pH and temperature, on the adsorptive capacity of the modified cellulose ball was investigated. Methylene blue and

methyl violet were used as model dyes for revealing adsorption behaviors, including kinetics and adsorption isotherm.

## **2.2 Experimental**

### **2.2.1 Materials**

The cellulose used in this study was from filter paper (Qualitative P4, porosity: Medium – Fine; Flow Rate: Slow, Fisher Scientific). The diatomite, CaCO<sub>3</sub> powder ( $\leq 30 \mu\text{m}$ ), maleic anhydride, and urea, all purchased from Sigma-Aldrich, were of laboratory reagent grade and used without further purification. Two basic dyes, including methylene blue and methyl violet, and NaOH were purchased from Fisher Scientific as well.

### **2.2.2 Preparation of cellulose/diatomite beads (CDBs)**

The diatomite with a size smaller than 150 mesh was collected, washed three times with distilled water to remove impurities, and then dried in an oven at 100 °C for 10h. A strong base (NaOH 5M) was used to carry out the chemical treatment of the diatomite. Specifically, diatomite was mixed with NaOH at a solid (g)/liquid (mL) ratio of 15%, then stirred at 100 °C for 2 h and filtered. The resulting samples were washed with distilled water several times and dried in an oven at 100 °C for 10 h. Scanning electron micrographs (JEOL JSM-6400 SEM instrument, Japan) of alkali-treated diatomite are presented in Figure.2.1.

Filter paper (2g) was dissolved into NaOH (7 wt %) /Urea (12 wt %) at -10 °C and dispersed using a homogenizer (Stanfen, Germany). The concentration of cellulose

solution was 4 %. Then, a certain amount of treated diatomite (2g) and  $\text{CaCO}_3$  with different weight ratios were added. The mixtures were dropped into an acidic solution (1 M HCl) using a syringe after being dispersed using a homogenizer. The reaction between  $\text{CaCO}_3$  and HCl happens immediately and the  $\text{CO}_2$  released from the reaction promote the formation of the pore structure of fibre matrix. The cellulose/diatomite beads (CDBs) were then immersed in distilled water for 24 h to dissolve  $\text{CaCl}_2$  and transferred into acetone immediately. After 24 h, the CDBs were put into vacuum oven at 50 °C for 10h (Figure.2.1).

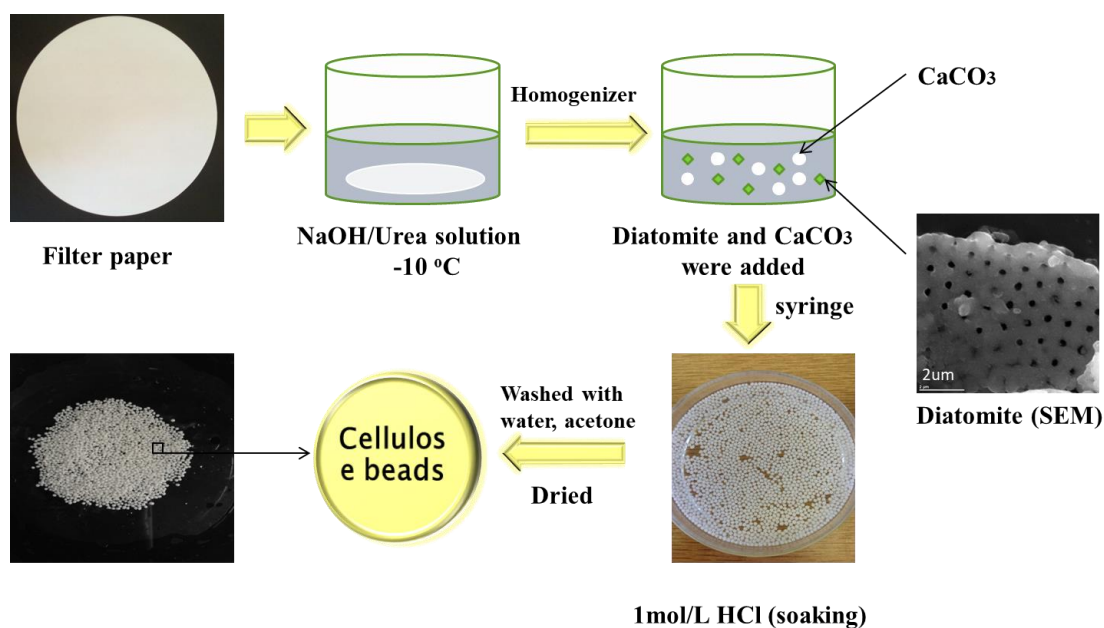


Figure.2.1 The preparation of CDBs.

### 2.2.3 Modification of CDBs

The cellulose/diatomite beads (2g) were treated with maleic anhydride (2g) dissolved in acetone (2g in 20 mL acetone) at room temperature for 1 h. After the treatment, the acetone was removed by the evaporation at 50 °C in vacuum oven for 1h. And then the

residual mixtures were heated in a vacuum oven at 100 °C for 3 h. After that, the resulting products (CDBs absorbents) were washed with distilled water, ethanol, and finally with acetone, then dried in a vacuum oven at 50 °C for 10h [10].

#### 2.2.4 Sample characterization

The chemical structure of CDBs and MCDBs was characterized with FT-IR (NEXUS 470 spectrophotometer, Nicolet Thermo Instruments, Canada) after being grinded with KBr. The BET adsorption was performed using an autosorb instrument (Belsorp-Max BEL Inc, Osaka, Japan). The specific surface areas and pore sizes were measured based on the N<sub>2</sub> gas adsorption isotherms of samples. The TGA curves were obtained using an instrument (Q600, TA Instruments, USA) in the temperature range from 25 to 600°C at a heating rate of 10 °C min<sup>-1</sup> under nitrogen flow.

The degree of the substitution of hydroxyl groups on cellulose with the carboxyl group of MCDBs was obtained using a titration method [14]. According to this method, 0.05g of MCDBs was added to 0.01N of HCl solution (15mL) in a round bottom flask at room temperature with constant stirring for 10 min. Then the NaOH (0.01N) was dropped into the mixture from a basic burette. The conductivity was measured using a digital conductivity meter (A22828, VWR international, USA). The experiment was conducted three times simultaneously. The concentration of carboxylic functions [ $C_{COOH}$  (mmol g<sup>-1</sup>)] was calculated based on Eq 2.1.

$$C_{COOH} = (V_2 - V_1) / m_{CDBs} \quad \text{Eq 2.1}$$

where  $V_2$  is the inflection point of conductivity increased (mL),  $V_1$  is the inflection point of conductivity unchanged (mL),  $m_{CDBs}$  is the mass of MCDBs (g).

Adsorption studies were carried out by soaking a certain amount (0.01g) of absorbents in 10mL of dye and shaking at 130rpm using a temperature-controlled shaker (SWB25, Thermo Electron Corporation, Germany). The comparative experiment between MCDBs and other materials was accomplished. The shaking time, temperature, pH, and the concentration of CaCO<sub>3</sub> were investigated, respectively. The concentration of the dye solution after filtration was measured with UV (Genesys 10-s, Thermo Electron Corporation) at 664nm (MB) and 590nm (MV), respectively [15]. The adsorption capacity (Q) and the fraction of removal R were calculated by Eq 2.2 and Eq 2.3:

$$Q = (C_0 - C_e) / m \times v \quad \text{Eq 2.2}$$

$$R = (C_0 - C_e) / C_0 \times 100 \quad \text{Eq 2.3}$$

where Q is the adsorption of the dye (mg/g), C<sub>0</sub> (mg/L) is the initial concentration of dye, C<sub>e</sub> (mg/L) is the equilibrium concentration of dye, m is the mass of absorbent (g), and V (L) is the volume of dye solution, respectively.

The desorption studies were carried out by soaking a certain amount (0.01g) of absorbents after adsorption in 10mL of HCl (1mol L<sup>-1</sup>) for 24h. After that, the absorbents were washed by distilled water and acetone, and then dried in a vacuum oven at 50 °C for 10h, then measured the adsorption capacity of MCDBs.

## 2.3 Results and discussion

### 2.3.1 FT-IR spectroscopy

The FTIR spectra of CDBs and MCDBs are presented in Figure.2.2. A strong adsorption at 3443 and 3446 cm<sup>-1</sup> is due to stretching of O-H group, and the peaks at 2901 and 2899 cm<sup>-1</sup> are related to the C-H stretching from cellulose. The most change observed

between CDBs and MCDBs is the appearance of bands at 1723 and 1632  $\text{cm}^{-1}$ . The adsorption band at 1723  $\text{cm}^{-1}$  corresponds to the carboxyl groups (C=O) and the one at 1632  $\text{cm}^{-1}$  relates to vibration of vinyl groups (C=C) [16]. The sharp peak at 1109  $\text{cm}^{-1}$  is mainly due to siloxane (Si–O–Si) stretching from alkali-treated diatomite and C–O stretching in cellulose [17]. Therefore, the maleic anhydride was grafted onto the cellulose surface successfully because of the presence of adsorption peaks from carboxyl and vinyl groups.

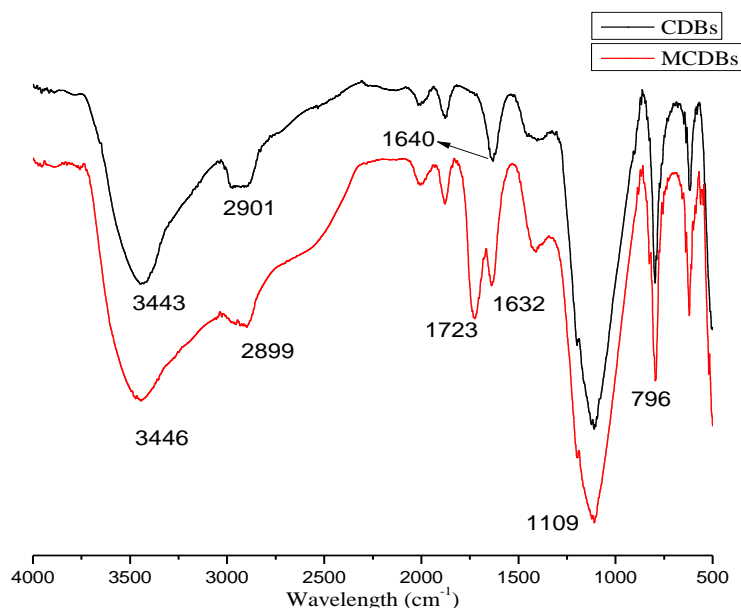


**Figure.2.2 FT-IR spectra for CDBs and MCDBs.**

### 2.3.2 TGA

TGA is an important tool for identifying the thermal stability of materials and can also provide that the reaction was successful. The TGA curves of CDBs and MCDBs are presented in Figure.2.3. The mass of diatomite remains unchanged with temperatures from 25 to 600°C. For CDBs, the total mass loss of 41% over the temperature range

between 290 and 374 °C corresponds to the major thermal degradation of cellulose fibers [18]. The MCDBs decomposition occurs in three events: the first mass loss of MCDBs in the TGA curve was attributed to a significant amount of water released from the MCDBs starting at 50°C; the second decomposition event occurred at around 140°C in the DTA curves, which may be due to the initial stage of thermal degradation; the third mass loss happened at temperatures higher than 290 °C, reflecting the major thermal degradation or thermal cleavage of cellulose fibers, which corresponded to an endothermic peak in the DTA curve around 350 °C [19].

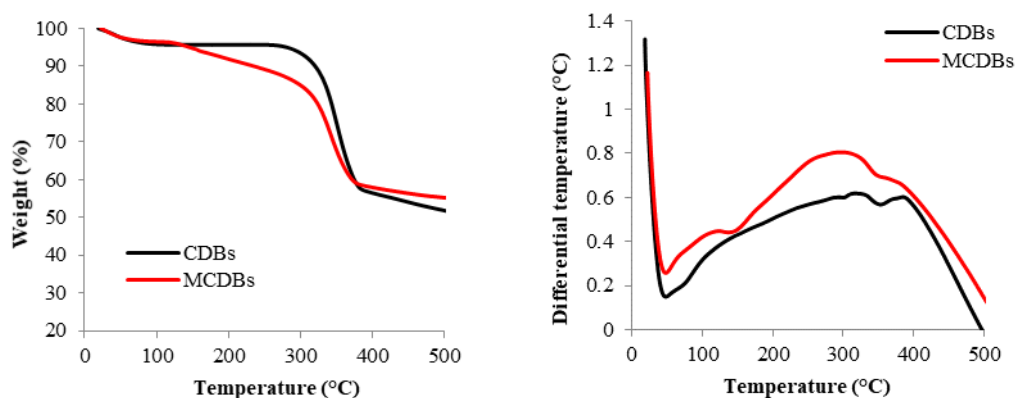


**Figure.2.3 TGA and DTA curves of the CDBs and MCDBs.**

### **2.3.3 Brunauer–Emmett–Teller (BET) adsorption**

From the data of BET, the specific surface area of CDBs increased from 1.00 m<sup>2</sup>/g to 1.53m<sup>2</sup>/g and the total pore volume was changed from 5.78 ×10<sup>-3</sup> to 9.42 ×10<sup>-3</sup> m<sup>3</sup>/g as the concentration of CaCO<sub>3</sub> increased from 10% to 30%. The specific surface area of CDBs (30% CaCO<sub>3</sub>) was changed from 1.53m<sup>2</sup>/g to 0.73 m<sup>2</sup>/g after modification with maleic anhydride. Meanwhile, the total pore volume changed from 9.42 ×10<sup>-3</sup> to

$4.89 \times 10^{-3} \text{ m}^3/\text{g}$ , implying the grafted maleic anhydride might fill up some pores. However, the adsorption capacity of the CDBs increased significantly after the modification with maleic anhydride due to the enhanced surface reactivity towards the adsorption. Therefore, the application of  $\text{CaCO}_3$  was conducive to the pore structure and the esterification was the main reason to increase the adsorption capacity of dye onto CDBs.

#### **2.3.4 Comparative experiment**

The dye removal capacity of various materials including filter paper, alkali-treated diatomite, CDBs, and MCDBs was studied at room temperature and neutral pH. The CDBs were prepared by filter paper and alkali-treated diatomite with a certain concentration of  $\text{CaCO}_3$ . The adsorption capacity of initial materials, such as filter paper and alkali-treated diatomite, is extremely low, which correspond to 1 and 2 in Figure.2.4. The CDBs has a higher fraction of removal compared to 1 and 2. Furthermore, after modified by maleic anhydride, the adsorption capacity of dye (MB and MV) increased immediately. The MCDBs showed the highest removal capacity, and the fraction of removal of MB and MV is 97.11% and 93.17%, respectively.

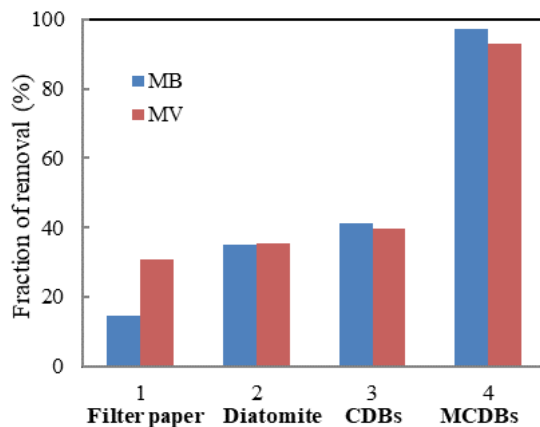


**Figure.2.4 Fraction of emoval of different materials: 1-filter paper; 2-alkali-treated diatomite; 3-CDBs; 4-MCDBs.**

### **2.3.5 Effects of the concentration of initial $\text{CaCO}_3$**

The effect of initial concentration of  $\text{CaCO}_3$  in the preparation of CDBs was studied at room temperature and neutral pH. As was shown in Figure.2.5, with the initial concentration of  $\text{CaCO}_3$  increased from 0 % to 30 %, the adsorption capacity of dye (MB and MV) increased. However, when further increasing the concentration of  $\text{CaCO}_3$  to 40 %, the capacity of dye removal was negatively affected. This result can be explained in terms of the function of  $\text{CaCO}_3$ . The key role played by  $\text{CaCO}_3$  is to create the pore structure by releasing  $\text{CO}_2$  at an acidic condition. The adsorption capacity increases with the increase in pore volume, which has been proved by the results of BET. However, the  $\text{CaCO}_3$  at over-dosage could induce the collapse of CDB pores, thus lowering adsorption capacity. The optimum concentration of  $\text{CaCO}_3$  was 30 %.

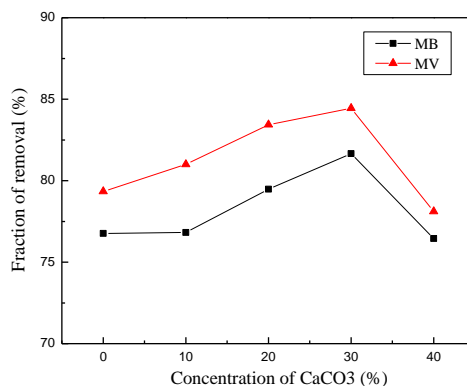


**Figure.2.5** Effects of CaCO<sub>3</sub> on adsorption of MB and MV (natural pH, room temperature and 2h).

### 2.3.6 Effects of pH on dye absorption

The effect of pH on dye absorption is shown in Figure.2.6. In general, pH will affect the degree of ionization and the surface charge of the MCDBs. As can be seen from Figure.2.6, the removal of dye from aqueous solutions is highly dependent on the pH of the solution. The Fraction of removal of dye is relatively low at a pH below is 3. The high concentration of H<sub>3</sub>O<sup>+</sup> at a low pH tends to reduce the active surface sites for dye adsorption [20]. The H<sub>3</sub>O<sup>+</sup> concentration was reduced at a high pH, so that the adsorbents became highly negative-charged. As a result, the dye removal was increased because of the electrostatic interaction. Furthermore, the amount of carboxylic acid groups on MCDBs would be reduced in basic condition when pH>7, resulting in a decrease in adsorption capacity. Overall, the optimum pH values for MB and MV removal were 7.0 and 6.5, respectively.

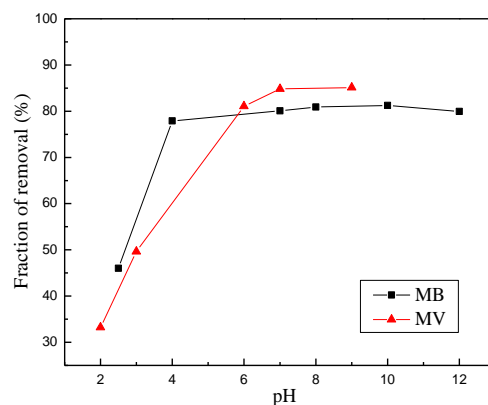


**Figure.2.6 Effects of pH on adsorption of dye (room temperature and 2h).**

### **2.3.7 Effects of temperature on adsorption**

The removal of dyes was studied at different temperatures under the optimum pH for adsorption in 2h, the results are presented in Figure.2.7. The adsorption of methyl violet changed significantly as the temperature increased from 20 to 30 °C, which indicates that the adsorption process of dye on MCDBs is an endothermic process, but leveled off after 30 °C. However, the adsorption capacity of methylene Blue was relatively stable regardless of temperature. Of all the experiments, the optimum temperature for MB and MV is 30 °C.

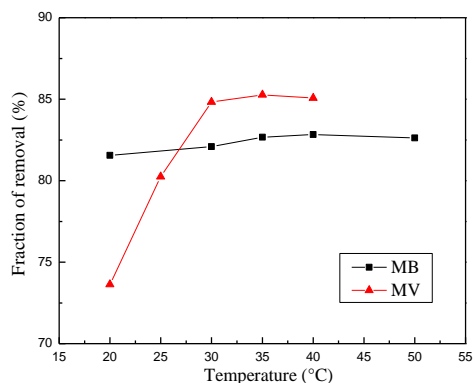


**Figure.2.7 Effects of temperature (for MB: pH 7.0, time 2h and for MV: pH 6.5, time 2h).**

### 2.3.8 Influence of shaking time on dye adsorption

The effects of adsorption time onto MCDBs are shown in Figure.2.8. Initially, the fraction of removal of dye increased rapidly with the shaking time changed from 0 to 300 min (MB) and 0 to 200 min (MV), then, the fraction of removal leveled off. Therefore, the optimum shaking times were around 300 min for MB and 200 min for MV; and the corresponding fraction of removal was 97.49 % and 93.23 %, respectively.

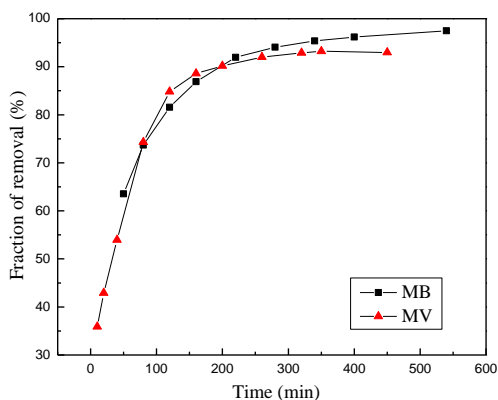


**Figure.2.8 Effects of contact time (for MB: pH 7.0, temperature 30 °C and for MV: pH 6.5, temperature 30 °C).**

### 2.3.9 Adsorption kinetics

There are two kinetic models for adsorption kinetics: Pseudo-first-order kinetics and Pseudo-second-order kinetics. Non-linear form and linear form are presented in Eq 2.4 and Eq 2.5, respectively [21].

$$d_q / d_t = k_1 (q_e - q) \quad \text{Eq 2.4}$$

$$q = q_e (1 - e^{-k_1 t}) \quad \text{Eq 2.5}$$

where  $q_t$  and  $q_e$  are the amounts of the dye adsorbed at any time  $t$  and at equilibrium ( $\text{mg g}^{-1}$ ), respectively.  $k_1$  is the rate constant for the adsorption ( $\text{g mg}^{-1} \text{min}^{-1}$ ). The value of  $R^2$  is carried out by the linear form Eq 2.6.

$$\ln (q_e - q) = \ln q_e - k_1 t \quad \text{Eq 2.6}$$

The initial and linear form of Pseudo-second-order kinetics is Eq 2.7 and Eq 2.8.

$$d_q / d_t = k_2 (q_e - q)^2 \quad \text{Eq 2.7}$$

$$t / q_t = 1 / k_2 q_e^2 + t / q_e \quad \text{Eq 2.8}$$

where  $k_2$  ( $\text{dm}^3 \text{mg}^{-1} \text{min}^{-1}$ ) is the constant rate of the adsorption process. The results of adsorption kinetics, calculated from Figure.2.8, are shown in Table.2.1 and Figure.2.9.

**Table.2.1 Adsorption kinetics of dyes**

Adsorbate	Kinetics model	$q_e$ ( $\text{mg g}^{-1}$ )	$K_1$ ( $\text{g mg}^{-1} \text{min}^{-1}$ )	$K_2$ ( $\text{g mg}^{-1} \text{min}^{-1}$ )	$R^2$
Methylene blue	Pseudo-first-order	8.77	$5.31 \times 10^{-2}$	-	0.9362
	Pseudo-second-order	19.84	-	$1.90 \times 10^{-3}$	0.9994
Methyl violet	Pseudo-first-order	1.18	$2.27 \times 10^{-2}$	-	0.8831
	Pseudo-second-order	9.87	-	$3.90 \times 10^{-3}$	0.9983

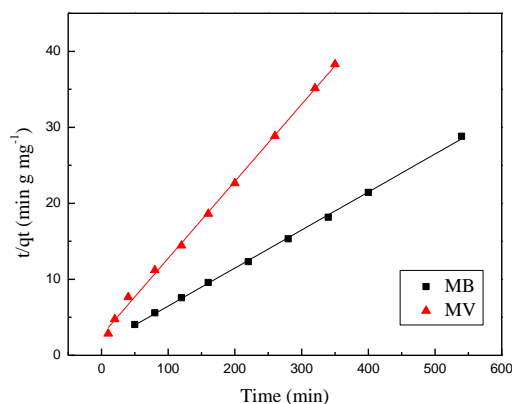


**Figure.2.9 Pseudo-second-order adsorption kinetics on MCDBs adsorbent**

As can be seen from Table.2.1, the adsorption process for basic dyes was better described by Pseudo-second-model, where the  $R^2$  for MB and MV are 0.9993 and 0.9985, respectively. The fitting results suggested that the adsorption rate was dominated by chemical adsorption, which involved the electron sharing or electron transfer between the adsorbent and the adsorbate [29]. In other words, the adsorption of MB and MV dominated with chemical adsorption.

### 2.3.10 Adsorption isotherm

The adsorption isotherm can be described as the equilibrium relationship between the adsorbate concentration in the liquid phase and on the adsorbent surface during specific conditions. There are many adsorption isotherms in the adsorption process. In this study, Langmuir, Freundlich, and Temkin isotherm models were chosen to describe the equilibrium data.

Langmuir isotherm model (Eq 2.9 and Eq 2.10) [22]:

$$q_e = (Q_{max}aC_e) / (1 + aC_e) \quad \text{Eq 2.9}$$

$$C_e/q_e = C_e/Q_{max} + 1/(Q_{max}a) \quad \text{Eq 2.10}$$

where  $Q_{max}$  ( $\text{mg g}^{-1}$ ) is the maximum adsorption capacity and  $a$  ( $\text{L mg}^{-1}$ ) is isotherm constant.  $C_e$  ( $\text{mg L}^{-1}$ ) and  $q_e$  ( $\text{mg g}^{-1}$ ) are the concentration and adsorption capacity at the equilibrium, respectively.

Freundlich isotherm model (Eq 2.11 and Eq 2.12) [23]:

$$q_e = K_f C_e^{1/n} \quad \text{Eq 2.11}$$

$$\ln q_e = \ln K_f + \ln C_e/n \quad \text{Eq 2.12}$$

where  $q_e$  and  $C_e$  are noted previously.  $K_f$  is roughly an indicator of adsorption capacity and  $n$  is adsorption intensity.

Temkin isotherm model and its linear form were represented with Eq 2.13 and Eq 2.14 [24].

$$q_e = RT/b_T (\ln A + \ln C_e) \quad \text{Eq 2.13}$$

$$q_e = RT/b_T \ln(AC_e) \quad \text{Eq 2.14}$$

where  $C_e$  and  $q_e$  are noted previously,  $A$  ( $\text{L mg}^{-1}$ ) and  $b_T$  ( $\text{J mol}^{-1}$ ) are the Temkin constants,  $T$  is the absolute temperature, and  $R$  is the universal gas constant  $8.314 \text{ J mol}^{-1} \text{ K}^{-1}$ .

The results of adsorption isotherm are calculated from three models and shown in Table.2.2 and Figure.2.10.

**Table.2.2 The isotherm models for adsorption**

Adsorbate	Isotherm models	$Q_{max}$	a	$K_f$	n	A	$b_T$	$R^2$
Methylene blue	Langmuir	117.65	0.0648	-	-	-	-	0.9982
	Freundlich	-	-	38.93	5.5679	-	-	0.9603
	Temkin	-	-	-	-	5.52	169.36	0.9878
Methyl violet	Langmuir	62.11	0.0573	-	-	-	-	0.9970
	Freundlich	-	-	24.28	6.6400	-	-	0.8552
	Temkin	-	-	-	-	17.59	369.63	0.8821

As can be seen from Table.2.2, the adsorption of dye onto MCDBs can be described by several isotherm models, and the Langmuir isotherm is the best fitting one. The  $R^2$  for MB and MV by using the Langmuir isotherm are 0.9982 and 0.9970, respectively. The definition of Langmuir isotherm is monolayer sorption where all of the adsorption sites are the same and the absorbed particles are totally independent; therefore, no further sorption can take place after a saturation value is reached [25]. The Langmuir constant is related to Gibbs free energy ( $\Delta G^0$ ) of sorption reaction as  $\Delta G^0 = -RT \ln a$ . Where T is absolute temperature and R is the gas constant. In this study, the value of a for MB and MV are 0.0648 and 0.0537 L/mg, respectively, the  $\Delta G^0$  for MB and MV are -10.4 kJ/mol and -10.1 kJ/mol, respectively. The negative value of the Gibbs free energy indicates that the process is feasibility and the adsorption is spontaneous. Thus, the sorption system is favorable [26]. The maximum monolayer capacity ( $Q_{max}$ ) for MB and MV were obtained at 117.65 and 62.11 mg g<sup>-1</sup>, respectively. Monolayer adsorption capacities for adsorption of dyes onto MCDBs and other materials are compared in Table.2.3.

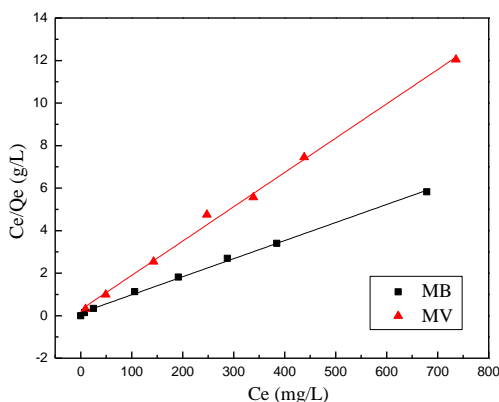


**Figure.2.10 Linear plots of Langmuir isotherm for adsorption on MCDBs at 30 °C**

The adsorption capacities of MCDBs and other materials are shown in Table.2.3, He et al. investigated the MB removal by carbon monoliths and nanocrystalline cellulose, the maximum adsorption capacity of MB were 127 mg/g and 101mg/g, respectively, which were close to MCDBs. The adsorption capacity of MCDBs is dominate compared to other studies, which indicates that it is potential as an absorbent for dye removal.

**Table.2.3 Results for adsorption of dyes by MCDBs and other materials**

Absorbent materials	Modified chemicals	Adsorption capacity(mg/L)	Reference
MCDBs	Maleic anhydride	MB: 117.65	This work
		MV: 61.11	
Carbon monoliths	N/A	MB: 127	He et al. [26]
Nanocrystalline cellulose		MB: 101	
Cellulose acetate	Titanium dioxide	MB: 54.38	Andrea et al. [27]
Banana peels	N/A	MB: 20.8	Annadurai et al. [28]
Orange peels		MB: 18.6	

### **2.3.11 Desorption of MB and MV from MCDBs**

The regenerated adsorbents were reused three times, the removal efficiencies under the optimal conditions were 97.1%, 88.3%, and 83.4% for MB and 93.4%, 92.6%, and 87.9%, respectively.

## **2.4 Conclusions**

A novel adsorbent consisting of the maleic anhydride-modified cellulose beads and alkali-treated diatomite (MCDBs) was successfully prepared. The dye removal efficiency was high under alkaline condition ( $\text{pH} > 6$ ) as the adsorbent had a negative-charge, thus, increasing its affinity to the cationic dye ion. This adsorbent was a cost-effective and renewable cellulose fibre beads. The dynamic and equilibrium data of adsorption fitted well with the Pseudo-second-model and the Langmuir isotherm equation, demonstrating that the adsorption process of dye is monolayer sorption and dominated by the chemical adsorption.

## 2.5 References

- [1] Zhou YM, Jin Q, Hu XY et al (2012) Heavy metal ions and organic dyes removal from water by cellulose modified with maleic anhydride, *J Mater Sci* 47: 5019-5029.
- [2] El Qada EN, Allen SJ, Walker GM (2008) Adsorption of basic dyes from aqueous solution onto activated carbons, *Chem Eng J* 135: 174-184.
- [3] Edson LF, Suellen B, Marcio AM et al (2013) Adsorption of a leather dye on mesoporous struvite obtained from swine wastewater, *Chem Eng Commun* 200: 1027-1038.
- [4] Parida KM, Sahu S, Reddy KH et al (2011) A Kinetic, Thermodynamic, and mechanistic approach toward adsorption of methylene blue over water-washed manganese nodule leached residues, *Ind Eng Chem Res* 50: 843-848.
- [5] Walker GM and Weatherley LR (1998) Fixed bed adsorption of acid dyes onto activated carbon, *Environ Pollut* 99: 133-136.
- [6] Han R, Ding D, Xu Y, Zou W et al (2008) Use of rice husk for the adsorption of congo red from aqueous solution in column mode, *Bioresour Technol* 99: 2938-2946.
- [7] David WO, Colin B, Thomas FO (2008) Heavy metal adsorbents prepared from the modification of cellulose: A review, *Bioresour Technol* 99: 6709-6724.
- [8] Wang LJ and Li J (2013) Adsorption of C.I. Reactive Red 228 dye from aqueous solution by modified cellulose from flax shive: kinetics, equilibrium, and thermodynamics, *Ind Crop Prod* 42: 153-158.
- [9] Lucinaldo SS, Luciano CBL, Fabricia CS et al (2013) Dye anionic sorption in aqueous solution onto a cellulose surface chemically modified with aminoethanethiol, *Chem Eng J* 218: 89-98.
- [10] Nada AM and Hassan ML (2006) Ion exchange properties of carboxylated bagasse, *J Appl Polym Sci* 102: 1399-1404.
- [11] Al-Ghouti MA, Khraisheh MAM, Allen SJ et al (2003) The removal of dyes from textile wastewater: a study of the physical characteristics and adsorption mechanisms of diatomaceous earth, *Environ Manage* 69: 229-238.
- [12] Al-Qodah Z, Lafi WK, Al-Anber Z et al (2007) Adsorption of methylene blue by acid and heat treated diatomaceous silica, *Desalination* 217: 212-224.
- [13] Lin JX, Zhan SL, Fang MH et al (2006) Modification of three types of absorbents and comparative study on their dye absorption capability, *ZJU Eng Sci* 40: 2031-2036.

- [14] Zhang K, Steffen F, Andreas G et al (2012) Analysis of carboxylate groups in oxidized never-dried cellulose II catalyzed by TEMPO and 4-acetamide-TEMPO, *Carbohydr Polym* 87: 894-900.
- [15] Gulay B, Begum A, Arica MY (2009) Adsorption kinetics and thermodynamic parameters of cationic dyes from aqueous solutions by using a new strong cation-exchange resin, *Chem Eng J* 152: 339-346.
- [16] Zhang W, Li C, Liang M et al (2010) Preparation of carboxylate-functionalized cellulose via solvent-free mechanochemistry and its characterization as a biosorbent for removal of Pb<sup>2+</sup> from aqueous solution, *J Hazard Mater* 181: 468-473.
- [17] Al-Degs Y, Khraisheh MA, Tutunji MF (2001) Sorption of lead ions on diatomite and manganese oxides modified diatomite, *Water Res* 35: 3724-3728.
- [18] Ma S, Yu SJ, Wang ZH et al (2013) Ultrasound-assisted modification of beet pulp cellulose with phthalic anhydride in ionic liquid, *Cellulose Chem Technol* 47: 527-533.
- [19] Aly AS, Sokker HH, Hashem A et al (2005) Preparation of cellulosic membrane containing pyrrolidone moiety via radiation induced grafting and its application in wastewater treatment, *American J Appl Sci* 2: 89-98.
- [20] Haluk A, Yasemin B, Cigdem Y (2008) Removal of Copper(II) from aqueous solution by adsorption onto low-cost adsorbents, *J Environ Manage* 87: 37-45.
- [21] Neelesh BS and Giridhar M (2013) Adsorption of anionic dyes on a reversibly swelling cationic superabsorbent polymer, *J Appl Polym Sci* 127: 2251-2258.
- [22] Irving Langmuir (1918) The adsorption of gases on plane surfaces of glass, mica and platinum, *JACS* 40: 1361-1403.
- [23] Iman K, Paul GP, Nadia GK et al (2012) New hydrogels based on symmetrical aromatic anhydrides: Synthesis, characterization and metal ion adsorption evaluation, *Carbohydr Polym* 87: 881-893.
- [24] Chen Z, Ma W, Han M (2008) Biosorption of nickel and copper onto treated alga (*undaria pinnatifida*): Application of isotherm and kinetic models, *J Hazard Mater* 155: 327-333.
- [25] Popuri SR, Jammala A, Reddy KVN et al (2007) Biosorption of hexavalent chromium using tamarind (*Tamarindus indica*) fruit shell-A comparative study, *Electron J Biotechnol* 10: 358-367.
- [26] He XY, Male KB, Nesterenko PN et al (2013) Adsorption and Desorption of Methylene Blue on Porous Carbon Monoliths and Nanocrystalline Cellulose, *Appl Mater inter* 5: 8796-8804.

[27] Andrea AH, Silvio LPD, Jordana RR et al (2008) Methylene Blue Immobilized on Cellulose Acetate with Titanium Dioxide: an Application as Sensor for Ascorbic Acid, J Braz Chem Soc 19: 943-949.

[28] Annadurai G, Juang RS, Lee DJ (2002) Use of cellulose-based wastes for adsorption of dyes from aqueous solutions, J Hazard Mater 92: 263-274.

[29] Wang H, Zhao A, Wang Y et al (2007) Mechanism study on adsorption of acidified multi-walled carbon nanotubes to Pb(II), J. Colloid Interface Sci 316: 277-283.

## Chapter 3 The cellulose-based hybrid beads for adsorption of lead ions in aqueous solutions<sup>2</sup>

### ABSTRACT

The adsorption of  $\text{Pb}^{2+}$  onto maleic anhydride modified cellulose/diatomite beads (MCDBs) was investigated. Instead of the general process for esterifying the cellulose beads, a solvent free synthesis which needs no catalyst or solvent was used. An appropriate amount of calcium carbonate was added during the formation of MCDBs to increase pore structure after being removed under an acidic condition. The synthesized adsorbent was characterized by FTIR, SEM, and BET. The degree of carboxyl group of MCDBs was found to be  $0.450 \text{ mmol g}^{-1}$  based on colloid titration. The effects of pH, temperature, contact time, and the concentration of  $\text{Pb}^{2+}$  on adsorption were studied in batch mode. The results indicated that the MCDBs had a good adsorption capacity toward  $\text{Pb}^{2+}$  with the maximum adsorption at  $44 \text{ mg g}^{-1}$ . The experimental kinetic data fit the pseudo-second order model very well. Moreover, the adsorption process for  $\text{Pb}^{2+}$  was better described by the Langmuir isotherm model. The regeneration of the MCDBs could be readily accomplished using HCl (1M) treatment without lowering adsorption capacity significantly.

**Keywords:** Lead ions, Hybrid beads, Adsorption

---

<sup>2</sup> This chapter has been published on RSC Advances, the format follows the requirements of the Journal. The entire experimental work was performed by candidate Yuan Li along with the preparation of manuscript. “Yuan Li, Mindong Chen, Xia Wan, Lu Zhang, Xu Wang, Huining Xiao. Solvent-free synthesis of the cellulose-based hybrid beads for adsorption of lead ions in aqueous solutions. RSC Advances (2017), 7: 53899-53906.”

### **3.1 Introduction**

Paper Environmental problems, especially aquatic environments, are main theme of scientific research in recent years. The removal of toxic heavy metal ions from industrial effluents, water supplies, and mine waters has received much attention. Heavy metal ions, such as Cu, Cd, Ni, and Pb, released into the environment, affect ecological life, owing to their tendency to accumulate in living organisms, and are highly toxic when absorbed into the body. [1] Heavy metals usually have a long residence times. Lead toxicity has been reported to decrease kidney functions and enzymatic activities and cause neuromuscular difficulties. [2] There are also many lead contamination incidents about drinking water reported in some countries. [3] Thus, it is necessary to remove heavy metal ions from wastewater. [4]

Various adsorbent materials have been explored for the removal of heavy metal ions from aqueous solutions. Of all the adsorbent materials, activated carbon has been widely used for the removal of heavy metals at trace levels. [5] However, activated carbon is costly as an adsorbent in water treatment. Therefore, the production of low-cost materials, such as cellulose and diatomite, has been the hotspot of researchers. Cellulose, as one of the natural and green materials, constitutes the most abundant natural polymer resource. However, the adsorption capacity is limited, and the selectivity is low when directly using of natural cellulose as an adsorbent. Because there are many hydroxyl groups on the polymer structure [6] and formation of hydrogen bonds between the molecular chains. [7] Chemical modification, such as esterification, halogenation, oxidation, and etherification, can be used to vary certain properties of cellulose such as

its hydrophilic or hydrophobic character, elasticity, water sorbency, adsorptive or ion exchange capability. [8]

Geay et al. [9] synthesized new adsorbents containing carboxyl groups by grafting acrylic acid onto sawdust, which was used for the sorption of  $\text{Cu}^{2+}$  from aqueous solution. McSweeney et al. [10] milled aspen wood, then, the Milled aspen wood was thermochemically modified with citric acid to improve the copper ( $\text{Cu}^{2+}$ ) ion sorption capacity of the wood. Nada et al. [11] modified bagasse fibers using three different chemical methods to remove heavy metal ions from waste water. Very recently, Wang et al. [12] reported an eco-friendly sugarcane cellulose-based adsorbent with very high sorption capacities towards  $\text{Pb}^{2+}$ ,  $\text{Cu}^{2+}$  and  $\text{Zn}^{2+}$ . The application of such adsorbents was also extended to the binary component systems; and the adsorption behaviour was found to be well described with the competitive Langmuir isotherm model. Zhou et al. [13] synthesized a low-cost adsorbent by a cost-effective chemical modification for dyes and heavy metal ions removal. Yu et al. [14] prepared cellulose nanocrystals (CNCs) from cotton, then the CNCs was chemically modified with succinic anhydride to introduce carboxyl groups on the adsorbents. However, the pyridine reflux was used during the chemical modification, which was not conducive to the development of the environment. Diatomite, a soft lightweight rock available in large deposits around the world, is a highly porous structure and low-cost material. [15] Attributed to its physical and chemical properties, it has been used as an adsorbent in wastewater treatment. [16] Al-Degs et al. [17] improved the intrinsic exchange properties by the modification with manganese oxides; and the resulting adsorbent showed a high tendency for adsorbing lead ions from solution. Khraisheh et al. [18] modified diatomite by NaOH solution and

manganese oxide to improve the adsorption capacity of the diatomite for removal of heavy metals. However, the powdered diatomite and cellulose might lead to the difficulty for the application of the adsorbents. Cellulose-based beads facilitate the easy separation of hybrid adsorbents in batch operation. Yang et al. [19] prepared carboxymethyl cellulose hydrogel beads using epichlorohydrin (ECH) as a crosslinking agent and found that the additional carboxyl groups afforded a higher sorption capacity to metal ions as well. Recently, Yu et al. [20] have successfully prepared porous magnetic cellulose beads via one-pot synthesis, which created a new platform to prepare the cellulose-based functional nanocomposites.

Thus, the aim of the present study was to investigate modified cellulose beads in conjunction with alkali-treated diatomite (MCDBs) as a low-cost material for the removal of Pb ions from aqueous solutions. To enhance the absorption capacity of fibres and to facilitate the recovery of adsorbent, the cellulose fibres were dissolved and regenerated, and then reacted with maleic anhydride. During the formation of adsorbent particles, calcium carbonate was added to further increase the porosity of the adsorbent after being removed under acidic condition. The effects of solution pH, temperature, initial concentration, and contact time during the adsorption processes were also evaluated.

## **3.2 Experimental**

### **3.2.1 Materials**

The cellulose raw material was also from filter paper (Qualitative P4, porosity: Medium-Fine; Flow Rate: Slow, Fisher Scientific). Diatomite, hydroxylamine hydrochloride,

dithizone,  $\text{Pb}(\text{NO}_3)_2$ ,  $\text{CaCO}_3$  powder ( $\leq 30\mu\text{m}$ ), maleic anhydride, and urea, all purchased from Sigma-Aldrich, Canada. NaOH, NaOH (0.01M), HCl (0.01M), ammonium hydroxide, Poly-DADMAC (0.01N) and PVSX solutions (0.01N), were purchased from Fisher Scientific as well. Ammonium citrate tribasic and potassium sodium L-tartrate tetrahydrate were obtained from Alfa Aesar. Standard Pb ( $1.000\text{ g L}^{-1}$ ) solution was prepared by dissolving appropriated amounts of  $\text{Pb}(\text{NO}_3)_2$  in the distilled water.

### **3.2.2 Methods**

#### **3.2.2.1 Preparation of cellulose/diatomite beads (CDBs)**

The diatomite under 150 mesh was washed with distilled water to remove fines and other adhered impurities, and then desiccated. [21] Chemical modification was accomplished by treating the diatomite with NaOH (5 mol/L): 150g diatomite was mixed with 1L NaOH, then stirred at  $100\text{ }^\circ\text{C}$  for 2 h. The resulting samples were washed with distilled water, and desiccated in an oven at  $100\text{ }^\circ\text{C}$ , then stored in glass bottles.

Cellulose solution (4%) was prepared by dissolving filter paper with NaOH (7 wt %) /Urea (12 wt %) at  $-10\text{ }^\circ\text{C}$ , homogenizer (Stanfen, Germany) was used during this process. Then, the treated diatomite and  $\text{CaCO}_3$  were added at different weight ratios. The mixtures were dropped into HCL (1 mol/L) using a syringe after being dispersed by the homogenizer. The cellulose/diatomite beads (CDBs) were then washed with distilled water to remove  $\text{CaCl}_2$  after the reaction between  $\text{CaCO}_3$  and HCl accomplished and transferred into acetone immediately. After 24 h, the CDBs were desiccated in vacuum oven (Figure.3.1). [22] The synthesized absorbents were named MCDBs-0, MCDBs-10, MCDBs-20, MCDBs-30, and MCDBs-40 according to the varies amount of  $\text{CaCO}_3$ .



PVSK (0.01N) into the mixture automatically. The point of zero charge detected by Mutek titrator corresponded to the amount (i.e. volume) of PVSK neutralizing the excessive amount of PDADMAC [23]. The experiment was carried out three times simultaneously. The concentration of carboxylic functions [ $C_{COOH}$  (mmol  $g^{-1}$ )] was calculated by Eq 3.1.

$$C_{COOH} = (V_2 - V_1) \times C / m_{MCDBs} \quad \text{Eq. 3.1}$$

where  $V_2$  is the volume of PVSK dropped into solution with MCDBs (mL),  $V_1$  is the volume of PVSK dropped into blank solution (mL),  $C$  is the concentration of PVSK and Poly-Dadmac,  $m_{MCDBs}$  is the mass of MCDBs (g).

### **3.2.3 Characterization**

#### **3.2.3.1 FTIR**

FT-IR spectra were recorded using a NEXUS 470 spectrophotometer (Nicolet Thermo Instruments, Canada) after being grinded with KBr.

#### **3.2.3.2 Scanning Electron Microscopy (SEM)**

The morphology of the unmodified and modified beads for both the surface and cross section were observed on a scanning electron microscope (JEOL 6400 SEM, JEOL Ltd., Japan) after carbon coated with 10 kV accelerating voltage.

#### **3.2.3.3 Brunauer–Emmett–Teller (BET) adsorption**

BET adsorption was carried out using an Autosorb instrument (Belsorp-Max BEL Inc, Osaka, Japan).

### 3.2.4 Batch experiments

Pb<sup>2+</sup> was chosen to evaluate the effectiveness of synthesized adsorbents for water treatment. All solutions with various concentrations were obtained by successive dilution. The pH was adjusted by adding either 0.01 M HCl or 0.01 M NaOH. Adsorption experiments were carried out using 10 mL of lead ions solution of desired concentration (10 mg L<sup>-1</sup>) at an initial pH of 7.0, and adsorbent dosage 0.01 g per 10 mL in agitation speed of 130 rpm on a temperature-controlled shaker (SWB25, Thermo Electron Corporation, Germany). In the preliminary experiment, this speed was found to be suitable to reach equilibrium. The shaking time, temperature, pH, and the concentration of CaCO<sub>3</sub> were investigated, respectively. Residual Pb<sup>2+</sup> concentration in the filtrate was determined using UV (Genesys 10-s, Thermo Electron Corporation). [24] The percent metal ions removal R (%) was calculated by the Eq 3.2. [25]

$$R = (C_1 - C_e) / C_1 \times 100 \quad \text{Eq 3.2}$$

where C<sub>1</sub> (mg L<sup>-1</sup>) and C<sub>e</sub> (mg L<sup>-1</sup>) were the initial and final concentration of metal ions, respectively. The adsorption capacity (Q) was calculated by the Eqn (3).

$$Q = (C_1 - C_e) / m \times V \quad \text{Eq 3.3}$$

where Q is the adsorption capacity (mg g<sup>-1</sup>), V is the volume of solution (L) and M is the mass of adsorbent (g) used.

#### 3.2.4.1 Adsorption kinetics

The pseudo-second-order kinetic model was used to describe the adsorption kinetic data of Pb<sup>2+</sup> measured on MCDBs. Non-linear form and linear form are presented in Eq 3.4 and Eq 3.5, respectively. [26]

$$dq/dt = k_1 (q_e - q)^2 \quad \text{Eq 3.4}$$

$$t/q_t = 1/(k_1 \times q_e^2) + t/q_e \quad \text{Eq 3.5}$$

where  $q_t$  ( $\text{mg g}^{-1}$ ) and  $q_e$  ( $\text{mg g}^{-1}$ ) are the amounts of the  $\text{Pb}^{2+}$  adsorbed at time  $t$  (min) and at equilibrium, respectively.  $k_1$  ( $\text{g mg}^{-1} \text{min}^{-1}$ ) is the rate constant of the adsorption process.

### 3.2.4.2 Adsorption isotherms

The isotherms were carried out by shaking the MCDBs (0.01g) with 10mL of metal ions solution at different initial concentrations. The corresponding adsorption isotherms for lead ions were described by fitting the experimental data to the Langmuir, Freundlich, [27] and Temkin isotherms, [28] respectively. The Langmuir equation using the linear form Eq 3.6: [29]

$$C_e/q_e = aC_e/K_L + 1/K_L \quad \text{Eq 3.6}$$

where  $q_e$  and  $C_e$  are the solution ( $\text{mg g}^{-1}$ ) and surface concentrations ( $\text{mg L}^{-1}$ ) for the adsorbate at the equilibrium, respectively, and  $K_L$  ( $\text{L g}^{-1}$ ) and  $a$  ( $\text{L mg}^{-1}$ ) are the isotherm constants.  $K_L$  can be obtained from the relationship between  $C_e/q_e$  and  $C_e$ . The constant,  $a$ , corresponds the energy of adsorption process. A dimensionless separation factor  $R_L$  is the essential characteristics of the Langmuir equation, which was described by Eq 3.7. [30]

$$R_L = 1/(1+C_0 \times K_L) \quad \text{Eq 3.7}$$

where  $C_0$  is the highest initial  $\text{Pb}^{2+}$  concentration ( $\text{mg L}^{-1}$ ), the value of  $R_L$  indicates the nature of the interaction and the isotherm type: unfavourable ( $R_L > 1$ ), linear ( $R_L = 1$ ), favourable ( $0 < R_L < 1$ ), or irreversible ( $R_L = 0$ ).

### 3.3 Results and discussion

#### 3.3.1 FTIR spectra and colloid titration

The FTIR spectra of CDBs before and after modification with maleic anhydride are shown in Figure.3.2. The widely peaks at 3442 and 3443  $\text{cm}^{-1}$  are due to the stretching of O-H group. The adsorption at 2891 and 2897  $\text{cm}^{-1}$  is related to the C-H stretching, the band at 1630  $\text{cm}^{-1}$  is attributed to the bending mode of the absorbed water. The absorption bands at 1112 and 1110  $\text{cm}^{-1}$  correspond to C-O antisymmetric bridge stretching<sup>31</sup> and siloxane (Si-O-Si) stretching from alkali-treated diatomite. [32] The main difference between CDBs and MCDBs is the new peak at 1724 and 1638  $\text{cm}^{-1}$ . The adsorption at 1724  $\text{cm}^{-1}$  indicates the carboxyl groups (C=O) [33] and the one at 1638  $\text{cm}^{-1}$  relates to vibration of vinyl groups (C=C). The -OH stretching adsorption band at 3442  $\text{cm}^{-1}$  do not significantly change after modification. Because only the surface hydroxyls that are available to maleic anhydride can be grafted during the chemical reaction. [34]

According to the results obtained by colloid titration, the concentration of carboxyl groups on the surface of MCDBs was 0.45mmol  $\text{g}^{-1}$ , which corresponds to the surface charge density of MCDBs.

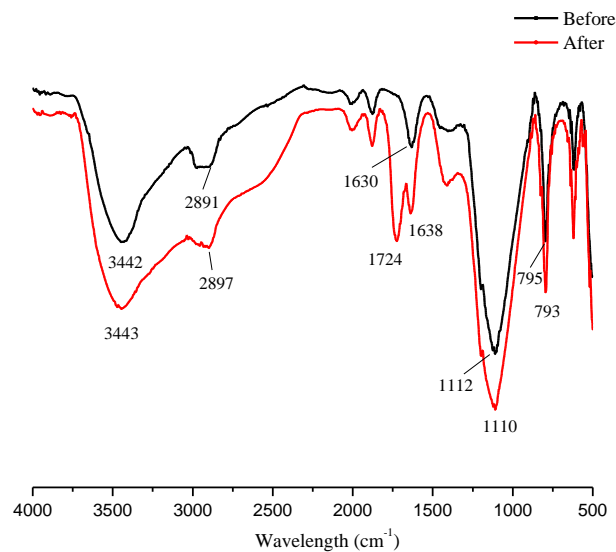


**Figure.3.2 FTIR spectrum of CDBs before and after modification.**

### 3.3.2 SEM

The surface structure of cellulose beads obtained was revealed by SEM and the images are shown in Figure.3.3. The CDBs obtained exhibited good spherical shape together with porous structure (Fig. 3 (a)). More pores can be observed in Figure.3.3 (c) and Figure.3.3 (e) than Figure.3.3 (b). The application of  $\text{CaCO}_3$  was conducive to the pore structure. The pores may be formed from the reaction between  $\text{CaCO}_3$  and  $\text{HCl}$ , during which the  $\text{CaCO}_3$  rich regions were transformed into pores due to the release of carbon dioxide and dissolution of  $\text{CaCO}_3$ . The alkali-treated diatomite exists in CDBs independently (Figure.3.3 (d)), which can preserve the adsorption capacity of adsorbate. After modification, maleic anhydride was grafted onto cellulose, which leads to decreasing pores in CDBs (Figure.3.3 (c) and Figure.3.3 (f)), due to the grafted maleic

anhydride which might fill up some pores on the spheres (Figure.3.3 (g) and Figure.3.3 (h)). This can be proved with the results of BET.

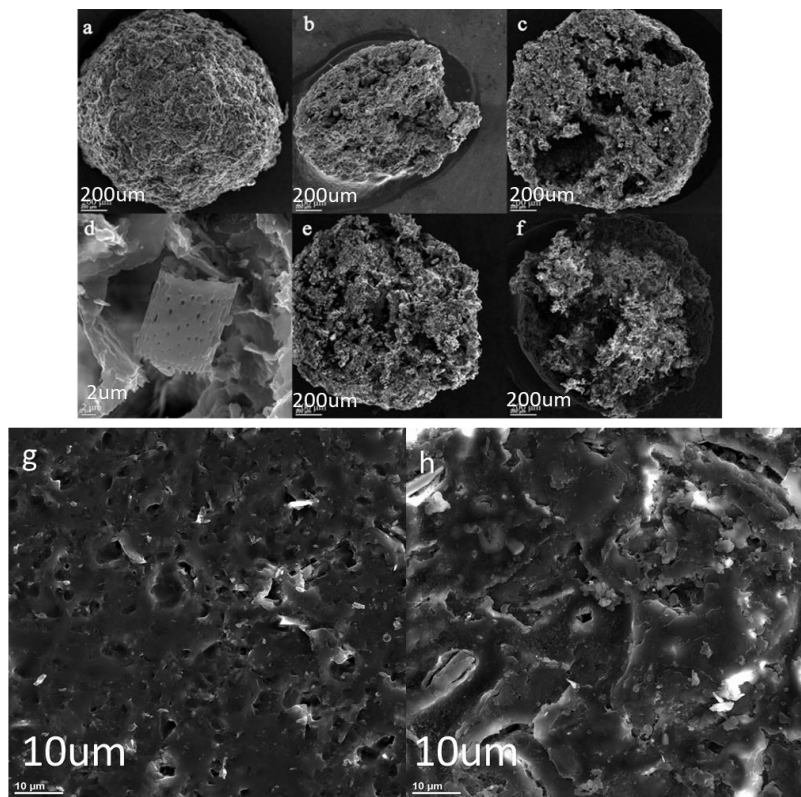


**Figure.3.3 SEM images of surface morphology (a), cross-section structure of MCDBs-10 (10% CaCO<sub>3</sub>) (b), MCDBs-30 (30% CaCO<sub>3</sub>) before modification (c, d, and g), MCDBs-30 (30% CaCO<sub>3</sub>) after modification (f, h), MCDBs-40 (40% CaCO<sub>3</sub>) (e) of regenerated cellulose beads.**

### **3.3.3 BET**

The specific surface areas of the CDBs and MCDBs were evaluated by BET analysis; and the results are presented in Table.3.1. The specific surface area of CDBs increased significantly when the concentration of CaCO<sub>3</sub> changed from 10% to 30%, at the same time, the total pore volume was changed from  $5.78 \times 10^{-3}$  to  $9.42 \times 10^{-3} \text{ m}^3 \text{ g}^{-1}$ , which

indicates the application of  $\text{CaCO}_3$  is conducive to the pore structure. After modification with maleic anhydride, the specific surface area of CDBs reduced to  $0.73 \text{ m}^2 \text{ g}^{-1}$ , meanwhile, the total pore volume changed from  $9.42 \times 10^{-3}$  to  $4.89 \times 10^{-3} \text{ m}^3/\text{g}$ , implying the grafted maleic anhydride might fill up some pores. However, the adsorption capacity of CDBs (30%  $\text{CaCO}_3$ ) is much lower than MCDBs-30 (30%  $\text{CaCO}_3$ ), which means the esterification is the main reason to increase the adsorption capacity of  $\text{Pb}^{2+}$  onto CDBs. MCDBs-40 does not have any results from BET, which might be due to the collapse of pores. In addition, the specific surface area of MCDBs-0 could not be detected by BET, which indicated that MCDBs-0 had very limited or no micro or mesoporous structures.

**Table.3.1 The BET results of CDBs and MCDBs.**

MCDBs	Specific surface ( $\text{m}^2 \text{ g}^{-1}$ )	Pore volume ( $\text{m}^3 \text{ g}^{-1}$ )
MCDBs-0 (before modification)	-	$1.1 \times 10^{-3}$
MCDBs-10 (before modification)	1.00	$5.78 \times 10^{-3}$
MCDBs-20 (before modification)	1.21	$6.64 \times 10^{-3}$
MCDBs-30 (before modification)	1.53	$9.42 \times 10^{-3}$
MCDBs-30 (after modification)	0.73	$4.89 \times 10^{-3}$
MCDBs-30 (before modification)	-	$6.23 \times 10^{-3}$

### 3.3.4 Comparative test

The  $\text{Pb}^{2+}$  fraction of removal (%) on different adsorbents including raw materials, CDBs and MCDBs is shown in Figure.3.4. The adsorption capacity of raw materials is extremely low, which is 44.95% for filter paper and 9.30% for alkali-treated diatomite, respectively. The CDBs has a higher fraction of removal compare with the raw materials.

Furthermore, the adsorption capacity of  $Pb^{2+}$  significantly increased after modified by maleic anhydride. These results demonstrated that the MCDBs are good carriers or adsorbents toward  $Pb^{2+}$ . The effect of  $CaCO_3$  concentration was studied at room temperature and neutral pH; and the results are also shown in Fig.3.4. The fraction of removal (%) increased significantly with the initial concentration of  $CaCO_3$  increase from 0 % to 30 %, and the fraction of removal was negatively affected when further increasing the concentration of  $CaCO_3$  up to 40 %, because the  $CaCO_3$  at over-dosage can induce the collapse of CDB pores. Therefore,  $CaCO_3$  play a role to the pore structure, the optimum concentration of  $CaCO_3$  is 30%.

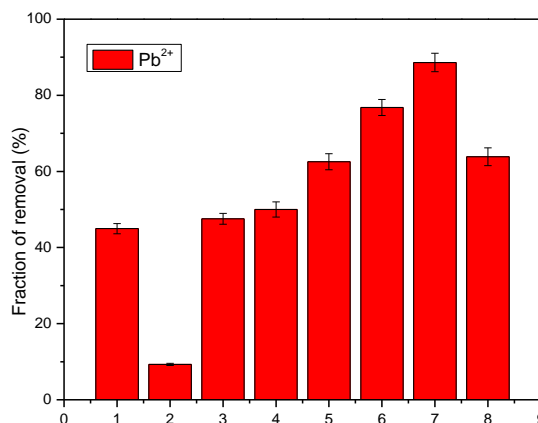


**Figure.3.4 Fraction of removal on different materials: 1-filter paper; 2-alkali-treated diatomite; 3-CDBs-0; 4-MCDBs-0; 5-MCDBs-10; 6-MCDBs-20; 7-MCDBs-30; 8-MCDBs-40**

### 3.3.5 Effect of pH

The removal of  $Pb^{2+}$  from aqueous solutions by adsorption depends on pH which affects the ionization of metal ions and the concentration of counter  $H^+$  ions on the surface of

the adsorbent. To study the effect of  $H^+$  concentration on metal removal, the solution pH is varied from 2 to 6. The results are shown in Figure.3.5.

The optimum pH value for adsorption of  $Pb^{2+}$  by MCDBs was found to be pH 6.0 (Figure.3.5). For MCDBs-30, fraction of removal is observed to be 88.89% for  $Pb^{2+}$  adsorption at this pH. In aqueous solutions,  $Pb^{2+}$  is dominant at pH 2-6. Other species ( $PbOH^+$ ) can exist at a higher pH. The removal of  $Pb^{2+}$  is extremely low at a pH below 3. The higher concentration of  $H_3O^+$ , which means lower pH, the concentration of protons competing with metal ions for the active sites are higher. The surface of adsorbents is positive charged, which is hard to adsorb heavy metals with positive charged. [35,36] With increasing pH ( $pH > 3$ ), the concentration of protons decreased, and the surface is negative charged which is advantageous for adsorption.

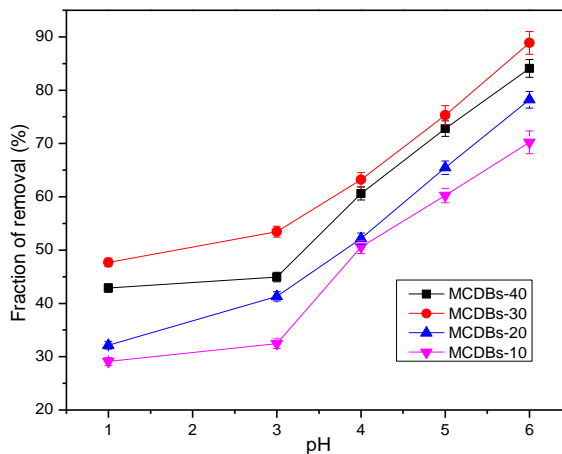


Figure.3.5 Effect of pH on adsorption of  $Pb^{2+}$ .

### 3.3.6 Effect of temperature

The effects of the temperature on adsorption of  $Pb^{2+}$  was studied by changing the temperature from 15 to 50 °C under the optimum pH in 2h, the results are presented in Figure.3.6. The adsorption of  $Pb^{2+}$  increased significantly as the temperature changed from 20 to 30 °C, which indicates that the adsorption process on MCDBs is an endothermic process. It changes indistinctive after 30 °C. So, the optimum temperature of  $Pb^{2+}$  adsorption on MCDBs is elected to be 30 °C.

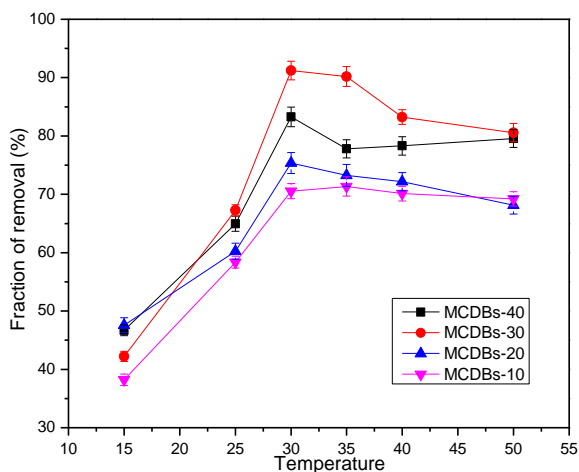


Figure.3.6 Effect of temperature on adsorption of  $Pb^{2+}$ .

### 3.3.7 Adsorption behaviour

#### 3.3.7.1 Adsorption kinetics

The effect of contact time on the adsorption of  $Pb^{2+}$  by MCDBs-30 is shown in Figure.3.7 and the results of adsorption kinetics, calculated from Figure.3.7, is shown in Figure.3.8. Experiments were performed at different temperatures (20, 30 and 45°C) at

pH 6. During short contact times, adsorption process is very fast (within 10min more than 50% is adsorbed) due to the numerous active sites on the surface of MCDBs-30, then, the fraction of removal levelled off. Over 84% adsorption efficiency is obtained at a certain temperature indicating that  $Pb^{2+}$  is absorbed by available adsorption sites. The sorption of  $Pb^{2+}$  onto MCDBs-30 is mainly mediated through complexation with surface functional groups (especially carboxyl groups) which can react with  $Pb^{2+}$  to form bound complexes. [37]

The adsorption process for  $Pb^{2+}$  is described by Pseudo-second-model, where the  $R^2$  are 0.9959, 0.9950, and 0.9981 at the temperature of 20, 30 and 45 °C, respectively (Figure.3.8). The fitting results suggested that the adsorption rate was dominated by chemical adsorption, which involved the electron sharing or electron transfer between the adsorbent and the adsorbate. The  $q_e$  values for  $Pb^{2+}$  adsorption is in a good agreement with the experimental one. This indicates the good agreement of the pseudo-second-order model to describe the kinetics of the adsorption. [38]

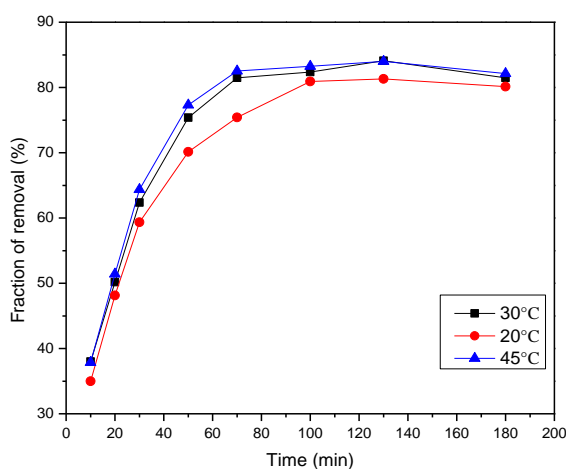


**Figure.3.7** Effect of contact time on adsorption of  $Pb^{2+}$ .

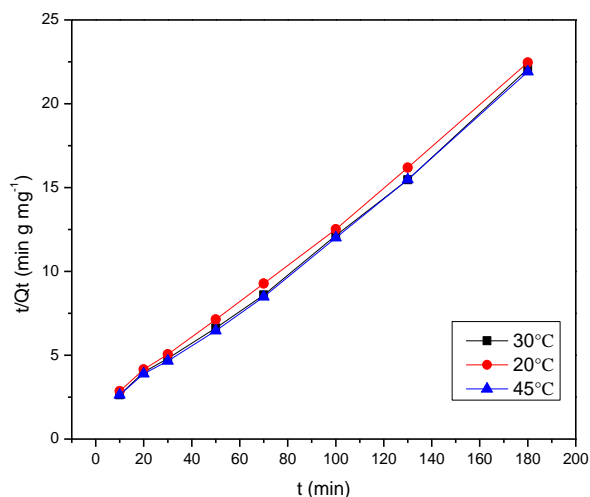


**Figure.3.8 Pseudo-second-order adsorption kinetics on MCDBs.**

### 3.3.7.2 Adsorption isotherms

The results of adsorption isotherms, calculated from different models, are shown in Table.3.2 and Figure.3.9. Langmuir model fit the experimental data well and the correlation coefficients of the equations ( $R^2=0.9952$ ) indicate that this model can explain the adsorption process satisfactorily. Langmuir isotherm is monolayer sorption where the adsorption sites are the same and the absorbed particles are independent, therefore, no further sorption can take place after a saturation value is reached. [39] In this study, the  $R_L$  value is between 0 and 1, indicates that the adsorption process is favorable. The estimated  $q_m=46.04 \text{ mg g}^{-1}$  ( $K_L/a$ ) is very close to the experimentally ( $44.54 \text{ mg g}^{-1}$ ) obtained maximum metal uptakes for  $\text{Pb}^{2+}$ . Monolayer adsorption capacities for adsorption of  $\text{Pb}^{2+}$  onto MCDBs-30 and other materials are compared in Table.3.3.

In addition, the thermodynamic parameters, such as enthalpy ( $\Delta H^\circ$ ), entropy ( $\Delta S^\circ$ ) and Gibb's free energy ( $\Delta G^\circ$ ) were estimated using the Van't Hoff equation. [44] Table.3.4 listed the thermodynamic parameters obtained from the temperature effect on  $Pb^{2+}$  adsorption, the values of free energy changes  $\Delta G^\circ$  are negative, confirming that adsorption of  $Pb^{2+}$  onto MCDBs is spontaneous and thermo-dynamically favorable. The  $\Delta G^\circ$  value decreased as the temperature increased, indicating less driving force for the adsorption. The negative values of  $\Delta H^\circ$  and  $\Delta S^\circ$  indicated that the  $Pb^{2+}$  adsorption on MCDBs was exothermic in nature and the stability of adsorption process with no structural change at solid-liquid interface.

**Table.3.2 the isotherm models for  $Pb^{2+}$  adsorption**

Adsorbate	Isotherm models	$K_L$	a	$K_f$	n	A	$b_T$	$R^2$
$Pb^{2+}$	Langmuir (20°C)	0.3776	0.0047	-	-	-	-	0.9949
	Langmuir (30°C)	0.5109	0.0116	-	-	-	-	0.9952
	Langmuir (45°C)	0.5666	0.0171	-	-	-	-	0.9958
	Freundlich (20°C)	-	-	3.552	1.649	-	-	0.9732
	Freundlich (30°C)	-	-	3.606	2.601	-	-	0.8921
	Freundlich (45°C)	-	-	3.596	2.784	-	-	0.9141
	Temkin (20°C)	-	-	-	-	0.3095	29.07	0.9268
	Temkin (30°C)	-	-	-	-	0.3607	53.91	0.9706
	Temkin (45°C)	-	-	-	-	0.4064	80.02	0.8711

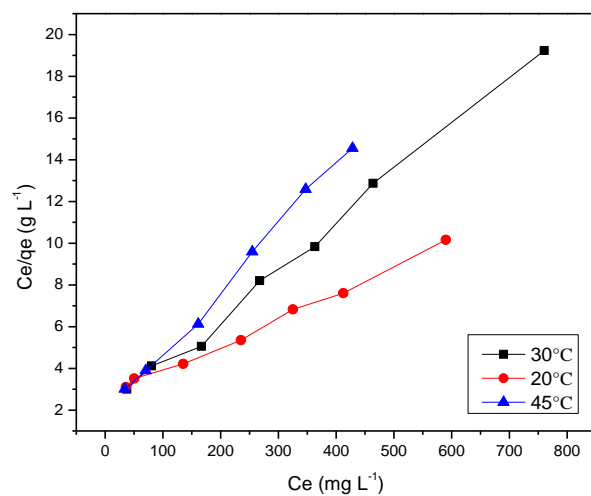


Figure.3.9 Linear plots of Langmuir isotherm for adsorption on MCDBs.

Table.3.3 Results for adsorption of Pb<sup>2+</sup> by MCDBs and other materials

Absorbent materials	Adsorbent capacity (mg/g)
Pine cones [40]	27.53
Soybean hulls [41]	44.37
MCDBs-30	44.54
Kaolinite clay [42]	113.63
Apricot stone [43]	22.85

Table.3.4 The calculation of  $\Delta G^\circ$ ,  $\Delta H^\circ$ , and  $\Delta S^\circ$

Temperature (K)	$\Delta G^\circ$ (kJ mol <sup>-1</sup> )	$\Delta S^\circ$ (kJ mol <sup>-1</sup> K <sup>-1</sup> )	$\Delta H^\circ$ (kJ mol <sup>-1</sup> )
293.15	-1.285	-0.0604	-20.66
298.15	-1.137		
303.15	-1.045		
318.15	-0.623		

### 3.3.8 Desorption of Pb<sup>2+</sup> from MCDBs-30

Desorption of the Pb<sup>2+</sup> was investigated, this procedure is necessary to restore the original adsorption capacity of the adsorbent and it also enables recovering valuable metals from wastewater streams. In this study, Pb<sup>2+</sup> was desorbed from MCDBs-30 using 1M HCl for 24h. Then the adsorbent was washed with distilled water, ethanol, and finally acetone. The adsorbent was reused three times at the same conditions (Pb<sup>2+</sup> concentration: 10 mg L<sup>-1</sup>; adsorbent: 0.01 g; volume of solution: 0.01 L), resulting in the fraction of removal (%) at 94.96, 90.74, and 87.13, respectively. The removal of Pb<sup>2+</sup> is substantially unchanged after reusing three times (the third time is 87.13%), indicates that the MCDBs-30 are renewable adsorbent for Pb<sup>2+</sup> removal.

## 3.4 Conclusions

Maleic anhydride modified CDBs (combine cellulose and alkali-treated diatomite) was found to effectively adsorb Pb<sup>2+</sup> from aqueous solutions. The pore structure of the adsorbents was enhanced by introducing CaCO<sub>3</sub> during the preparation. Further experiment data revealed that the adsorption process of Pb<sup>2+</sup> on the MCDBs-30 follows a pseudo-second-order kinetics and the equilibrium data can be well fitted with a Langmuir isotherm. The maximum adsorption capacities of adsorbent (Langmuir) was 44 mg g<sup>-1</sup> from an initial concentration of 800 mg L<sup>-1</sup> at pH 6 and at 30 °C. The capacity of the adsorbents in Pb<sup>2+</sup> removal was remained unchanged after reusing three times. The MCDBs-30 is a green-based, cost-effective, and renewable adsorbent. It could be used to adsorb more heavy metal ions which are positive charged.

### 3.5 References

- [1] B. Volesky and Z.R. Holan, Biosorption of Heavy Metals. *Biotechnol. Prog.*, 1995, 11, 235-250.
- [2] H.G. Seiler, H. Sigel and A. Sigel, Handbook on toxicity of inorganic compounds, 1988, Marcel Dekker, New York.
- [3] K. Li and X. Wang, Adsorptive removal of Pb (II) by activated carbon prepared from *Spartina alterniflora*: equilibrium, kinetics, and thermodynamics. *Bioresour. Technol.*, 2009, 100, 2810-2815.
- [4] J. Mohsen and A. Fathemeh, Sunflower stalk, an agricultural waste, as an adsorbent for the removal of lead and cadmium from aqueous solutions. *J. Mater. Cycles. Waste. Manag.*, 2013, 15, 548-555.
- [5] K.S. Low, C.K. Lee and S.M. Mak, Sorption of copper and lead by citric acid modified wood. *Wood Sci. Technol.*, 2004, 38, 629-640.
- [6] X.F. Ma, C.Z. Liu, D.P. Anderson and P.R. Chang, Porous cellulose spheres: Preparation, modification, and adsorption properties. *Chemosphere.*, 2016, 165, 399-408.
- [7] C. Emo, C. Andrea, D. Salvatore and S. Roberto, Biodegradation of poly (vinyl alcohol) based materials. *Prog. Polym. Sci.*, 2003, 28, 963-1014.
- [8] D.J. McDowall, B.S. Gupta and V.T. Stannett, Grafting of vinyl monomers to cellulose by ceric ion initiation. *Prog. Polym. Sci.*, 1984, 10, 1-50.
- [9] G. Magali, M. Veronique, C. Andre, L. Bernard and G. Philippe, Decontamination of synthetic solutions containing heavy metals using chemically modified sawdusts bearing polyacrylic acid chains. *J. Wood Sci.*, 2000, 46, 331-333.
- [10] D.M. James, M.R. Roger and M.S. Hong, Effect of Citric Acid Modification of Aspen Wood on Sorption of Copper Ion. *J. Nat. Fib.*, 2006, 3, 43-58.
- [11] A.M.A. Nada and M.L. Hassan, Ion Exchange Properties of Carboxylated Bagasse. *J. Appl. Polym. Sci.*, 2006, 102, 1399-1404.
- [12] F.T. Wang, Y.F. Pan, P.X. Cai, T.X. Guo, H.N. Xiao, Single and binary adsorption of heavy metal ions from aqueous solutions using sugarcane cellulose-based adsorbent. *Bioresour. Technol.*, 2017, 241, 482-490.
- [13] Y. Zhou, Q. Jin, X. Hu, Q. Zhang and T. Ma, Heavy metal ions and organic dyes removal from water by cellulose modified with maleic anhydride. *J. Mater. Sci.*, 2012, 47, 5019-5029.

- [14] X. Yu, S. Tong, M. Ge, L. Wu, J. Zuo, C. Cao and W. Song, Adsorption of heavy metal ions from aqueous solution by carboxylated cellulose nanocrystals. *J. Environ. Sci.*, 2013, 25, 933-943.
- [15] M.A.M. Khraisheh, Y.S. Al-degs and W.A.M. Mcminn, Remediation of Wastewater Containing Heavy Metals Using Raw and Modified Diatomite. *Chem. Eng. J.*, 2004, 99, 177-184.
- [16] P. Pusit, T. Pilaiporn and P. Sukon, Removal of Heavy Metals from Aqueous Solution by Natural and Modified Diatomite. *J. Microsc. Society of Thailand.*, 2011, 4, 103-107.
- [17] Y. Al-Degs, M.A.M. Khraisheh and M.F. Tutunji, Sorption of lead ions on diatomite and manganese-oxides modified diatomite. *Wat. Res.*, 2001, 35, 3724-3728.
- [18] M.A.M. Khraisheh, M.A. Al-Ghouti, S.J. Allen and M.N.M. Ahmad, The effect of pH, temperature and molecular size on the removal of dyes from textile effluent using manganese oxides modified diatomite. *Wat. Environ. Res.*, 2004a, 76, 2655-2663.
- [19] S.P. Yang, S.Y. Fu, H. Liu, Y.M. Zhou, X.Y. Li, 2011. Hydrogel Beads Based on Carboxymethyl Cellulose for Removal Heavy Metal Ions. *J. Appl. Polym. Sci.* 119, 1204-1210.
- [20] X. Yu, D. Kang, Y. Hu, S. Tong, M. Ge, C. Cao and W. Song, One-pot synthesis of porous magnetic cellulose beads for the removal of metal ions. *RSC Adv.*, 2014, 4, 31362-31369.
- [21] W.S. Moore, D. Reid and J. Geophys, Extraction of radium from natural waters using manganese-impregnated acrylic fibers. *J. Geophys. Res.*, 1973, 78, 8880-8886.
- [22] Y. Li, H. Xiao, M. Chen, Z. Song and Y. Zhao, Absorbents based on maleic anhydride-modified cellulose fibers/diatomite for dye removal. *J. Mater. Sci.*, 2014, 49, 6696-6704.
- [23] A. Musyanovych, R. Rossmannith, C. Tontsch, K. Landfester, Effect of Hydrophilic Comonomer and Surfactant Type on the Colloidal Stability and Size Distribution of Carboxyl- and Amino-Functionalized Polystyrene Particles Prepared by Miniemulsion Polymerization. *Langmuir*, 2007, 23, 5367-5376.
- [24] Y. Wang and M. Zhu, The determination of trace lead in propolis using improved Dithizone colorimetric. *Sci. Technol. Food Ind.*, 2006, 8, 164-165.
- [25] K. Mukhopadhyay, A. Ghosh, S.K. Das, B. Show, P. Sasikumar and U.C. Ghosh, Synthesis and characterisation of cerium(IV)-incorporated hydrous iron(III) oxide as an adsorbent for fluoride removal from water. *RSC Adv.*, 2017, 7, 26037-26051.

- [26] Y. He, T. Xu, J. Hu, C. Peng, Q. Yang, H. Wang and H. Liu, Amine functionalized 3D porous organic polymer as an effective adsorbent for removing organic dyes and solvents. *RSC Adv.*, 2017, 7, 30500-30505.
- [27] X. Jiang, S. Wang, L. Ge, F. Lin, Q. Lu, T. Wang, B. Huang and B. Lu, Development of organic–inorganic hybrid beads from sepiolite and cellulose for effective adsorption of malachite green. *RSC. Adv.*, 2017, 7, 38965-38972.
- [28] Z. Chen, W. Ma and M. Han, Biosorption of nickel and copper onto treated alga (*Undaria pinnatifida*): Application of isotherm and kinetic models. *J. Hazard. Mater.*, 2008, 155, 327-333.
- [29] F. Lu, C. Huang, L. You, J. Wang and Q. Zhang, Magnetic hollow carbon microspheres as a reusable adsorbent for rhodamine B removal. *RSC Adv.*, 2017, 7, 23255-23264.
- [30] G. McKay, Adsorption of dyestuffs from aqueous solutions with activated carbon I: Equilibrium and batch contact-time studies. *J. Chem. Tech. Biotechnol.*, 1982, 32, 759-772.
- [31] Q. Lu, X. Li, L. Tang, B. Lu and B. Huang, One-pot tandem reactions for the preparation of esterified cellulose nanocrystals with 4-dimethylaminopyridine as a catalyst. *RSC Adv.*, 2015, 5, 56198-56204.
- [32] Y. Al-Degs, M.A. Khraisheh and M.F. Tutunji, Sorption of lead ions on diatomite and manganese oxides modified diatomite. *Wat. Res.*, 2001, 35, 3724-3728.
- [33] H. Sanna, R. Evelliina and S. Mika, Removal of heavy metals from aqueous solutions by succinic anhydride modified mercerized nanocellulose. *Chem. Eng. J.*, 2013, 223, 40-47.
- [34] H. Zhao, J.H. Kwak, Z.C. Zhang, H.M. Brown, B.W. Arey and J.E. Holladay, Studying cellulose fiber structure by SEM, XRD, NMR and acid hydrolysis. *Carbohydr. Polym.*, 2007, 68, 235-241.
- [35] Z.X. Wang, G. Li, F. Yang, Y.L. Chen and P. Gao, Electro-Fenton degradation of cellulose using graphite/PTFE electrodes modified by 2-ethylanthraquinone. *Carbohydr. Polym.*, 2011, 86, 1807-1813.
- [36] M. Iqbal, A. Saeed and I. Kalim, Characterization of adsorptive capacity and investigation of mechanism of  $\text{Cu}^{2+}$ ,  $\text{Ni}^{2+}$  and  $\text{Zn}^{2+}$  adsorption on mango peel waste from constituted metal solution and genuine electroplating effluent. *Sep. Sci. Technol.*, 2009, 44, 3770-3791.
- [37] J.H. Park, Y.S. Ok, S.H. Kim, J.S. Cho, J.S. Heo, R.D. Delaune and D.C. Seo, Competitive adsorption of heavy metals onto sesame straw biochar in aqueous solutions. *Chemosphere.*, 2016, 142, 77-83.

- [38] M.D. Ahmed, A.A. Asem and S.Y. Shereen, Efficient adsorption of Cu(II) and Hg(II) from their aqueous solutions using amine functionalized cellulose. *J. Disper. Sci. Technol.*, 2013, 34, 1230-1239.
- [39] Z.H. Ding, R. Yu, X. Hu, Y.J. Chen and Y.F. Zhang, Graft copolymerization of epichlorohydrin and ethylenediamine onto cellulose derived from agricultural by-products for adsorption of Pb(II) in aqueous solution. *Cellulose.*, 2014, 21, 1459-1469.
- [40] M. Milan, M. Milovan, B. Aleksandar, Z. Aleksandra and R. Marjan, Removal of lead (II) ions from aqueous solutions by adsorption onto pine cone activated carbon. *Desalination.*, 2011, 276, 53-59.
- [41] M.M. Johns, W.E. Marshall and C.A. Toles, Agricultural by-products as granular activated carbons for adsorbing dissolved metals and organics. *J. Chem. Technol. Biotechnol.*, 1998, 71, 131-140.
- [42] O. Waid and Al. Hossam, Removal of Pb<sup>2+</sup> ions from aqueous solutions by adsorption on kaolinite clay. *Am. J. Appl. Sci.*, 2007, 4, 502-507.
- [43] M. Kobya, E. Demirbas, E. Senturk and M. Ince, Adsorption of heavy metal ions from aqueous solutions by activated carbon prepared from apricot stone. *Bioresour. Technol.*, 2005, 96, 1518-1521.

## **Chapter 4 Novel composite adsorbent consisting of dissolved cellulose fibre/microfibrillated cellulose for dye removal from aqueous solution<sup>3</sup>**

### **ABSTRACT**

A novel composite adsorbent was developed based on dissolved cellulose fibres (as matrix) reinforced with microfibrillated cellulose (MFC). Both cellulose fibres and microfibrillated cellulose were functional-modified using an organic solvent-free approach to introduce carboxyl groups onto cellulose and the surface of MFC. To further enhance the adsorption capacity, nano-sized CaCO<sub>3</sub> was added as a pore forming agent during the formation of dissolved cellulose/MFC (CMFC) composites and removed in an acidic condition afterwards. The structure and morphology of as-synthesized adsorbents were characterized by using Fourier Transform Infrared Spectroscopy (FT-IR), Scanning Electron Microscope (SEM), Thermo Gravimetric Analyzer (TGA), and Brunauer-Emmet-Teller (BET) measurements. An orthogonal experimental design and software SPSS were utilized to reveal the impact of influencing factors (pH, temperature, and the concentration of pore forming agent) on dye removal. The results were imitated by kinetic models and adsorption isotherms, which indicated that the MCMFCs had a dominated adsorption capacity toward MB with the maximum adsorption at 303.03 mg g<sup>-1</sup>. The pseudo-second-order kinetic model and Langmuir

---

<sup>3</sup> This chapter has been published on ACS Sustainable Chemistry & Engineering, the format follows the requirements of the Journal. The entire experimental work was performed by candidate Yuan Li along with the preparation of manuscript. “Yuan Li, Huining Xiao, Yuanfeng Pan, Lidong Wang. Novel Composite Adsorbent Consisting of Dissolved Cellulose Fiber/ Microfibrillated Cellulose for Dye Removal from Aqueous Solution. ACS Sustainable Chemistry & Engineering (2018), 6: 6994-7002.”

isotherm model fit well, indicating the adsorption was monolayer and governed by chemisorption.

**Keywords:** Green composite adsorbents, Microfibrillated cellulose spheres, Dye adsorption, Kinetics, Isotherms

#### **4.1 Introduction**

There is an increasing demand for clean water due to the rapid urbanization and expanding industrial activities. The fresh water sources are limited on earth and this demand should be addressed by utilizing water clarification techniques. However, the technique depends on various contaminants and pollutants, such as organic compounds, heavy metal ions, dyes, and pharmaceuticals [1]. Dyes, coloring most consumer products, produce vast discharges to the body and endanger humans. The cationic dyes are difficult to degrade due to the complex aromatic molecular structures and xenobiotic properties [2]. Dyes in the aqueous solution can be removed by the adsorption technique due to its benefits such as low cost, simplicity, and ease of operation [3]. Various adsorbents, such as alumina nanoparticles [4], modified metal oxides [5], silica mesoporous materials [6], and cellulose based adsorbents [7] were widely investigated by researchers in recent years to overcome the high-cost production of activated carbon [8], resulting in an attentive, rapid, and efficient solution for sewage treatment.

Cellulose, the most abundant naturally-occurring biopolymer with a mass of hydroxyl groups along its chain [9], is an ideal raw material for producing new functional materials because of the growing demand for innovative and biodegradable products recently [10]. In addition, cellulose is multifunctional and renewable material which can

be used to replace many other non-renewable materials [11]. However, as an adsorbent the adsorption capacity of unmodified cellulose is limited and the selectivity is low because of the formation of hydrogen bonds between the molecular chains [12]. The hydroxyl group is one of the principle structural components in the cell walls of cellulose [13], which can be easily modified to introduce the functional groups via various derivation reactions including esterification, halogenation, oxidation, and etherification [14]. Such modifications improve the properties of cellulose substantially, particularly including the adsorptive and ion exchange capability [15].

The natural cellulosic materials have many advantages compared with other inorganic adsorbent. Apart from low density and cost, they are renewable and biodegradable. Nevertheless, few studies of the cellulose composites as the adsorbents for the removal of pollutant have been reported [16,17]. The powdered shape of such adsorbents might cause difficulty for the operation, filtration, and separation effectively, resulting in the lower potential application in large-scale water treatment [18]. The study of large-scale adsorbents, such as beads and other shaped particles, is therefore necessary and has been the hot topic for researchers. Zhang et al. prepared magnetic cellulose beads consisting of activated carbon to remove dyes including methylene blue and methyl orange [19]. The cellulose hybrid beads had been successfully investigated for the removal of cationic dyes, which offered a new platform to prepare the organic-inorganic hybrid adsorbents [20]. A novel cellulose-based adsorbent was synthesized to remove anionic dyes, and the adsorption ability was specially investigated [21].

Compared with conventional cellulose fibers, microfibrillated cellulose (MFC) is superior due to its advantages in structure, performance, and application. MFC is an

ideal material which would provide a variety of shapes and be biocompatible and absorbable [22]. Microfibrillated cellulose is an excellent environmentally friendly adsorbent due to high specific surface area. The application of MFC in the preparation of composite-type adsorbent is expected to increase the strength of the adsorbents and thermal stability significantly owing to its high bonding potential. However, little work has been reported on combining dissolved cellulose fibres reinforced with microfibrillated cellulose (MFC) as a composite type of adsorbent.

Therefore, in this work, we explored an innovative approach to prepare the dissolved cellulose fibre/microfibrillated cellulose composite beads as an environmental-friendly adsorbent for the removal of dyes from aqueous solutions. The key novelty relies on the unique porous structures in the green-based adsorbent consisting of dissolved fibres as matrix reinforced with cellulose filament in micro-scale. The nano-sized  $\text{CaCO}_3$  particle as an effective pore forming agent further enhanced the porosity of the adsorbent, thus leading to extremely high adsorption capacity towards to dyes (as a model compound for contaminants). In addition, both cellulose fibres and microfibrillated cellulose were functional-modified using an organic solvent-free method. Apart from developing an appropriate protocol for the synthesis of all green-based adsorbent, the structure, morphology, thermal properties, and adsorption behaviors of as-synthesized adsorbents were also systematically investigated in this work to evaluate their potential application for the removal of dyes. Various kinetic and isotherm models were fit to reveal the mechanism of adsorption. The applications of such green-based adsorbents could be readily extended to the removal of heavy metal ions from industrial wastewater.

## 4.2 Experimental

### 4.2.1 Materials

The source of cellulose material was filter paper (Qualitative P4, porosity: Medium - Fine; Flow Rate: Slow, Fisher Scientific). Microfibrillated cellulose (MFC) was kindly provided by FPIinnovations Canada (Pointe Claire, QC, Canada), which was obtained via processing cellulose fibres mechanically based on a technology invented by FPIinnovations. The resulting fibres in nano- or micro- range have the lengths from 50 to 800  $\mu\text{m}$  with the aspect ratios from 300 to 3000 and high surface area ( $> 80 \text{ m}^2/\text{g}$ ).  $\text{CaCO}_3$  nanoparticles (Product # 1951RH,  $\leq 30\text{nm}$ , 97.5%) was supplied by SkySpring Nanomatierials, Inc. NaOH, maleic anhydride (MA), urea, methylene blue, and methyl violet (MV) were all purchased from Sigma-Aldrich, Canada. Poly-DADMAC solution (0.01N) and PVSK solution (0.01N) was purchased from Fisher Scientific. Standard Methylene blue and methyl violet ( $1.000 \text{ g L}^{-1}$ ) solution was prepared by dissolving appropriated amounts of dyes in the distilled water.

### 4.2.2 Methods

#### 4.2.2.1 Preparation of Cellulose/Microfibrillated cellulose spheres (CMFCs) and carbonylated CMFCs (MCMFCs).

The cellulose solution (4%) was prepared by the method reported elsewhere [23]. During the process, the filter paper was cut into pieces and then dissolved in the solution containing NaOH (7 wt %) /Urea (12 wt %) at  $-10 \text{ }^\circ\text{C}$ , and the homogenizer (Stanfen, Germany) was used. Then, the dried microfibrillated cellulose and nano- $\text{CaCO}_3$  were

added at different weight ratios into the dissolved fibre solution. The mixtures were added into HCL (1 mol/L) dropwise using a syringe after to generate the beads via precipitation since cellulose is insoluble under such conditions. Over this process, the dissolution of nano-CaCO<sub>3</sub> and CO<sub>2</sub> released from the dissolution under acidic conditions created the pores with the size in a broad range. The cellulose/microfibrillated cellulose spheres (CMFCs) were washed with distilled water to remove the water-soluble residues, which were produced by the reaction between nano-CaCO<sub>3</sub> and HCl. The precipitated CMFCs were then soaked into acetone for 24 h, and the CMFCs were desiccated in a vacuum oven (Figure.4.1).

The preparation of carbonylated CMFCs (MCMFCs) followed the procedure reported in our previous work [20]. First, the CMFCs (5g) was added in maleic anhydride solution (5 g of MA dissolved in 40 mL of acetone) and soaked in the solution for 20 minutes. Afterwards, the mixture was placed in a vacuum oven at 50 °C for 1h, followed by heating up to 100°C for 3 h. The MCMFCs was then washed with distilled water, ethanol, and finally with acetone several times to remove the impurities or unreacted MA, and then desiccated in a vacuum oven overnight. As a result, the carboxylic groups were introduced onto cellulose through the esterification reaction. The entire process is illustrated schematically in Figure.4.1.

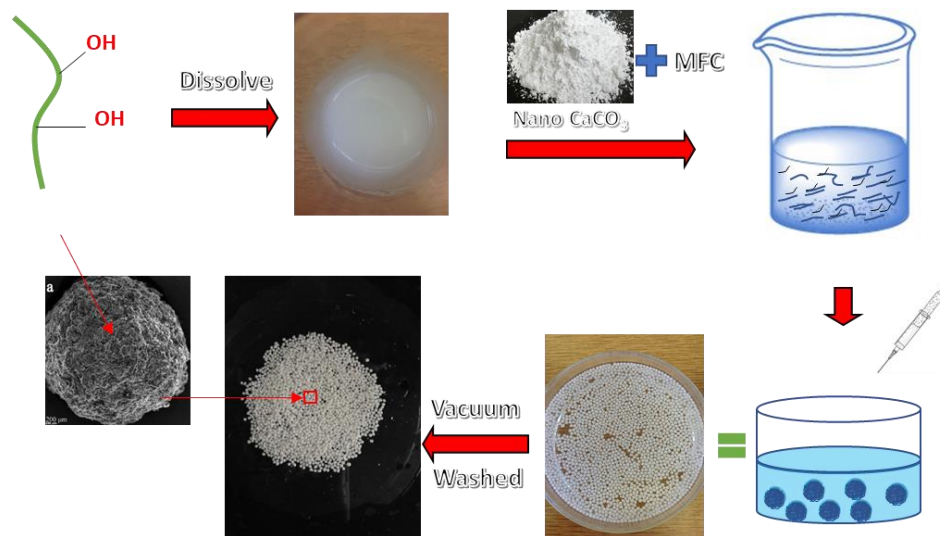


**Figure.4.1 The Schematic of CMFCs Preparation.**

#### 4.2.2.2 Charge density determination

The surface charge density of cellulose MCMFCs was determined via a colloid back titration method using a titrator (PCD 03, Mutek, UK). In the test, 0.05g of oven-dried MCMFCs was added to 0.01N Poly-DADMAC solution (5mL) at room temperature with constant stirring for 1h. Then, titration analysis was conducted for both control and fiber samples by adding the PVSK (0.01N) into the mixture automatically. The point of zero charge detected by Mutek titrator corresponded to the amount (i.e. volume) of PVSK neutralizing the excessive amount of PDADMAC which unabsorbed on the surfaces of MCMFCs. The experiment was carried out three times simultaneously. The charge density of carboxylic-modified cellulose beads ( $\text{mmol g}^{-1}$ ] was calculated by Eq 4.1.

$$C_{COOH} = (V_2 - V_1) \times C / m_{MCMFCs} \quad \text{Eq 4.1}$$

Where  $V_2$  is the volume of PVSK dropped into solution with MCMFCs (mL),  $V_1$  is the volume of PVSK dropped into blank solution (mL),  $C$  is the concentration of PVSK and Poly-Dadmac,  $m_{\text{MCMFCs}}$  is the mass of MCMFCs (g).

#### **4.2.2.3 Structural and morphologic characterization of adsorbents**

Fourier transform infrared spectroscopy (FTIR): prior to measurement, the tested specimens were prepared by grinding the KBr with dried samples. The FT-IR spectra of the samples were recorded using NEXUS 470 spectrophotometer (Nicolet Thermo Instruments, Canada) with a detector at  $1\text{ cm}^{-1}$  resolution from  $450$  to  $4000\text{ cm}^{-1}$  and 64 scans per sample. Scanning electron microscope (SEM): the surface structure and morphology of the samples were observed using a JEOL JSM-6400 SEM instrument (Japan). Prior to observation, the surface of the samples was coated with a thin film of carbon using a sputter coater. Thermal analysis: analysis of the thermal stability of the samples was performed using the Thermo Gravimetric Analyzer (TGA and DTG) (Q600, TA Instruments, USA) from the ambient temperature to  $600\text{ }^\circ\text{C}$  under  $\text{N}_2$  atmosphere at  $10\text{ }^\circ\text{C}/\text{min}$  heating rate. Brunauer-Emmet-Teller (BET): the BET adsorption was carried out using an Autosorb instrument (Belsorp-Max BEL Inc, Osaka, Japan). The liquid nitrogen was used during the measurement. The specific surface areas and pore sizes were measured based on the  $\text{N}_2$  gas adsorption isotherms of samples.

#### **4.2.2.4 Adsorption of cationic dyes**

Adsorption experiments were carried out in a batch mode to study the effect of shaking time, temperature, pH, and  $\text{CaCO}_3$  content on adsorption behavior. In this work, the adsorbents (10 mg) were immersed into 10 mL of dye aqueous solution of 20 mg/L at

room temperature. Prior to adsorption, the temperature-controlled shaker (SWB25, Thermo Electron Corporation, Germany) was used during the process of adsorption, shaking at 130rpm. After preset time intervals, the supernatant concentration of the MB was measured using a UV-vis spectrophotometer (Genesys 10-s, Thermo Electron Corporation) at 664nm [24]. The adsorption capacity of the MCMFCs at time  $t$  ( $Q_t$ , mg/g), the equilibrium adsorption capacity ( $Q_e$ , mg/g) and the fraction of removal ( $R$ , %) was calculated based on the equations mentioned in Chapter 3 [25].

#### **4.2.2.5 Regeneration Analysis**

HCl (1mol/L) was used as the eluent in the test. MB-loaded MCMFCs (10mg) was added to the eluent (20 mL) 60 min at room temperature. The desorbed adsorbent was washed and dried, and the so-regenerated adsorbent was examined to determine its reusability. After desorbing MB, the MCMFCs was dried under vacuum before its reuse.

#### **4.2.2.6 The orthogonal design**

The statistical software version SPSS 16.00. was used in orthogonal design ( $P < .05$  means statistical difference;  $P < .01$  means significantly statistical difference) [26], which involved the trials of 3 factors in 5 levels of adsorption processes to simplify the calculation and limit trial scope to achieve statistic efficiency. The results are shown in Table.4.1. The three factors in five levels were set as follows: pH, temperature, and concentration of nano- $\text{CaCO}_3$  as factors A, B, and C, respectively. Among them, five levels of pH were set from 3 to 11; temperatures from 20 to 50 °C; and the concentration of  $\text{CaCO}_3$  at wt% from 0 to 40 %, respectively.

**Table.4.1 Three factors with 5 levels**

pH	Temperature (°C)	CaCO <sub>3</sub> (%)	Experiment	pH	Temperature (°C)	CaCO <sub>3</sub> (%)	Experiment
3	30	10	1	11	25	20	13
3	25	5	2	11	30	30	14
5	30	0	3	5	50	10	15
7	20	5	4	11	50	5	1
9	30	5	5	3	40	20	17
7	50	0	6	3	50	30	18
7	30	20	7	3	20	0	19
9	40	10	8	9	50	20	20
11	40	0	9	11	20	10	21
5	40	5	10	5	25	30	22
7	40	30	11	7	25	10	23
9	20	30	12	9	25	0	24
				5	20	20	25

#### 4.2.2.7 Adsorption kinetics

Prior to kinetic studies, the synthesized MCMFCs (0.01g) were immersed in 10mL of dye at the desired pH and optimum temperature for preset time intervals. The initial concentration of MB was fixed at 20.0 mg/L. The concentration of dye solution was measured and then the pseudo-first-order, the pseudo-second-order [27], and Elovich kinetic models imitated the adsorption data [28]. The linear forms for the three models are presented as follows (Eq 4.2, Eq 4.3, and Eq 4.4):

$$\ln (q_e -q) = \ln q_e - k_1 t \quad \text{Eq 4.2}$$

$$t/q_t = 1/(k_2 q_e^2) + t/q_e \quad \text{Eq 4.3}$$

$$q_t = (1/\beta) \ln \alpha\beta + (1/\beta) \ln t \quad \text{Eq 4.4}$$

Where  $q_t$  and  $q_e$  are the amounts of the dye adsorbed at any time  $t$  and at equilibrium ( $\text{mg g}^{-1}$ ), respectively.  $k_1$  and  $k_2$  are the rate constants of the adsorption ( $\text{g mg}^{-1} \text{min}^{-1}$ ) for the pseudo-first-order and pseudo-second-order model, respectively.  $\alpha$  and  $\beta$  are the initial adsorption rate at zero coverage and the desorption constant related to the extent of surface coverage and activation energy for chemisorption in the Elovich model.

#### 4.2.2.8 Adsorption isotherms

The experiments were carried out at the desired pH and optimum temperature by shaking the MCMFCs (0.01g) with 10mL of dye solutions at different initial concentrations. The experimental procedures were the same as addressed previously. Different isotherm models, including Langmuir, Freundlich and Temkin model were used to imitate the adsorption results. Following are the equations detailing each model [29,30]:

Langmuir model (Eq 4.5):

$$C_e/q_e = C_e/Q_{max} + 1/(Q_{max} a) \quad \text{Eq 4.5}$$

where  $Q_{max}$  ( $\text{mg g}^{-1}$ ) and  $a$  ( $\text{L mg}^{-1}$ ) are isotherm constants.  $C_e$  ( $\text{mg L}^{-1}$ ) and  $q_e$  ( $\text{mg g}^{-1}$ ) are the concentration and adsorption capacity at the equilibrium, respectively.

Freundlich model (Eq 4.6):

$$\ln q_e = \ln K_f + (1/n) \ln C_e \quad \text{Eq 4.6}$$

where  $q_e$  and  $C_e$  are noted previously.  $K_f$  is roughly an indicator of adsorption capacity and  $n$  is adsorption intensity.

Temkin model (Eq 4.7):

$$q_e = RT/b_T \ln A + RT/b_T \ln C_e \quad \text{Eq 4.7}$$

where  $A$  ( $\text{L mg}^{-1}$ ) and  $b_T$  ( $\text{J mol}^{-1}$ ) are the Temkin constants,  $T$  is the absolute temperature, and  $R$  is the universal gas constant  $8.314 \text{ J mol}^{-1}\text{K}^{-1}$ .

### 4.3 Results and discussion

#### 4.3.1 FT-IR spectra

The FT-IR was employed to investigate the changes of the functional groups on CMFCs after modification. The spectra of both modified and control samples are presented in Figure.4.2.

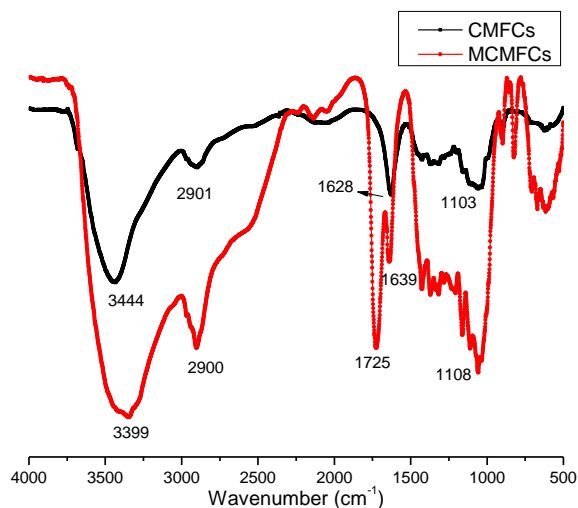


**Figure.4.2 FT-IR spectrum for control and modified CMFCs**

Some characteristic peaks of cellulose were identified, the band at  $3444 \text{ cm}^{-1}$  corresponded to the hydrogen bond O-H stretching vibration, the C-H symmetric

stretching vibration assigned at  $2901\text{ cm}^{-1}$ , the absorbance at  $1628\text{ cm}^{-1}$  was associated with O-H bending of the absorbed water, and the band at  $1103\text{ cm}^{-1}$  was the C-O stretching vibration [31]. Compared with the spectra of CMFCs, the new peaks at  $1725$  and  $1639\text{ cm}^{-1}$ , were observed on MCMFCs. After modification, characteristics peaks at  $1725\text{ cm}^{-1}$ , and  $1639\text{ cm}^{-1}$  occurred, which corresponded to carbonyl groups (C=O) and the vibration of vinyl groups (C=C), respectively [32]. Hence, the chemical reaction between maleic anhydride and CMFCs was proved. Moreover, the peak assigned to -OH stretching adsorption shifted from  $3444\text{ cm}^{-1}$  to  $3399\text{ cm}^{-1}$  after modification, which further demonstrated the reaction between the hydroxyl groups on CMFCs and maleic anhydride during modification [33]. In addition, the successful introduction of carboxyl groups on MCMFCs could be verified via the colloidal titration method, which gave the anionic charge density of  $0.573\text{ mmol g}^{-1}$ , was proportional to the amount of carboxyl groups on cellulose glucose repeat units.

#### **4.3.2 Surface morphology of CMFCs and MCMFCs**

To facilitate the observation with SEM, the cellulose/microfibrillated cellulose composite spheres were embedded in the epoxy resin, and then cut and polished. To get insight into the inner or porous structures of as-synthesized adsorbents, the morphologies of CMFCs (10%  $\text{CaCO}_3$ ), CMFCs (30%  $\text{CaCO}_3$ ), the cross sections of CMFCs and MCMFCs were revealed under SEM, respectively (Figure.4.3). Figure.4.3a and Figure.4.3b indicated that the dissolved cellulose matrix reinforced with MFC formed a honeycomb-like structure with pores at various sizes; the cross section of CMFCs presented a porous morphology, and more porous structure was observed on the

spheres with the higher concentration of nano- $\text{CaCO}_3$  added, demonstrating the role of nano- $\text{CaCO}_3$  in pore forming processes. Clearly, the pores could be created via the reaction between  $\text{CaCO}_3$  and  $\text{HCl}$ , during which the dissolution of  $\text{CaCO}_3$  occurred while the carbon dioxide was released, thus leading to porous structure. In comparison with the morphology of CMFCs (10%  $\text{CaCO}_3$ ) Figure.4.3c, the CMFCs (30%  $\text{CaCO}_3$ ) (Figure.4.3d) exhibited more porous and wrinkled structure. However, the beads consisting of maleic anhydride-grafted cellulose appeared to be less porous (Figure.4.3d and Figure.4.3e), due to the grafted maleic anhydride which might fill up some pores on the spheres.

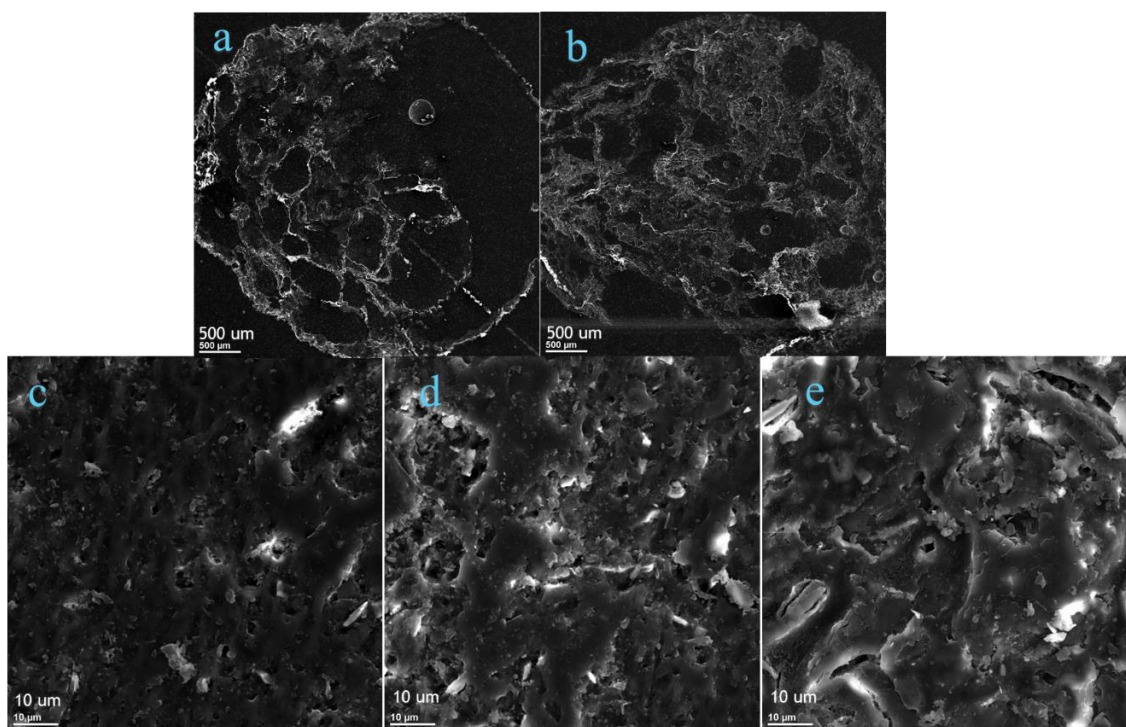


**Figure.4.3 SEM images of cross-section of CMFCs (10%  $\text{CaCO}_3$ ) (a), cross-section of CMFCs (30%  $\text{CaCO}_3$ ) (b), CMFCs (10%  $\text{CaCO}_3$ ) (c), CMFCs (30%  $\text{CaCO}_3$ ) (d) and CMFCs-30 (30%  $\text{CaCO}_3$ ) after being modified by MA (e).**

### 4.3.3 Thermal analysis

To reveal the thermal properties of cellulose/microfibrillated cellulose beads (CMFCs) and MCMFCs, the TGA and DTG curves are shown in Figure.4.4. As for CMFCs and MCMFCs, a total mass loss of 92.7% and 93.3% over the temperature range between 25 °C and 700 °C were observed (see Figure.4.4a), respectively. Both CMFCs and MCMFCs showed an initial weight loss of 8% between 25 °C and 100 °C, which was due to the evaporation of bound water from the samples. And the release of water from samples was the same for both samples, presumably due to the similar hydrophilic properties associated with cellulose and microfibrillated cellulose [34]. Compared to the CMFCs, the decomposition of MCMFCs occurred in three events: the first weight loss of 8%, starting at 50 °C in the TGA curve, was attributed to a bound water released from the MCMFCs; the second decomposition occurred around 160°C, presumably due to the initial stage of thermal degradation; the third weight loss happened at the temperature higher than 290 °C, corresponding to the major thermal cleavage of cellulose and microfibrillated cellulose, which also reflected to an endothermic peak in the Figure.4.4b at around 338 °C [35]. However, the results in Figure.4.4b indicated that the thermal decomposition peak of the maximum weight loss was 349 °C for CMFCs, which was 11 °C higher than that of MCMFCs. Obviously, the cellulose/CMF spheres showed higher thermal resistance than the spheres modified by maleic anhydride.

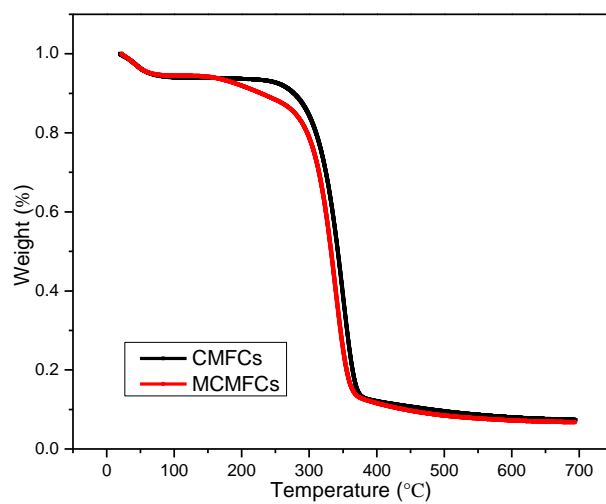


**Figure.4.4a**

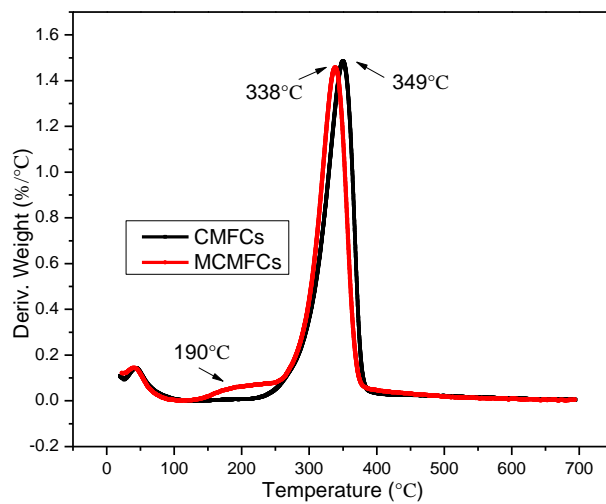


**Figure.4.4b**

**Figure.4.4 The TGA and DTG curves of CMFCs and MCMFCs**

#### 4.3.4 Brunauer-Emmet-Teller (BET)

From the data of BET, the specific surface area of CMFCs increased from 0.0765 m<sup>2</sup>/g to 11.30 m<sup>2</sup>/g and the total pore volume was changed from 1.4 ×10<sup>-2</sup> to 2.4 ×10<sup>-2</sup> cm<sup>3</sup>/g when the concentration of nano-CaCO<sub>3</sub> was increased from 10% to 30% (wt). Whereas the specific surface area for MCMFCs prepared at 30% CaCO<sub>3</sub> changed to 6.73 m<sup>2</sup>/g, suggesting that the esterification with maleic anhydride lowered surface areas. Meanwhile, the total pore volume changed from 2.4 ×10<sup>-2</sup> to 9.62×10<sup>-3</sup> cm<sup>3</sup>/g, presumably due to the collapse of pores and the grafted maleic anhydride which might fill up some pores inside beads. In addition, when the spheres were modified by maleic anhydride, the pore structure was gradually destroyed and the agglomeration pores on spheres increased, resulting in a decrease in the total pore volume and the specific surface area. However, the adsorption capacity of synthesized MCMFCs increased significantly after the modification, and such a phenomenon may be due to the enhanced surface reactivity towards the adsorption. Therefore, the nano-CaCO<sub>3</sub> was conducive to the pore structure, and the negative charge of the MCMFCs was the main reason to increase the adsorption capacity of dye onto CMFCs. In addition, the specific surface area of CMFCs without CaCO<sub>3</sub> could not be detected by BET, which indicated that CMFCs had very limited or no micro or mesoporous structures. It is worth noting that BET testing is only capable of detecting the micro- or mesopores on the adsorbents, which often exist on the walls of the pores on the adsorbent. However, those micro or mesoporous structures could play an important role in the adsorption of dyes.

### 4.3.5 Adsorption behavior

#### 4.3.5.1 The orthogonal experiments

The results obtained from the orthogonal experiments were analyzed using the software SPSS under “General Linear Model - Univariate”. After inputting the data from Table.4.1 into SPSS and defining the variables, we obtained the following outputs (see Tables.4.2 and Table.4.3), including dependent variables and tests of between - subject effects:

**Table.4.2 pH, temperature, and percentages of CaCO<sub>3</sub> - Dependent variable: fraction of removal**

pH	Mean	95% Confidence Interval	
		Lower Bound	Upper Bound
3	.559	.444	.674
5	.687	.572	.802
7	.960	.845	1.075
9	.948	.833	1.063
11	.862	.747	.977

Temperature °C	Mean	95% Confidence Interval	
		Lower Bound	Upper Bound
20	.824	.709	.939
25	.843	.728	.958
30	.781	.666	.896
40	.791	.676	.906
50	.777	.662	.893

CaCO <sub>3</sub> concentration Wt%	Mean	95% Confidence Interval	
		Lower Bound	Upper Bound
0	.720	.605	.835
5	.828	.713	.943
10	.850	.735	.965
20	.762	.647	.877
30	.857	.742	.972

**Table.4.3 Tests of Between-Subjects Effects – Dependent Variable**

Source	Type III Sum of Squares	df	Mean Square	F	Sig.
Corrected Model	.699 <sup>a</sup>	12	.058	4.179	.010
Intercept	16.131	1	16.131	1.157E3	.000
pH	.612	4	.153	10.969	.001
Temperature	.016	4	.004	.296	.875
CaCO <sub>3</sub> conc.	.071	4	.018	1.273	.334
Error	.167	12	.014		
Total	16.997	25			
Corrected Total	.867	24			

Table.4.2 indicated the dependent variable of fraction of removal by pH (A), temperature (B), and the concentration of CaCO<sub>3</sub> (C). As can be seen in the Table.4.2, the mean values varied for different levels, and the order of the influence of each factor level on the results were: A3>A4>A5>A2>A1, B2>B1>B4>B3>B5, C5>C3>C2>C4>C1. Table.4.3 revealed the significant order of the factors for the test results, i.e., A>C>B. The analysis of variance showed that the pH impact on the fraction of removal of dyes was significant (P <0.05); whereas temperature (B) had no significant effect on the dye removal, and the influence of CaCO<sub>3</sub> concentration was standing somewhere in between [36]. Combined with various factors, the optimal conditions for the dyes adsorption were A3B2C5. Due to the limited effect of the

concentration of CaCO<sub>3</sub>, C3 (20%) was selected in the following experiments. As a result, the optimal conditions were: pH 7, temperature 25°C, and 20% CaCO<sub>3</sub>, which, in fact, are the conditions easy to be accomplished in applications.

#### **4.3.5.2 Adsorption kinetics**

The adsorption kinetics was analyzed by employing pseudo-first-order, pseudo-second-order, and Elovich kinetics models to demonstrate the adsorption process of MB on MCMFCs. The parameters are illustrated in Table.4.4 and the effect of contact time is shown in Figure.4.5a from 5min to 150min. The pseudo-first-order and the pseudo-second-order are the models to imitate a surface-controlled adsorption rate. Another kinetic model, the Elovich kinetics, describes the adsorption that is limited by the surface-controlled adsorption onto energetically heterogeneous sites.

A good linearity was observed in the plot of  $t/q_t$  versus  $t$ , which was further confirmed by the high correlation coefficient ( $R^2 = 0.9989$  (20 °C),  $0.9997$  (25 °C), and  $0.9997$  (40 °C), respectively) determined by the pseudo-second-order model. These results revealed that the adsorption of MB onto the synthesized adsorbents were better fit using the pseudo second-order kinetic model, which indicated that the rate controlling step in adsorption of the dyes was the chemical-sorption between the adsorbent and adsorbate [37]. The rate constant ( $k_2$ ) of MCMFCs (40 °C) was higher than those of MCMFCs (25 °C) and MCMFCs (20 °C), indicating a faster uptake of dyes onto the adsorbents. In addition, the suitability of Elovich model ( $R^2 = 0.9702$  (20 °C),  $0.9760$  (25 °C), and  $0.9142$  (40 °C), respectively) indicated that the adsorption rate was limited by heterogeneous energetic barriers corresponded to the surface adsorption [38]. In

summary, for the case of dye adsorption onto the MCMFCs, the adsorption capacity is governed by the porous structure of adsorbent, the chemical adsorption sites, and the intra-particle diffusion. It seems like that one or more of these three factors control the MCMFCs adsorption rate under the different experimental conditions; whereas the correlation coefficient of pseudo-second-order is the highest, followed by pseudo-first-order and Elovich kinetics model. Thus, the faster adsorption rate might be related to the introduction of carboxylic groups in the adsorbents; and the chemical modification is essential in improving the adsorption capacity of MCMFCs.

From Figure.4.5a, the adsorption quantities increased rapidly in the initial 30 minutes with the fraction of removal at 90%; and the equilibrium was reached after 90 min for MB. The adsorption processes of MB onto the porous MCMFCs were essentially relevant to three continuous events, which were marked in Figure.4.5. The first step, circled via the black line, was due to an external or instantaneous surface adsorption process. The second step, indicated via the red line, was the gradual adsorption process, where the intraparticle diffusion was rate-controlled. The third step, circled via the purple line, was the equilibrium adsorption process, in which the intraparticle diffusion rate was low owing to the extremely low concentration of MB in solution [39].

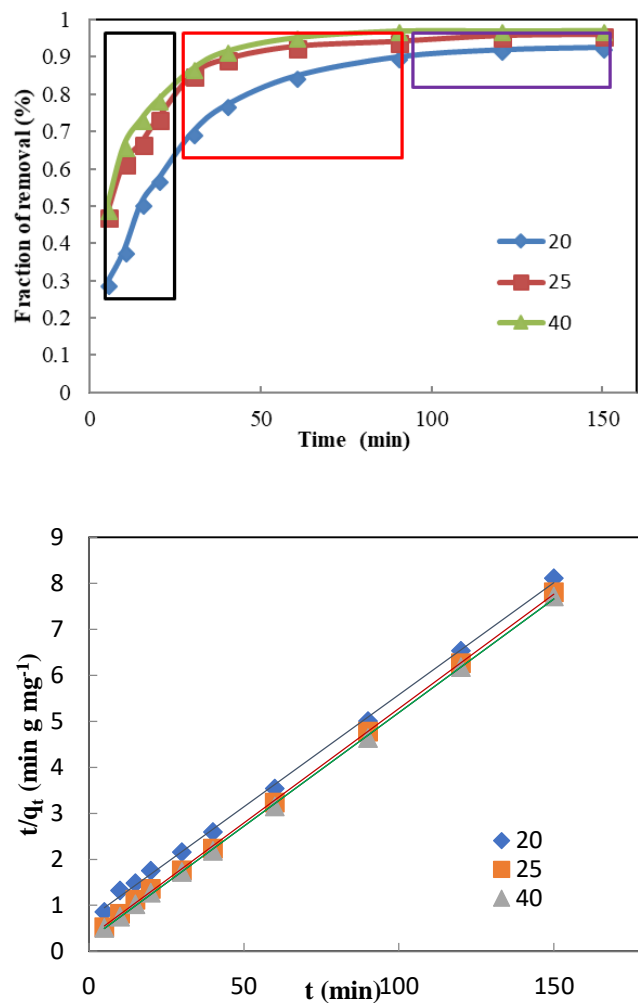


**Figure.4.5** The effect of contact time (a) and the linear of pseudo second order kinetic (b) at 20, 25, and 40 °C

**Table.4.4** The kinetic parameters for the pseudo-first, pseudo-second-order and Elovich models

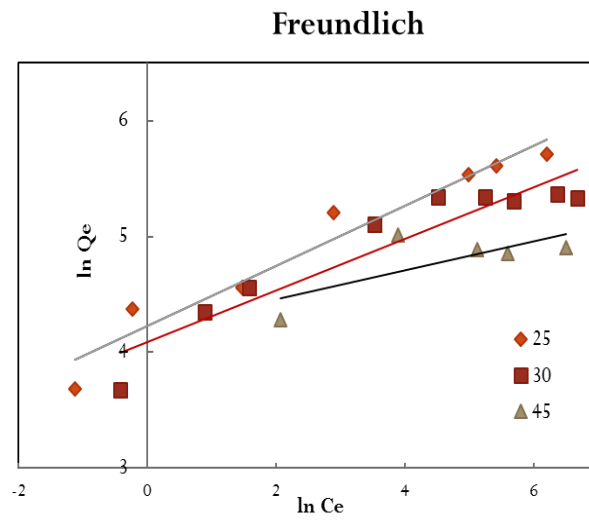
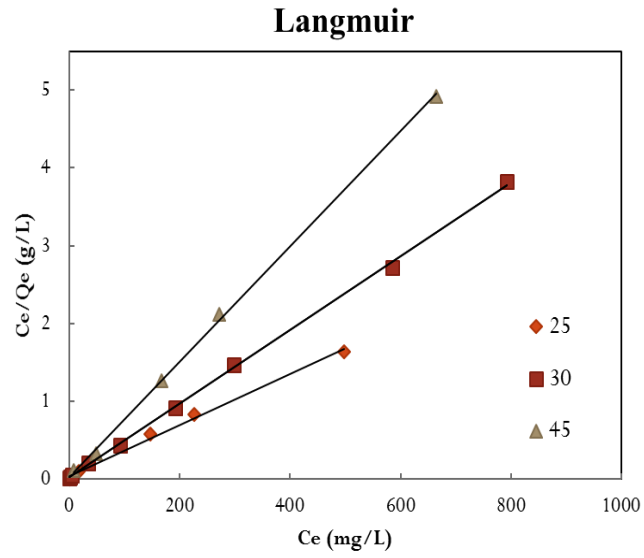
Adsorbate	Kinetics model	$Q_{e,exp}$ (mg/g)	$K_1$ (g mg <sup>-1</sup> min <sup>-1</sup> )	$K_2$ (g mg <sup>-1</sup> min <sup>-1</sup> )	$\alpha$	$\beta$	$R^2$
MB (20°C)	Pseudo-first-order	52.15	0.079	-	-	-	0.7620
	Pseudo-second-order	20.53	-	$3.36 \times 10^{-3}$	-	-	0.9989
	Elovich	-	-	-	3.371	0.2437	0.9702

MB (25°C)	Pseudo-first-order	9.641	0.041	-	-	-	0.9760
	Pseudo-second-order	20.08	-	$8.21 \times 10^{-3}$	-	-	0.9997
	Elovich	-	-	-	3.157	0.5088	0.9760
MB (40°C)	Pseudo-first-order	11.71	0.059	-	-	-	0.9804
	Pseudo-second-order	20.24	-	$9.84 \times 10^{-3}$	-	-	0.9997
	Elovich	-	-	-	32.61	0.3587	0.9142

### 4.3.5.3 Adsorption isotherms

Prior to studying the adsorption mechanism onto MCMFCs systematically, the experimental data were fitted using Langmuir, Freundlich, and Temkin isotherms. The results, imitated from different adsorption isotherms, are shown in Figure.4.6. The Langmuir plot of  $C_e/Q_e$  versus  $C_e$  showed a linear curve with the slope of  $1/Q_{\max}$  and intercept of  $1/(a*Q_{\max})$  as well as a higher  $R^2$  of 0.9992 at 45 °C (Figure.4.6a), demonstrating the excellent fit. In contrast, the Freundlich isotherm (Figure.4.6b) and Temkin isotherm (Figure.4.6c) had a much lower  $R^2$  of 0.5396 and 0.4725, respectively, showing a poorer fit. Therefore, the well-fitted Langmuir isotherm could well explain the adsorption process, i.e., MB adsorbed as a monolayer on the MCMFCs surfaces with the maximum adsorption capacity  $Q_{\max}$  at 301.76 mg g<sup>-1</sup>. In this study, the estimated adsorption capacity (303.03 mg g<sup>-1</sup>) is very close to the maximum dye uptake obtained experimentally. Such a high adsorption capacity enables MCMFCs to be a very promising green-based adsorbent for dye removal. The comparison of the dye

adsorption capacity of MCMFC with other adsorbents reported elsewhere is presented in Table.4.5.



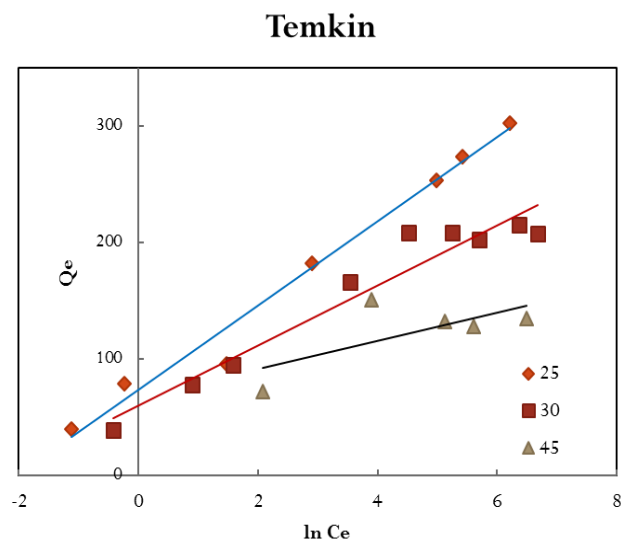


**Figure.4.6** Linear plots of Langmuir, Freundlich, and Temkin isotherm for adsorption on MCMFCs.

**Table.4.5** Comparison of dye adsorption capacity of MCMFCs with other adsorbents

Adsorbent materials	Adsorption capacity (mg/g)
Cellulose Nanocrystal [40]	MB: 106
Cellulose nanofibrils [41]	Malachite green (MG): 212.7
MCMFCs (this work)	MB: 303.03
MCDBs (previous work) [20]	MB: 117.65; MV: 62.11
APE/bentonite-CCMF (CAC) composite [42]	Brilliant Green (BG): 52.63
Hydrogel nanocomposites (HNCs) [43]	Rhodamine B (RhB): 137

#### 4.3.5.4 The effect of temperature

The thermodynamic parameters, such as enthalpy ( $\Delta H^\circ$ ), entropy ( $\Delta S^\circ$ ) and Gibb's free energy ( $\Delta G^\circ$ ) were determined using the Van't Hoff equation [44]. Table.4.6 lists the thermodynamic parameters obtained from the temperature effect on adsorption, the

values of free energy changes  $\Delta G^\circ$  are negative, confirming that adsorption of dyes onto MCMFCs is spontaneous and thermo-dynamically favorable. The more negative values of  $\Delta G^\circ$ , the greater driving force to the adsorption process. As the temperature increased, the  $\Delta G^\circ$  value decreased, indicating less driving force, and hence resulting in lesser adsorption capacity at higher temperatures. The value of  $\Delta H^\circ$  is negative, indicating that the adsorption process is exothermic in nature. The negative value of  $\Delta S^\circ$  indicates the stability of adsorption process with no structural change at solid-liquid interface.

**Table.4.6 The calculation of  $\Delta G^\circ$ ,  $\Delta H^\circ$ , and  $\Delta S^\circ$**

Temperature (K)	$\Delta G^\circ$ (kJ mol <sup>-1</sup> )	$\Delta S^\circ$ (kJ mol <sup>-1</sup> K <sup>-1</sup> )	$\Delta H^\circ$ (kJ mol <sup>-1</sup> )
298.15	-4.31	-0.0881	-35.93
303.15	-3.82		
313.15	-3.63		
318.15	-3.46		

#### 4.3.5.5 Regeneration Analysis

The regeneration was carried out by immersing the dye-laden adsorbent into hydrochloride acid (1mol/L) solution for 60 min. Once recovered, the MCMFCs were reused for the MB removal in future five cycles (Figure.4.7). The recycling of adsorbent is critical for the application, the desorption rate is presented along with the different cycle time. As can be seen from Figure.4.7, both desorption rate and fraction of removal of MB decreased gradually as the cycle time increased but maintained at 87.1% and 85.1% at the 5th recycle, respectively. Thus, the results demonstrate that MCMFCs is an efficient and cost-effective adsorbent with great potential for regeneration.

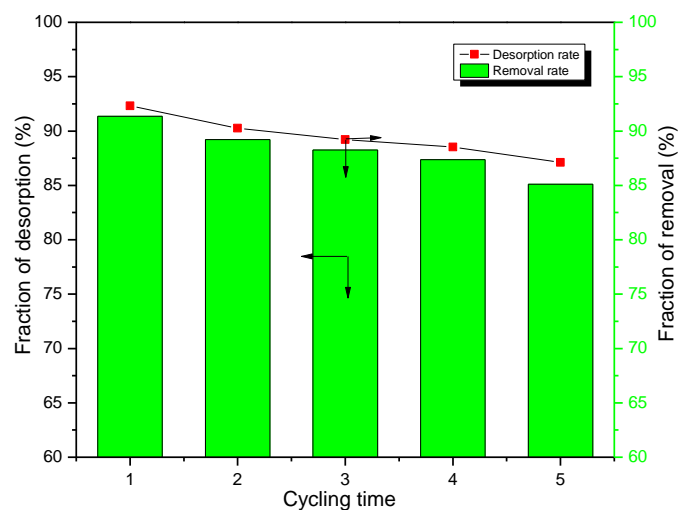


**Figure.4.7 Reusability of MCMFCs for MB adsorption (at the initial concentration of 20 mg/L at 298 K).**

#### **4.4 Conclusions**

In summary, an easily operated and environmentally-friendly process was developed to prepare green and renewable composite adsorbents which consist of dissolved cellulose fibres as matrix and microfibrillated cellulose as reinforced microparticles. The combination of microfibrillated cellulose not only significantly enhanced the adsorption efficiency but also simplified the operation, filtration, and separation. The grafted carboxyl groups on both dissolved cellulose fibres and MFC and large specific surface area of CMFCs created by pore forming agent are believed to be the key factors for the superior capacity of the adsorbents. The maximum adsorption capacity of adsorbent (Langmuir) toward methylene blue dye was  $303.03 \text{ mg g}^{-1}$ , which is higher than most bio-adsorbents reported elsewhere. Therefore, the MCMFCs are expected to be a

promising cost-effective and renewable absorbent for highly efficient removal of organic pollutants.

#### 4.5 References

- [1] Kumari, S.; Chauhan, G. S.; Ahn, J. H. Novel cellulose nanowhiskers-based polyurethane foam for rapid and persistent removal of methylene blue from its aqueous solutions. *Chem. Eng. J.* 2016, 304, 728-736.
- [2] Parida, K. M.; Sahu, S.; Reddy, K. H.; Sahoo, P. C. A Kinetic, Thermodynamic, and mechanistic approach toward adsorption of methylene blue over water-washed manganese nodule leached residues. *Ind. Eng. Chem. Res.* 2011, 50, 843-848.
- [3] Garg, V. K.; Kumar, R.; Gupta, R. Removal of malachite green dye from aqueous solution by adsorption using agro-industry waste: A case study of *Prosopis cineraria*. *Dyes Pigments.* 2004, 62, 1-10.
- [4] Banerjee, S.; Gautam, R. K.; Jaiswal, A.; Chattopadhyaya, M. C.; Sharma, Y. C.; Rapid scavenging of methylene blue dye from a liquid phase by adsorption on alumina nanoparticles. *RSC Adv.* 2015, 5, 14425-14440.
- [5] Hua, M.; Zhang, S.; Pan, B.; Zhang, W.; Lv, L.; Zhang, Q. Heavy metal removal from water/ by nanosized metal oxides: A review. *J. Hazard. Mater.* 2015, 211-212, 317-331.
- [6] Zhou, Q.; Lin, Y.; Shu, J.; Zhang, K.; Yu, Z.; Tang, D. Reduced graphene oxide-functionalized FeOOH for signal-on photoelectrochemical sensing of prostate-specific antigen with bioresponsive controlled release system. *Biosens. Bioelectron.* 2017, 98, 15-21.
- [7] Liu, S.; Xu, M.; Yu, T.; Han, D.; Peng, J.; Li, J.; Zhai, M. Radiation synthesis and performance of novel cellulose-based microsphere adsorbents for efficient removal of boron (III). *Carbohydr. Polym.* 2017, 174, 273-281.
- [8] Bhatnagar, A.; Hogland, W.; Marques, M.; Sillanpaa, M. An overview of the modification methods of activated carbon for its water treatment applications. *Chem. Eng. J.* 2013, 219, 499-511.
- [9] Keijbets, M. J. H. Potato Processing for the Consumer: Developments and Future Challenges. *Potato Res.* 2008, 51, 271-281.
- [10] Zhang, W.; Sha, Z.; Huang, Y.; Bai, Y.; Xi, N.; Zhang, Y. Glow discharge electrolysis plasma induced synthesis of cellulose-based ionic hydrogels and their multiple response behaviors. *RSC Adv.* 2015, 5, 6505-6511.

- [11] Jonoobi, M.; Oladi, R.; Davoudpour, Y.; Oksman, K.; Dufresne, A.; Hamzeh, Y.; Devoodi, R. Different preparation methods and properties of nanostructured cellulose from various natural resources and residues: a review. *Cellulose*. 2015, 22, 935-969.
- [12] Perez, S.; Samain, D. Structure and engineering of celluloses. *Adv. Carbohydr. Chem. Bi.* 2010, 64, 5-116.
- [13] Zhang, J.; Xiao, H.; Yang, Y. Preparation of hemicellulose-containing latex and its application as absorbent toward dyes. *J. Mater. Sci.* 2015, 50, 1673-1678.
- [14] O'Connell, D. W.; Birkinshaw, C.; O'Dwyer, T. F. Heavy metal adsorbents prepared from the modification of cellulose: A review. *Bioresource Technol.* 2008, 99, 6709-6724.
- [15] Pan, Y.; Wang, F.; Wei, T.; Zhang, C.; Xiao, H. Hydrophobic modification of bagasse cellulose fibers with cationic latex: Adsorption kinetics and mechanism. *Chem. Eng. J.* 2016, 302, 33-43.
- [16] Alain, D.; Danie, L. D.; Michel, R. V. Cellulose Microfilaments from Potato Tuber Cells: Processing and Characterization of Starch–Cellulose Microfibril Composites. *J. Appl. Polym. Sci.* 2000, 76, 2080-2092.
- [17] Wang, F.; Pan, Y.; Cai, P.; Guo, T.; Xiao, H. Single and binary adsorption of heavy metal ions from aqueous solutions using sugarcane cellulose-based adsorbent. *Bioresource Technol.* 2017, 241, 482-490.
- [18] Jiang, X.; Wang, S.; Ge, L.; Lin, F.; Lu, Q.; Wang, T.; Huang, B.; Lu, B. Development of organic-inorganic hybrid beads from sepiolite and cellulose for effective adsorption of malachite green. *RSC Adv.* 2017, 7, 38965-38972.
- [19] Luo, X.; Zhang, L. High effective adsorption of organic dyes on magnetic cellulose beads entrapping activated carbon. *J. Hazard. Mater.* 2009, 171, 340-347.
- [20] Li, Y.; Xiao, H.; Chen, M.; Song, Z.; Zhao, Y. Absorbents based on maleic anhydride-modified cellulose fibers/diatomite for dye removal. *J. Mater. Sci.* 2014, 49, 6696-6704.
- [21] Wang, Y.; Zhao, L.; Peng, H.; Wu, J.; Liu, Z.; Guo, X. Removal of anionic dyes from aqueous solutions by cellulose-based adsorbents: equilibrium, kinetics, and thermodynamics. *J. Chem. Eng. Data.* 2016, 61, 3266-3276.
- [22] Wu, H.; Bremner, D. H.; Wang, H.; Wu, J.; Li, H.; Wu, J.; Niu, S.; Zhu, L. Fabrication and investigation of a biocompatible microfilament with high mechanical performance based on regenerated bacterial cellulose and bacterial cellulose. *Mater. Sci. & Eng.: C.* 2017, 79, 516-524.

- [23] Cai, J.; Zhang, L. Unique gelation behavior of cellulose in NaOH/Urea aqueous solution, *Biomacromolecules*. 2006, 7, 183-189.
- [24] Dai, H. J.; Huang, H. H. Synthesis, characterization, and properties of pineapple peel cellulose-g-acrylic acid hydrogel loaded with kaolin and sepia ink. *Cellulose*. 2017, 24, 69-84.
- [25] Štefelová, J.; Slovák, V.; Siqueira, G.; Olsson, R. T.; Tingaut, P.; Zimmermann, T.; Sehaqui, H. Drying and Pyrolysis of Cellulose Nanofibers from Wood, Bacteria, and Algae for Char Application in Oil Absorption and Dye Adsorption. *ACS Sustainable Chem. Eng.* 2017, 5(3), 2679-2692.
- [26] Xie, P.; Li, Z.; Tian, Z. The optimal combination of mechanical ventilator parameters under general anesthesia in obese patients undergoing laparoscopic surgery. *J. Clin. Anesth.* 2016, 34, 290-294.
- [27] Wang, N.; Ouyang, X. K.; Yang, L. Y.; Omer, A. M. Fabrication of a Magnetic Cellulose Nanocrystal/Metal–Organic Framework Composite for Removal of Pb(II) from Water. *ACS Sustainable Chem. Eng.* 2017, 5(11), 10447-10458.
- [28] Zhou, H.; Gao, B.; Zhou, Y.; Qiao, H.; Gao, W.; Qu, H.; Liu, S.; Zhang, Q.; Liu, X. Facile preparation of 3D GO/CNCs composite with adsorption performance towards [BMIM][Cl] from aqueous solution. *J. Hazard. Mater.* 2017, 337, 27-33.
- [29] Luo, X.; Yuan, J.; Liu, Y.; Liu, C.; Zhu, X.; Dai, X.; Ma, Z.; Wang, F. Improved Solid-Phase Synthesis of Phosphorylated Cellulose Microsphere Adsorbents for Highly Effective Pb<sup>2+</sup> Removal from Water: Batch and Fixed-Bed Column Performance and Adsorption Mechanism. *ACS Sustainable Chem. Eng.* 2017, 5(6), 5108-5117.
- [30] Koushkbaghi, S.; Zakialamdari, A.; Pishnamazi, M.; Ramandi, H. F.; Aliabadi, M.; Irani, M. Aminated-Fe<sub>3</sub>O<sub>4</sub> nanoparticles filled chitosan/PVA/PES dual layers nanofibrous membrane for the removal of Cr(VI) and Pb(II) ions from aqueous solutions in adsorption and membrane processes. *Chem. Eng. J.* 2018, 337, 169-182.
- [31] Lu, J.; Askeland, P.; Drzal, L. T. Surface modification of microfibrillated cellulose for epoxy composite applications. *Polymer*. 2008, 49, 1285-1296.
- [32] Liu, L.; Gao, Z. Y.; Su, X. P.; Chen, X.; Jiang, L.; Yao, J. M. Adsorption Removal of Dyes from Single and Binary Solutions Using a Cellulose-based Bioadsorbent. *ACS Sustainable Chem. Eng.* 2015, 3(3), 432-442.
- [33] Zhao, H.; Kwak, J. H.; Zhang, Z. C.; Brown, H. M.; Arey, B. W.; Holladay, J. E. Studying cellulose fiber structure by SEM, XRD, NMR and acid hydrolysis. *Carbohydr. Polym.* 2007, 68, 235-241.

- [34] Lu, Q.; Li, X.; Tang, L.; Lu, B.; Huang, B. One-pot tandem reactions for the preparation of esterified cellulose nanocrystals with 4-dimethylaminopyridine as a catalyst. *RSC Adv.* 2015, 5, 56198-56204.
- [35] Aly, A. S.; Sokker, H. H.; Hashem, A.; Hebeish, A. Preparation of cellulosic membrane containing pyrrolidone moiety via radiation induced grafting and its application in wastewater treatment. *American J. Appl. Sci.* 2005, 2, 89-98.
- [36] Scott, W. F.; Lu, S.; Lo, C. N. Orthogonal polynomials, repeated measures, and SPSS. *Commun. Stat-Theor. M.* 2017, 46, 3342-3364.
- [37] Huang, H.; Wang, X.; Ge, H.; Xu, M. Multifunctional Magnetic Cellulose Surface-Imprinted Microspheres for Highly Selective Adsorption of Artesunate. *ACS Sustainable Chem. Eng.* 2016, 4(6), 3334-3343.
- [38] Schmidt, M. P.; Martínez, C. E. Kinetic and Conformational Insights of Protein Adsorption onto Montmorillonite Revealed Using in Situ ATR-FTIR/2D-COS. *Langmuir.* 2016, 32, 7719-7729.
- [39] Zhang, J.; Zhou, Q.; Ou, L. Kinetic, isotherm, and thermodynamic studies of the adsorption of methyl orange from aqueous solution by chitosan/alumina composite. *J. Chem. Eng. Data* 2012, 57, 412-419.
- [40] Nekouei, F.; Nekouei, S.; Keshtpour, F.; Noorizadeh, H.; Wang, S. Cr(OH)<sub>3</sub>-NPs-CNC hybrid nanocomposite: a sorbent for adsorptive removal of methylene blue and malachite green from solutions. *Environ. Sci. Pollut. R.* 2017, 24, 1-18.
- [41] Jiang, F.; Dinh, D. M.; Hseih, Y. Adsorption and desorption of cationic malachite green dye on cellulose nanofibril aerogels. *Carbohydr. Polym.* 2017, 173, 286-294.
- [42] Azha, S. F.; Shahadat, M.; Ismail, S. Acrylic polymer emulsion supported bentonite clay coating for the analysis of industrial dye. *Dyes Pigments.* 2017, 145, 550-560.
- [43] Hosseinzadeh, H.; Bahador, N. Novel CdS quantum dots templated hydrogel nanocomposites: Synthesis, characterization, swelling and dye adsorption properties. *J. Mol. Liq.* 2017, 240, 630-641.
- [44] Namasivayam, C.; Yamuna, R. T. Adsorption of chromium (VI) by a low-cost adsorbent: Biogas residual slurry. *Chemosphere.* 1995, 30, 561-578.

## **Chapter 5 Novel cellulose filaments based composite spheres: microwave-assisted synthesis, characterization, and application in water treatment<sup>4</sup>**

### **ABSTRACT**

A novel method for synthesizing temperature-responsive polymer-modified cellulose filaments/Poly (N-isopropylacrylamide) spheres (P-MCCBs) was successfully developed in this study. The cellulose filaments spheres were first prepared using a vacuum drying method in the presence of a pore forming agent (nano-sized CaCO<sub>3</sub>). Afterwards, NIPAM (N-isopropylacrylamide), a temperature-sensitive monomer, was polymerized and grafted onto the cellulose filaments spheres through in situ free radical polymerization by using microwave-assisted polymerization. The morphology, chemical structure, and thermal sensitivity of the spheres were characterized. The dye and heavy metal desorption capability of hybrid spheres were also investigated. The spheres grafted with PNIPAM exhibited a controllable desorption rate at different temperatures (25 and 45 °C). The temperature effect on the dye and heavy metal adsorption rate was also observed. The adsorption kinetics followed the pseudo-second-order model, and the desorption process could be fit by using Higuchi and Korsmeyer-Peppas models. These results indicated that porous P-MCCBs could act as a novel material for controllable adsorption and desorption processes of contaminants (Methylene Blue and Pb<sup>2+</sup>).

---

<sup>4</sup> This chapter has been submitted on Journal of Environmental Management, the format follows the requirements of the Journal. The entire experimental work was performed by the candidate Yuan Li along with the preparation of the manuscript.

**Keywords:** Cellulose filaments spheres, Microwave-assisted, Thermal-responsive, Kinetics.

## 5.1 Introduction

The rapid development of economy and expanding industrial activities introduced the increasing levels of hazardous dyes and heavy metal ions into waste water, which has been accepted as major concerns of our environment [1]. These contaminants are hazardous and endanger humans at even low concentrations. Dyes and toxic heavy metal ions are utilized in the most industrial units such as printing, leather, mining, textile, pulp mills, etc [2]. The industrial wastewaters should be discharged with adequate treatment due to the potentially endanger the environment. However, the degradation products are also carcinogenic and cannot be degraded or destroyed [3]. Among the conventional methods such as ion exchange, chemical precipitation, solvent extraction, adsorption etc., the adsorption onto a solid substrate is dominating due to the benefits such as cost effective, high efficient, easy operating, and without by-products [4]. A variety of adsorbents have been studied by researchers in recent years [5-7]. To minimize the shortages of utilizing activated carbon, some low-cost adsorbents, such as agricultural by-products [8], bio-adsorbents [8], diatomite, and clay, have been investigated widely. Particularly, cellulose, as a natural material, gained increasing emphasis as an efficient solution for the wastewater treatment [10].

Recently, smart materials, thermo- and pH-responsive materials, were reported by some researchers [11-13] which could be utilized in the fields of biotechnology and pharmaceutical. Poly (N-isopropyl acrylamide) (Poly-NIPAM), an insoluble polymer

with the lower critical solution temperature (LCST) at 32 °C, was usually used as the thermo-sensitive polymer to prepare thermos-responsive materials [14], Pan et al. [15] synthesized thermo-responsive regenerated cellulose membranes by grafting with PNIPAM using atom transfer radical polymerization (ATRP), and found the membranes had obvious thermally modulated properties. Yang et al. [16] synthesized cellulose-graft-poly (N-isopropylacrylamide) (cellulose-g-PNIPAM) copolymers, which exhibited clear temperature-sensitive behavior and might be attractive substrates for some biomedical applications, such as drug release and tissue engineering. In addition, the typical pH-sensitive polymers including poly (acrylic acid) (PAA) [17] and poly(4-vinylpyridine) (P4VP) [18] have been reported as a stable and highly binding capacity resources compared to the low-molecular-weight species. Up to now, the functional materials with dual-responsive properties have been reported. Jin et al. [19] prepared a kind of core-shell hybrid composite as a drug carrier, copolymer poly(N-isopropylacrylamide)-co-poly(acrylic acid) [P(NIPAM-co-AA)] with pH- and temperature-responsive characteristics was introduced to control the properties of the composite. Thermo- and pH-responsive N-isopropylacrylamide (NIPAM) nanogels were synthesized by copolymerization of acrylic acid (AA) comonomer through differential microemulsion polymerization, the as-prepared nanogels had higher drug release properties [20]. Furthermore, some researchers have studied the microwave-assisted polymerization due to the drawbacks of conventional method including the uncontrollable reaction rate, long reaction time, and by-products, which includes step-growth polymerizations [21], free radical polymerizations [22], and ring-opening polymerizations [23].

In this study, we synthesize temperature-responsive composite cellulose filaments/Poly (N-isopropylacrylamide) (CF/Poly-NIPAM) spheres via microwave-assisted synthesis. The precipitated cellulose/CF composite spheres will be firstly prepared, afterwards, the modification of as-prepared spheres will be carried out by microwave-assisted synthesis featuring temperature responsiveness through free radical polymerization using N, N'-methylenebisacrylamide (MBA) as the crosslinker and potassium persulfate (KPS) as the initiator. The synthesized adsorbents were characterized using FTIR, TGA, and SEM. Finally, the as-synthesized adsorbents were applied for the adsorption of methylene blue (MB) ions, as a representative of dyes, and lead (Pb (II)) ions, as a representative of heavy metals, from aqueous solution.

## **5.2 Experimental**

### **5.2.1 Materials**

The source of cellulose was filter paper (Qualitative P4, Fisher Scientific). Microfibrillated cellulose (MFC) was kindly provided by FPInnovations Canada (Pointe Claire, QC, Canada), which was obtained via processing cellulose fibres mechanically based on a technology invented by FPInnovations. The resulting fibres in nano- or micro- range have the lengths from 50 to 800  $\mu\text{m}$  with the aspect ratios from 300 to 3000 and high surface area ( $> 80 \text{ m}^2/\text{g}$ ).  $\text{CaCO}_3$  nanoparticles (Product # 1951RH,  $\leq 30\text{nm}$ , 97.5%) was supplied by SkySpring Nanomaterials, Inc. Sodium hydroxide (solid), maleic anhydride (MA), urea, methylene blue, Lead (Pb (II)) nitrate, N-isopropylacrylamide (NIPAM), all purchased from Sigma-Aldrich Chemical Co., N, N'-

methylenebisacrylamide (MBA), N, N, N, N-tetramethylethylene diamine (TEMED), and potassium persulfate (KPS) were all of analytical grade chemicals (Aldrich).

## **5.2.2 Experimental methods**

### **5.2.2.1 Preparation of precipitated cellulose/CFs composite spheres**

The synthesis of polymer grafted precipitated cellulose/CFs composite spheres (P-MCCBs) were carried out by following procedures: commercial filter paper and CFs were used as the starting material for the preparation of precipitated cellulose/CFs composite spheres. Dry cellulose was dissolved by using the matrix solution (7% NaOH/12% urea) at -10 °C, and then the CFs and the pore forming agent (CaCO<sub>3</sub>) were dispersed in the cellulose solution using a high-speed shear homogenizer (Stanfen, Germany) for 5 min to obtain a constant CFs suspension. After that, the CFs suspension was added into 1N HCl solution dropwise. The precipitated cellulose/CF composite spheres were formed, at the mean time, the pore forming agent was dissolved by HCl. The as-prepared spheres were then washed with distilled water and acetone for several times and finally dried via a vacuum drying process.

### **5.2.2.2 Microwave-assisted synthesis of polymer grafted precipitated cellulose/CFs composite spheres**

The preparation of carbonylated cellulose/CFs composite spheres (MCCBs) was reported in our previous work [24]. The polymer grafted precipitated cellulose/CFs composite spheres (P-MCCBs) were prepared by concurrent crosslinking and microwave-assisted free radical polymerization of NIPAM inside the MCCBs (as

indicated in Figure.5.1). First, prior to make a uniform solution, the monomer NIPAM, the crosslinking agent MBA and initiator KPS were dissolved in distilled water by gently stirring. The concentrations of NIPAM were controlled by 5, 10, and 15% (w/v), respectively. The MBA and KPS concentrations were 10% and 2% based on the weight of NIPAM. Afterwards, the dry MCCBs were soaked in the mixed solution. The spheres were saturated by gently shaking at 130 rpm using the shaker (SWB25, Thermo Electron Corporation, Germany). The excess solution was removed, and the sample was transferred into the baker containing paraffin oil and emulsifier span 80. The sample was fully dispersed by vigorous shaking and transferred into the microwave reactor. The proper conditions were used for the polymerization (70 °C and 100 w). After the polymerization at different reaction time, the P-MCCBs composites were washed by excessive distilled water and acetone several times. The purified sample was dried by a vacuum-drier. The corresponding samples were named P1-MCCBs, P2-MCCBs, and P3-MCCBs according to the concentrations of NIPAM during the process of preparation.

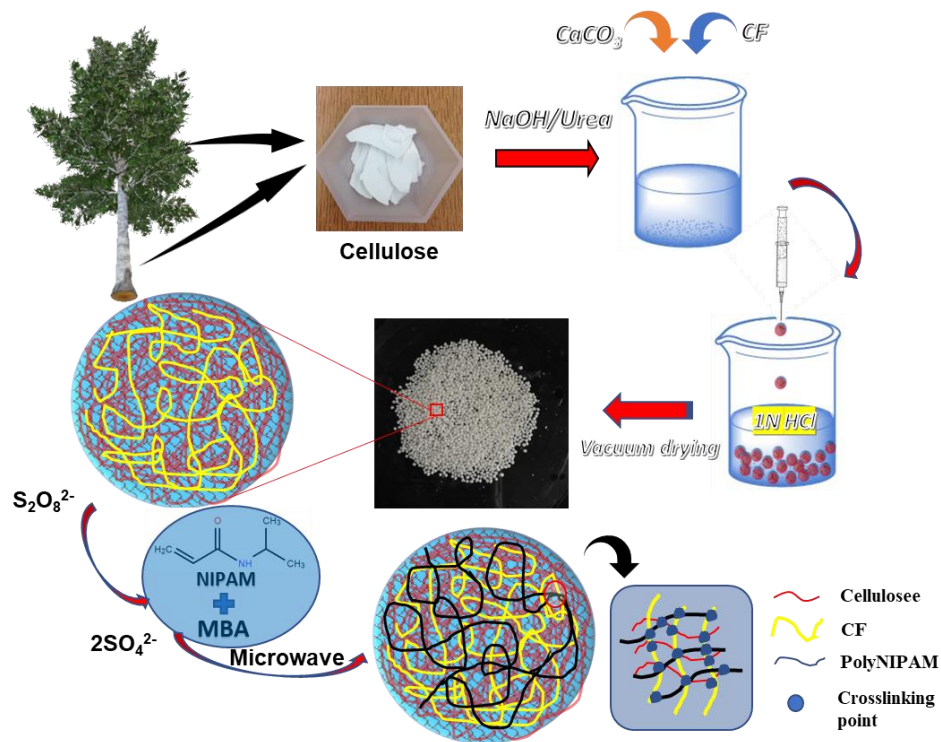


Figure.5.1 The preparation of polymer grafted precipitated cellulose/CFs composite spheres (P-MCCBs)

### 5.2.3 Characterization of P-MCCBs

The samples were grinded and analyzed by Fourier transform infrared spectroscopy (FTIR). The test was carried out using NEXUS 470 spectrophotometer (Nicolet Thermo Instruments, Canada) with a detector at  $1\text{ cm}^{-1}$  resolution from  $500$  to  $4000\text{ cm}^{-1}$  and 16 scans per sample. Thermal stability of the adsorbents was tested by using Thermogravimetric Analyzer (TGA, Q600, TA Instruments, USA). Approximately 10 mg of the samples was used for every test. The experiment was carried out at a heating rate of  $10\text{ }^{\circ}\text{C min}^{-1}$  under nitrogen flow of  $100\text{ ml min}^{-1}$ . Scanning electron microscopy (SEM, JEOL JSM-6400, Japan) was used for morphological characterization. Prior to

observation, samples were attached to the holders and coated with gold before the tests. Bulk density was tested by transferring a known quality of adsorbents to a measuring cylinder and repeat three times. The bulk density of the samples was calculated by dividing the weight (g) by the volume (cm<sup>3</sup>).

#### **5.2.4 Adsorption of MB and Pb<sup>2+</sup>**

Prior to study the effect of shaking time, temperature, and pH, the batch mode adsorption was carried out in this experiment. The stock solutions of 1000 mg L<sup>-1</sup> MB and Pb<sup>2+</sup> were prepared by dissolving a certain amount of MB and Pb(NO<sub>3</sub>)<sub>2</sub> into the distilled water and the working concentrations were obtained by diluting the stock solutions accurately.

Adsorption experiments were conducted at a constant speed of 130 rpm using 50 mL glass containers containing 10 mg of adsorbents with 10 mL of MB and Pb<sup>2+</sup> solution at a controlled temperature. The temperature-controlled shaker (SWB25, Thermo Electron Corporation, Germany) was used during the adsorption process at a fixed agitation speed at 130 rpm for all experiments. The initial pH of the solutions was adjusted by adding 1 M HCl or 1 M NaOH. The optimal pH was determined and used throughout the adsorption experiments. The concentration of MB was measured using a UV-vis spectrophotometer (Genesys 10-s, Thermo Electron Corporation) and the concentration of Pb<sup>2+</sup> was detected by using Inductive Coupled Plasma Emission Spectrometer (VISTA-MPX CCD, USA). The adsorption capacity of MB and Pb(II) ( $Q_e$ ) was calculated by Eq 5.1:

$$Q_e = (C_i - C_e) \times V/W \quad \text{Eq 5.1}$$

where  $C_i$  and  $C_e$  are initial and equilibrium concentrations (mg/L), respectively;  $W$  is the mass of the samples (g); and  $V$  is volume of the solution (L).

The removal percentage was presented by Eq 5.2:

$$R = (C_i - C_e)/C_i \quad \text{Eq 5.2}$$

where  $C_i$  and  $C_e$  have been mentioned above (mg/L).

### 5.2.5 Desorption of MB and $Pb^{2+}$

The feasibility of desorption of the adsorbents was investigated using 0.001 mol/L HCl (pH ~3). After agitating 10 mg of the dried adsorbents with 10 mL of MB and  $Pb^{2+}$  solution at a controlled temperature under optimum conditions, MB and  $Pb^{2+}$  loaded adsorbent was washed, dried, and added into 5 mL of 0.001 mol/L HCl solution for desorption at 130 rpm. The desorption rate at each period was calculated.

## 5.3 Results and discussion

### 5.3.1 FTIR spectra

The FTIR spectra of MCCBs, P3-MCCBs, and dye-laden MCCBs are compared in Figure.5.2. For MCCBs, the absorption bands at 3400 and 2900  $cm^{-1}$  were corresponded to the stretching of O-H and C-H bonds, respectively. The absorbance at 1636  $cm^{-1}$  was associated with O-H bending vibration of the absorbed water and the vibration of vinyl groups (C=C). The band 1430  $cm^{-1}$  was due to the in-plane bending vibrations of H-CH and O-CH groups from cellulose. The peak at 1722  $cm^{-1}$  attributed to the carbonyl groups (C=O) [25]. After the polymerization, the peaks at 1563, 1636, and 1722  $cm^{-1}$  were due to amide groups and N-H groups of NIPAM. The absorption band of isopropyl

groups at  $1372\text{ cm}^{-1}$  was also observed in the spectra. In addition, the peak at  $1722\text{ cm}^{-1}$  was weakened after polymerization, indicating that the carboxyl groups were occupied during the reaction. This peak was even weaker after the adsorption of dye, revealing that the carboxy groups participated in the adsorption process. Moreover, the peak attributed to  $\text{-OH}$  stretching ( $3440\text{ cm}^{-1}$ ) was widened after polymerization, which further revealed the reaction between the hydroxyl groups and the monomer during polymerization. These results indicated that the preparation of carbonylated MCCBs was successful and the P-MCCBs had been successfully synthesized through radical polymerization using microwave-assisted synthesis.

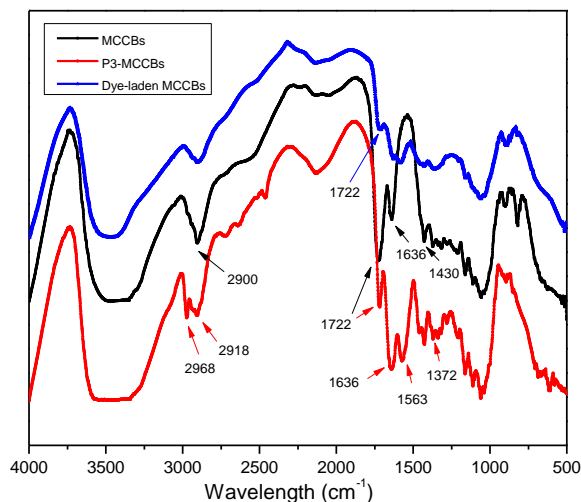


**Figure.5.2** FTIR spectra of MCCBs, P3-MCCBs, and Dye-laden MCCBs

### 5.3.2 SEM images

The SEM images of pure cellulose spheres and P3-MCCBs are shown in Figure.5.3. From Figure.5.3a, clearly, the pure cellulose spheres were highly porous, and the

morphology of precipitated cellulose and the CFs appeared as a heterogeneous network structure. Figure.5.3b and Figure.5.3c indicated the cross-section of pure cellulose spheres, where the inner morphology of the spheres could be identified dramatically. The precipitated cellulose reinforced with CFs successfully and formed the pores at various sizes. More importantly, the individual CFs could be clearly observed in Figure.5.3c, demonstrating the successful application of nano-CaCO<sub>3</sub> in pore forming processes. The SEM images (d and e) showed that PNIPAM polymer chains were distributed in the cellulose spheres network. The morphology of P3-MCCBs (d and e) hybrid spheres was significantly different from that of cellulose spheres (a, b, and c). Though the P3-MCCBs were less porous than cellulose spheres, the porous structure with different pore sizes was also clearly seen on the SEM image (Figure.5.3e). Due to the uneven porous structure of cellulose spheres, the pore size of P3-MCCBs varied widely from nanometers to even micrometers [26].

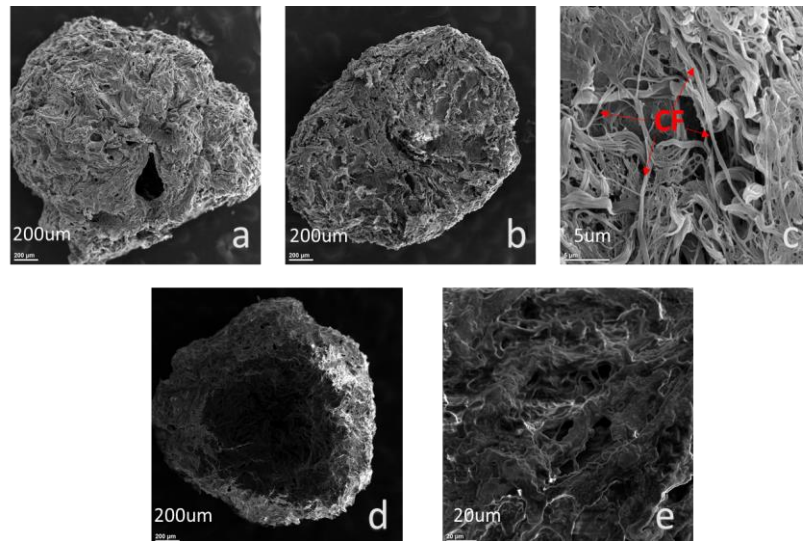


**Figure.5.3 SEM images (a, b, and c - cellulose spheres; d and e - P3-MCCBs)**

### 5.3.3 TGA

The TG and DTG curves show the thermal stability and the temperatures of decomposition, respectively. The Figure.5.4 revealed that the thermal decomposition of pure cellulose spheres mainly occurred at temperatures at 50 and 302 °C, where 10 and 60% of the total weight were thermally degraded. From the DTG curves of P3-MCCBs, the maximum decomposition rate occurred at about 314 °C, which indicated that the thermal stability of P3-MCCBs was significantly different from that of pure cellulose spheres because of the properties such as high specific area, porous structure, etc. Particularly, from DTG curve of P3-MCCBs, the decomposition rates were observed at about 225 and 380 °C, which reflected the thermal decomposition of the Poly-NIPAM staying in the channels of the spheres and the Poly-NIPAM grafted cellulose spheres. By comparing the pure cellulose spheres and P3-MCCBs, P3-MCCBs showed higher thermal stability than pure cellulose spheres, indicating that the polymerization obviously affected the thermal stability of cellulose spheres.

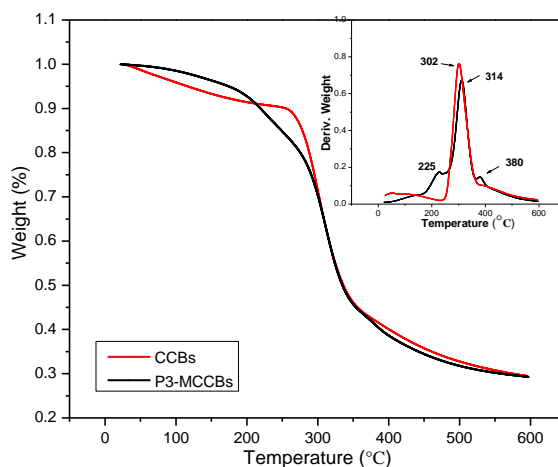


**Figure.5.4 TG and DTG curves of pure cellulose spheres and P3-MCCBs.**

### 5.3.4 Bulk density of the spheres

Bulk density reflects the quality of the spheres, the porous structure of the adsorbents, and further evaluates the potential of the spheres. It can be calculated by dividing the weight by the volume of the spheres. The volume was determined by transferring a certain quantity of spheres to a measuring cylinder. The corresponding results are indicated in Figure.5.5. Clearly, the bulk density of MCCBs increased with the increase of monomer ratio, showing an almost linear proportion to the NIPAM content, which indicated that more polymer had been grafted on or entrapped in the MCCBs. Ideally, the hydroxyl groups on the spheres could react with NIPAM via polymerization and no more active hydroxyl groups remained on the chains of cellulose and CFs. In this case, the more monomers added, the more polymers were produced. Such phenomenon matched the results of bulk density dramatically.

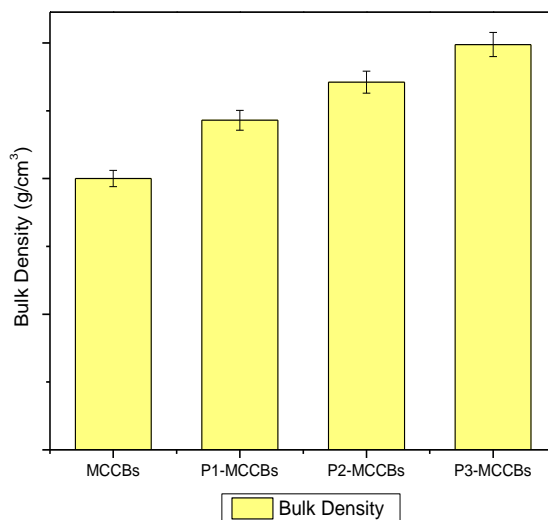


Figure.5.5 Bulk density of the polymer-modified spheres.

### 5.3.5 The effect of reaction time (microwave-assisted)

Fig.5.6 indicates the graft efficiency and weight gain of P3-MCCBs at the function of reaction time. As shown in Figure.5.6, the graft efficiency of P3-MCCBs increased dramatically along with the reaction time, reached 65% within 5 minutes. At the meantime, the weight gain was around 18.22%. In addition, when the reaction time was 10 minutes, the graft efficiency and weight gain of P3-MCCBs were 81% and 23%, respectively, showing a fast reaction process via microwave-assisted polymerization. When the reaction time was further increased to 20 minutes, the graft efficiency of P3-MCCBs increased up to 95.38%, and such efficiency peaked at 96.25% with the reaction time of 30 minutes, with the weight gain maintained at 28.01%. These results reflected that the microwave-assisted polymerization was a fast and stable process along with the high graft efficiency of monomers. The reaction time was set to 20 minutes in the following experiments.

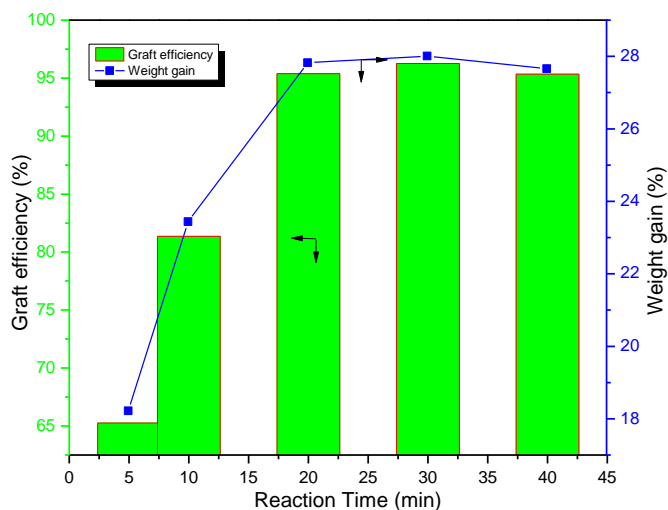


Figure.5.6 The graft efficiency and weight gain versus reaction time (5, 10, 20, 30, and 40min).

### 5.3.6 The graft efficiency of P1-MCCBs, P2-MMCCBs, and P3-MCCBs

The microwave-assisted polymerization was carried out by using the different concentrations of NIPAM (5, 10, and 15% w/v) with the optimal reaction time of 20 minutes, the corresponding results are indicated in Figure.5.7. From Figure.5.7, the polymerization accomplished in 20 minutes with the graft efficiency of P1-MCCBs, P2-MMCCBs, and P3-MCCBs at 88.84, 97.29, and 95.38%, respectively. Meanwhile, the weight gain was 6.34, 15.4, and 27.82%, reflecting a gradual increase. Such phenomenon revealed that the polymerization could be microwave accelerated and high efficiency could be obtained via microwave-assisted polymerization.

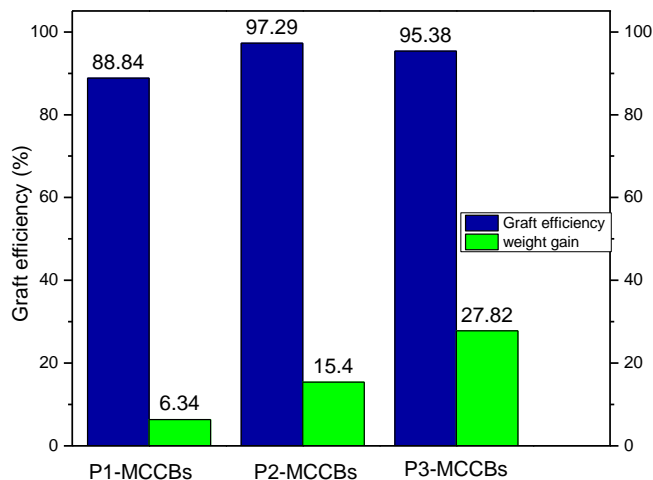
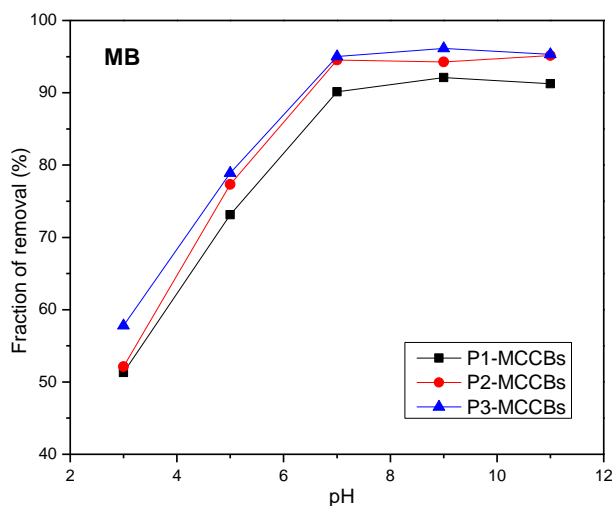


Figure.5.7 The graft efficiency of P1-MCCBs, P2-MMCCBs, and P3-MCCBs.

### 5.3.7 pH effects on the adsorption of MB and Pb<sup>2+</sup>

The removal of dye (MB) and heavy metal ion (Pb<sup>2+</sup>) as a function of pH were studied by varying the pH range from 3 to 11 and 2 to 6, respectively. The corresponding results

are shown in Figure.5.8. In aqueous solutions,  $Pb^{2+}$  is dominant at pH 2-6; other species ( $PbOH^+$ ) can exist at a higher pH. However, the dyes are stable to pH values. Generally, the pH value of solution is an important influencing factor affecting the adsorption of dyes and heavy metal ions. As shown in Figure.5.8, the fraction of removal of MB was extremely low and even lower for  $Pb^{2+}$ , indicated that the lower pH values of the solution, the lower adsorption capability of pollutants. The pH affects the concentration of hydrogen ions in the solution, which can compete with the dyes and heavy metal ions for the limited adsorptive sites on the adsorbents, resulting in the lower fraction of removal in the acidic conditions. As the pH value increased, the surface of adsorbents was negatively-charged, electrostatic attraction between pollutants and adsorbents was stronger than that in acidic conditions. Thus, the optimum pH values for the adsorption of MB and  $Pb^{2+}$  were found to be pH 7.0 and 6.0, respectively.



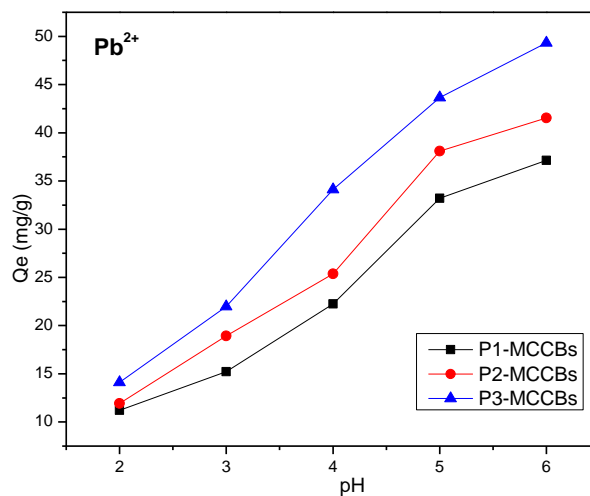


Figure.5.8 MB adsorption process by using polymer-modified spheres.

### 5.3.8 Dye and heavy metal adsorption at different temperatures

Prior to investigate the adsorption properties of polymer-modified spheres, the batch mode adsorption was carried out under the following conditions: pH was 7.0 for MB and 6.0 for  $Pb^{2+}$ ; initial concentrations of MB and  $Pb^{2+}$  were 40 and 50 ppm; the temperature was predetermined at 25 °C, followed by 45 °C after equilibrium; the adsorbent dosage was 1000 mg/L. The plots of adsorption abilities versus contact time are shown in Figure.5.9. The adsorption equilibrium was attained within 120 minutes for MB and 60 minutes for  $Pb^{2+}$ , respectively. The adsorption process of MB was fast in the initial 50 minutes and followed by a gradual adsorption process. The equilibrium reached when the fraction of removal was up to 95 %. In addition, the adsorption of  $Pb^{2+}$  by P-MCCBs was high and quick in the initial 40 minutes and leveled off afterwards. The adsorption capacity of P3-MCCBs was 42.5 mg g<sup>-1</sup>, while the amount of  $Pb^{2+}$

adsorbed by P1-MCCBs and P2-MCCBs was lower, 34 and 40 mg g<sup>-1</sup>, respectively. The thermal properties of the adsorbents could be revealed while the temperature of solution being changed to 45 °C. From Figure.5.9 and Figure.5.10, an obvious drop could be observed for the adsorption of MB and Pb<sup>2+</sup>, around 5-8% of adsorbed MB was released rapidly as the temperature changed, and the drop of Pb<sup>2+</sup> was around 20% as the temperature increased, which revealed that the adsorption of MB was more stable than that of Pb<sup>2+</sup> by using polymer grafted spheres. Figure.5.9 and Figure.5.10 indicated that P3-MCCBs reflected more thermal responsive properties than P1-MCCBs and P2-MCCBs, which were applicable for both MB and Pb<sup>2+</sup>. Ideally, the grafted Poly (N-isopropyl acrylamide) (Poly-NIPAM) shows a conformational change above the lower critical solution temperature (LCST) at 32 °C [27], resulting in the systole of Poly-NIPAM, where the structure of the spheres changed, and some molecules of MB were finally desorbed into the solution. Such process was reversible, indicating the successful synthesis of the “smart” adsorbents.

Prior to systematically investigate the comparison of adsorption capacity when temperature changed, the adsorbent P3-MCCBs was used in batch mode adsorption. The temperature was fixed at 25 and 45 °C and the corresponding results are indicated in Figure.5.11 and Figure.5.12. The adsorption processes could be divided to three continuous stages: the first stage, happened from 0 to 30 minutes, was the external surface adsorption; the second stage was gradual adsorption, in which the intraparticle diffusion was rate-controlled; the last stage was the equilibrium adsorption, where the low adsorption rate was due to the relatively low concentrations of MB and Pb<sup>2+</sup> in the solution. In addition, the adsorption capability of P3-MCCBs towards MB and Pb<sup>2+</sup> at

25 °C was stronger than that at 45 °C, showed that the lower temperature was conducive to the adsorption of adsorbate. The adsorptive sites on the adsorbents are limit based on the mechanism of adsorption. The Poly-NIPAM shrank when the temperature was over LCST and rendered the change on the morphology of P3-MCCBs. In this case, fewer adsorptive sites will be available for the MB and  $Pb^{2+}$  when the ambient temperature increased to 45 °C. The adsorption abilities therefore decreased with the increase of temperature.

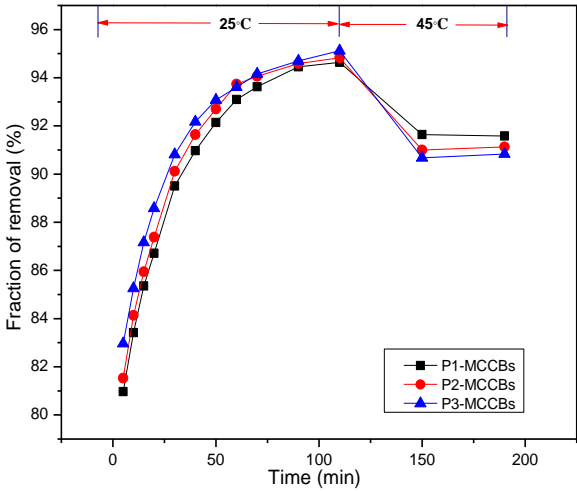


Figure.5.9 MB adsorption process by using polymer-modified spheres.

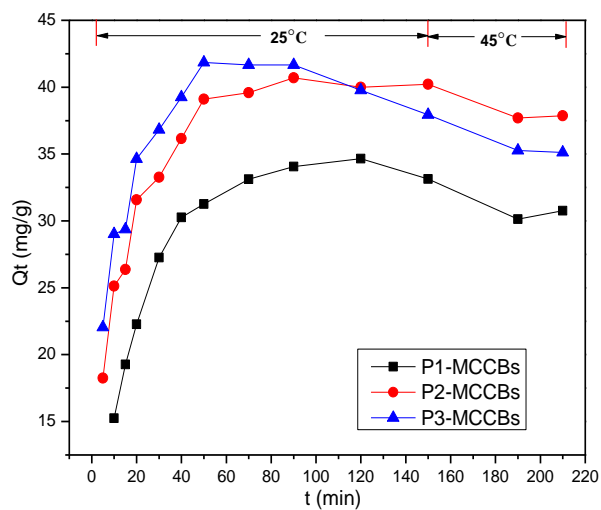


Figure.5.10  $Pb^{2+}$  adsorption process by using polymer-modified spheres.

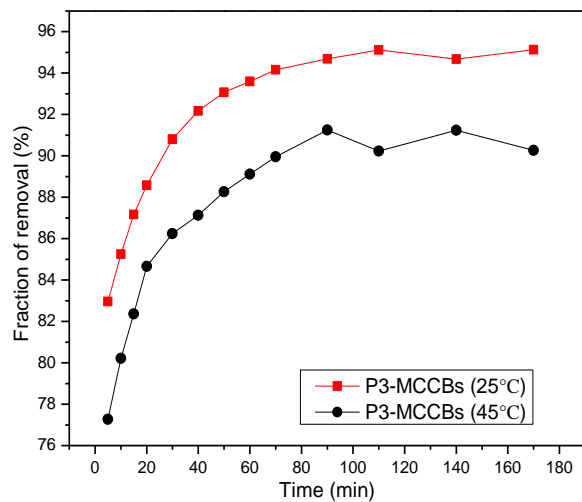
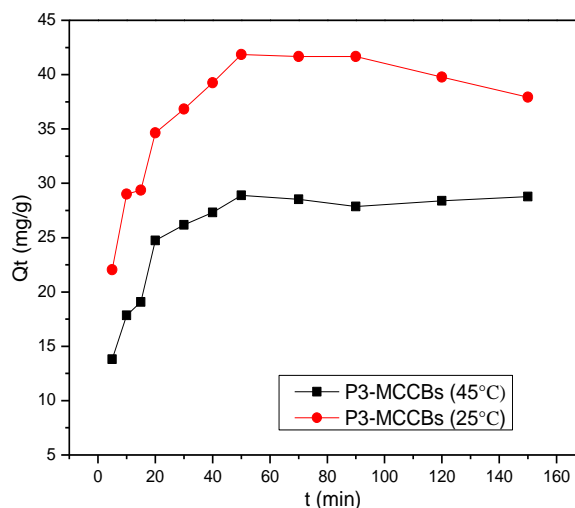


Figure.5.11 MB adsorption process at different temperatures.

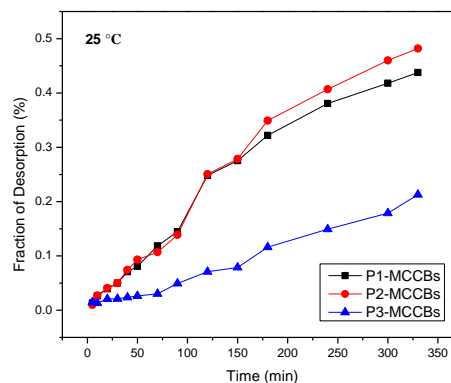
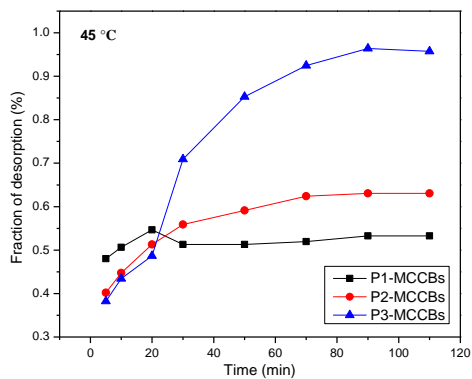


**Figure.5.12 Pb<sup>2+</sup> adsorption process at different temperatures.**

### 5.3.9 The MB desorption behaviors

Figure.5.13 shows the MB and Pb<sup>2+</sup> desorption from P1-MCCBs, P2-MCCBs, and P3-MCCBs at pH 7.0 and temperatures at 25 and 45 °C. MB and Pb<sup>2+</sup> were used as a model contaminant to study the relationship between desorption rates from different adsorbents at different temperatures. From Figure.5.13, P3-MCCBs exhibited a much higher desorption rate compared with other adsorbents at 45 °C for both MB and Pb<sup>2+</sup>. However, the desorption rate at 25 °C reflected an opposite trend, where the desorption rate of P3-MCCBs was lower than that of P1-MCCBs and P2-MCCBs. Such phenomenon has not been observed on P1-MCCBs and P2-MCCBs, indicating the thermal sensitive property of P3-MCCBs, which presumably due to the higher ratio of Poly-NIPAM grafted on the adsorbents. In addition, the thermal properties of P1-MCCBs and P2-MCCBs were not obvious, both adsorbents reflected the same trend of

desorption processes as the time increased, which may due to the lower ratio of Poly-NIPAM on the adsorbents. In this study, two factors control the desorption of model contaminant: the diffusivity of the pollutant and the swelling of the polymer [28]. Because there are fewer Poly-NIPAM molecules inside the P1-MCCBs and P2-MCCBs, the porous structure and polymer would maintain unchanged as the temperature changed, the model contaminant can diffuse out of the adsorbents with similar apparent resistance. However, the porous morphology of P3-MCCBs changed due to the systole of Poly-NIPAM, resulting in lower swelling capacity and higher desorption rate at the temperature at 45 °C. These results indicated that the introduction of Poly-NIPAM chains in the MCCBs could make the dye and heavy metal desorption controllable. The mechanism of desorption and adsorption will further be studied in the following sections.



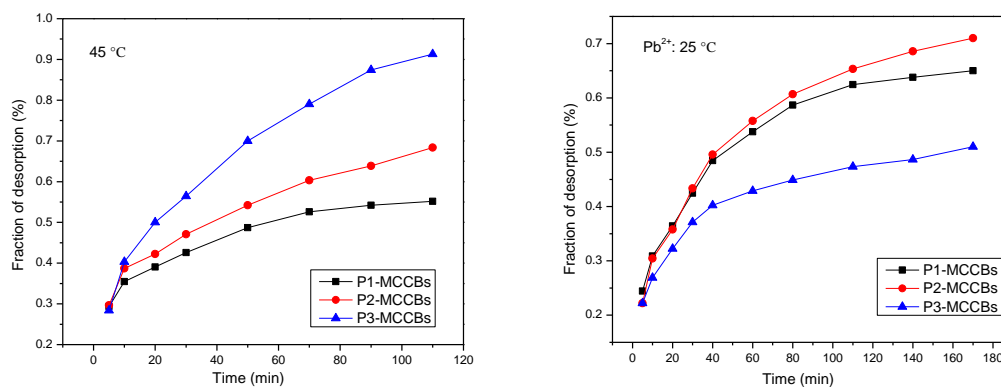


**Fig.5.13 Dye and Pb<sup>2+</sup> desorption process at different temperatures.**

### 5.3.10 Adsorption kinetics

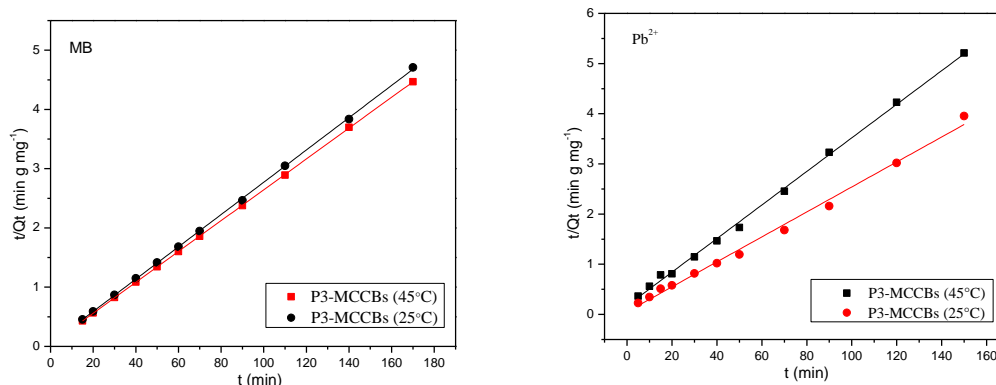


**Fig.5.14 The linear relation of pseudo-second-order kinetic at different temperatures.**

The adsorption kinetic profiles were modeled by fitting the Pseudo-second-model. The formula ( $t/q_t = 1/(k_2 \times q_e^2) + t/q_e$ ) was presented by Shaker and Albishri [29]. The corresponding results showed that the Pseudo-second-model was the well-fit model for all the samples (the correlation coefficients  $R^2 > 0.99$ ) at the temperature of 25 and 45 °C, respectively (Figure.5.14). The fitting results suggested that the adsorption rate was controlled by chemical adsorption, which involved the electron sharing or electron

transfer between the adsorbent and the adsorbate. The fast adsorption rate might be related to the introduction of carboxylic groups in the adsorbents.

### 5.3.11 The desorption kinetic models

The results of MB desorption at different temperatures were fit by desorption kinetic models. Four kinetic models were applied to model the kinetic profiles, including the zero order ( $Q_t = Q_0 + k_0t$ ), first order ( $Q_t = Q_0 e^{-kt}$ ), Higuchi ( $Q_t = k_t^{1/2}$ ) and Korsmeyer-Peppas ( $Q_t/Q_\infty = k_t^n$ ). [30] The corresponding results are shown in Table.5.1. A comparative study of correlation coefficients  $R^2$  showed that the Higuchi and Korsmeyer-Peppas models were the best-fit models for all the samples at the temperatures of 25 and 45 °C, respectively ( $R^2 > 0.9$ ). This is attributed to the swelling of the polymer chains, which leads to the formation of large pores that facilitate dyes desorption out of the adsorbents. The determined values of the diffusion exponent ( $n$ ) obtained from Korsmeyer-Peppas model ranged between 0.704 and 0.871 at 25 °C, (Table.5.1), indicating that the dye release from these P3-MCCBs followed anomalous transport. However, the values of the diffusion exponent ( $n$ ) were higher than 1.0 when the temperature was 45 °C, showing that the mechanism of dye transport was super case-II transport. These results reflected that the dye desorption process could be modally fit by using the Higuchi and Korsmeyer-Peppas models. The ambient temperature would affect the dye desorption eventually.

**Table.5.1 Kinetic model's constants and correlation coefficients ( $R^2$ )**

Sample-MB	Zero order		First order	
	P1-MCCBs (45 °C)	$Q_t=4.0316+0.0031t$	$R^2=0.7618$	$Q_t=4.031e^{-0.0007t}$
P2-MCCBs (45 °C)	$Q_t=3.6821+0.0165t$	$R^2=0.7946$	$Q_t=3.677e^{-0.0038t}$	$R^2=0.7552$
P3-MCCBs (45 °C)	$Q_t=3.5039+0.0479t$	$R^2=0.8568$	$Q_t=3.565e^{-0.0089t}$	$R^2=0.8089$
P1-MCCBs (25 °C)	$Q_t=0.1983+0.0114t$	$R^2=0.9628$	$Q_t=0.3337e^{-0.0091t}$	$R^2=0.7737$
P2-MCCBs (25 °C)	$Q_t=0.145+0.0125t$	$R^2=0.9730$	$Q_t=0.2924e^{-0.0109t}$	$R^2=0.7751$
P3-MCCBs (25 °C)	$Q_t=0.0061+0.005t$	$R^2=0.9857$	$Q_t=0.1431e^{-0.0085t}$	$R^2=0.9382$
Sample-MB	Higuchi		Korsmeyer-Peppas	
P1-MCCBs (45 °C)	$Q_t=0.0411t^{0.5}+3.917$	$R^2=0.9289$	$Q_t/Q_\infty=109.41t^{31.27}$	$R^2=0.9737$
P2-MCCBs (45 °C)	$Q_t=0.2282t^{0.5}+3.027$	$R^2=0.9139$	$Q_t/Q_\infty=83.29t^{6.36}$	$R^2=0.9779$
P3-MCCBs (45 °C)	$Q_t=0.6471t^{0.5}+1.705$	$R^2=0.9355$	$Q_t/Q_\infty=85.43t^{2.79}$	$R^2=0.9486$
P1-MCCBs (25 °C)	$Q_t=0.2398t^{0.5}-0.772$	$R^2=0.9730$	$Q_t/Q_\infty=0.007t^{0.871}$	$R^2=0.9885$
P2-MCCBs (25 °C)	$Q_t=0.2622t^{0.5}-0.904$	$R^2=0.9675$	$Q_t/Q_\infty=0.005t^{0.919}$	$R^2=0.9880$
P3-MCCBs (25 °C)	$Q_t=0.0996t^{0.5}-0.369$	$R^2=0.9047$	$Q_t/Q_\infty=0.012t^{0.704}$	$R^2=0.8881$

## 5.4 Conclusions

In summary, we successfully synthesized thermal-sensitive composite cellulose filaments/Poly (N-isopropylacrylamide) (CF/Poly-NIPAM) spheres via microwave-assisted polymerization by using native cellulose and cellulose filaments as the raw materials. The robust and highly porous structure of cellulose spheres allowed the as-prepared adsorbents to have good stability. The polymerization could be microwave accelerated and high efficiency could be obtained via microwave-assisted polymerization. Also, the P-MCCBs hybrid spheres were sensitive to the ambient temperature, and the adsorption and desorption behaviors of target contaminants (MB and Pb<sup>2+</sup>) changed greatly by varying the temperature from 25 to 45 °C. Moreover, the porous structure and physicochemical properties of the P-MCCBs hybrid spheres could

be controlled by changing the concentration of the NIPAM during the preparation process. The MB desorption rate from the composite spheres with various Poly-NIPAM content at temperatures of 25 and 45 °C changed significantly. Hence, the thermal-responsive spheres can be used as an excellent adsorbent with controllable contaminants adsorption and desorption characteristics. In addition, this synthesis technique offered a platform which could be extended to other approaches to prepare functional porous materials.

## 5.5 References

- [1] Chakraborty S, De S, Basu JK (2005) Treatment of a textile effluent: application of a combination method involving adsorption and nanofiltration. *Desalination* 174:73-85.
- [2] Crini G (2006) Non-conventional low-cost adsorbents for dye removal: a review. *Bioresource Technol.* 97:1061-1085.
- [3] Mahajan R, Bali M (2012) Analytical studies on metal speciation studies of river sutlej. *Int. J. Emerg. Technol. Adv. Eng.* 2: 551-554.
- [4] Garg VK, Kumar R, Gupta R (2004) Removal of malachite green dye from aqueous solution by adsorption using agro-industry waste: A case study of *Prosopis cineraria*. *Dyes and Pigments* 62: 1-10.
- [5] Hua M, Zhang S, Pan B, et al (2015) Heavy metal removal from water/ by nanosized metal oxides: A review. *J. Hazard. Mater.* 211-212: 317-331.
- [6] Zhou Q, Lin Y, Shu J, et al (2017) Reduced graphene oxide-functionalized FeOOH for signal-on photoelectrochemical sensing of prostate-specific antigen with bioresponsive controlled release system. *Biosens. Bioelectron.* 98: 15-21.
- [7] Lyu H, Gao B, He F et al (2018) Experimental and modeling investigations of ball-milled biochar for the removal of aqueous methylene blue. *Chem. Eng. J.* 335: 110-119.
- [8] Pelleria FM, Giannis A, Kalderis D et al (2012) Adsorption of Cu(II) ions from aqueous solutions on biochars prepared from agricultural by-products. *J. Environ. Manag.* 96: 35-42.

- [9] Mahmoud ME (2015) Water treatment of hexavalent chromium by gelatinimpregnated-yeast (GeleYst) biosorbent. *J. Environ. Manag.* 147: 264-270.
- [10] Kang H, Liu R, Huang Y (2015) Graft modification of cellulose: methods, properties and applications. *Polymer* 70: 1-16.
- [11] Jalili NA, Jaiswal MK, Peak CW (2017) Injectable nanoengineered stimuli-responsive hydrogels for on-demand and localized therapeutic delivery. *Nanoscale* 9: 15379-15389.
- [12] Atta AM, Al-Lohedan HA, El-Saeed AM et al (2017) Salt-controlled self-healing nanogel composite embedded with epoxy as environmentally friendly organic coating. *J. Coat. Technol. Res.* 14: 1225-1236.
- [13] Qian Z, Guye KN, Masiello DJ et al (2017) Dynamic Optical Switching of Polymer/Plasmonic Nanoparticle Hybrids with Sparse Loading. *J. Phys. Chem. B* 121: 1092-1099.
- [14] Liu P, Luo Q, Guan Y (2010) Drug release kinetics from monolayer films of glucose-sensitive microgel. *Polymer* 51: 2668-2675.
- [15] Pan K, Zhang X, Cao B (2010) Surface-initiated atom transfer radical polymerization of regenerated cellulose membranes with thermo-responsive properties. *Polym. Int.* 59: 733-737.
- [16] Yang L, Zhang J, He J (2015) Synthesis and characterization of temperature-sensitive cellulose-graft-poly (N-isopropylacrylamide) copolymers. *Chinese J. Polym. Sci.* 33: 1640-1649.
- [17] Pal A, Giri A, Bandyopadhyay A (2016) Influence of hydrodynamic size and zeta potential of a novel polyelectrolyte poly (acrylic acid) grafted guar gum for adsorption of Pb (II) from acidic waste water. *J. Environ. Chem. Eng.* 4: 1731-1742.
- [18] Behbahani M, Bide Y, Bagheri S et al (2016) A pH responsive nanogel composed of magnetite, silica and poly (4-vinylpyridine) for extraction of Cd (II), Cu (II), Ni (II) and Pb (II). *Microchim. Acta* 183: 111-121.
- [19] Jin X, Wang Q, Sun J et al (2018) P(NIPAM-co-AA) @ BMMs with mesoporous silica core and controlled copolymer shell and its fractal characteristics for dual pH- and temperature-responsive performance of ibuprofen release. *Int. J. Polym. Mater. Po.* 67: 131-142.
- [20] Pruettiphap M, Rempel GL, Pan Q et al (2017) Morphology and drug release behavior of N-isopropylacrylamide/acrylic acid copolymer as stimuli-responsive nanogels. *Iran. Polym. J.* 26: 957-969.

- [21] Komorowska-Durka M, Dimitrakis G, Bogdal D et al (2015) A concise review on microwave-assisted polycondensation reactions and curing of polycondensation polymers with focus on the effect of process conditions. *Chem. Eng. J.* 264: 633-644.
- [22] Zhang C, Liao L, Gong S (2007) Recent developments in microwave-assisted polymerization with a focus on ring opening polymerization. *Green Chem.* 9: 303-314.
- [23] Singla P, Mehta R, Berek D et al (2014) Ring opening polymerization of lactide in a monomode microwave using stannous octoate and dibutyltin dimethoxide catalysts. *J. Macromol. Sci. A* 51: 350-361.
- [24] Li Y, Xiao H, Chen M et al (2014) Absorbents based on maleic anhydride-modified cellulose fibers/diatomite for dye removal. *J. Mater. Sci.* 49: 6696-6704.
- [25] Liu L, Gao ZY, Su XP et al (2015) Adsorption Removal of Dyes from Single and Binary Solutions Using a Cellulose-based Bioadsorbent. *ACS Sustain. Chem. Eng.* 3: 432-442.
- [26] Cai H, Sharma S, Liu W et al (2014) Aerogel microspheres from natural cellulose nanofibrils and their application as cell culture scaffold. *Biomacromolecules* 15: 2540-2547.
- [27] Plunkett KN, Zhu X, Moore JS (2006) PNIPAM chain collapse depends on the molecular weight and grafting density. *Langmuir* 22: 4259-4266.
- [28] Bae YH, Okano T, Hsu R (1987) Thermo-sensitive polymers as on-off switches for drug release. *Macromol. Rapid Commun.* 8: 481-485.
- [29] Shaker MA, Albishri HM (2014) Dynamics and thermodynamics of toxic metals adsorption onto soil-extracted humic acid. *Chemosphere.* 111: 587-595.
- [30] Costa P, Lobo JMS (2001) Modeling and comparison of dissolution profiles. *Eur. J. Pharm. Sci.* 13: 123-133.

## **Chapter 6 Fabrication of dual-responsive semi-INP cellulose microfilaments/ Poly (N-isopropylacrylamide-co-acrylic acid) spheres for dye removal in single and binary systems<sup>5</sup>**

### **ABSTRACT**

Copolymer-modified cellulose microfilaments/Poly (N-isopropylacrylamide-co-acrylic acid) spheres (MPNAA) were developed and semi- interpenetrating network (semi-IPN) was formed by free radical copolymerization of N-isopropylacrylamide (NIPAM) and acrylic acid (AA) on cellulose microfilaments spheres. The cellulose microfilaments spheres (CCS) were first prepared using a vacuum drying method in the presence of a pore forming agent (nano-sized CaCO<sub>3</sub>). Afterwards, NIPAM (a temperature-sensitive monomer) and AA (a pH-sensitive monomer) were copolymerized and grafted onto the cellulose microfilaments spheres through in situ free radical polymerization in the microwave-reactor. The morphology, chemical structure, and thermal sensitivity of the as-prepared spheres were characterized. The MPNAA reflected pH-dependence and pH 9.0 was the optimum value for adsorption. The adsorption kinetics followed the pseudo-second-order and exhibited a three-stage intraparticle diffusion model. Adsorption isotherms (at 298, 313, and 328 K) were fit using Langmuir, Freundlich, and Temkin models, which indicated that the MPNAA dominated the adsorption capacity towards MB and MV, with the maximum adsorption at 497.5 and 840.3 mg g<sup>-1</sup> in a single system. These results indicated that the spheres with copolymers exhibited a controllable adsorption and desorption process as pH- and temperature-responsive adsorbents, and MPNAA could act as a new type of material for controlled dyes adsorption.

---

<sup>5</sup> This chapter has been submitted on Carbohydrate Polymers, the format follows the requirements of the Journal. The entire experimental work was performed by the candidate Yuan Li along with the preparation of the manuscript.

**Keywords:** Semi-IPN spheres, Cellulose microfilaments, Dual-responsive, Dye adsorption, Binary system

## 6.1 Introduction

The industrial discharge of hazardous dyes is currently critical and has aroused tremendous concern [1]. The complex aromatic molecular structures and xenobiotic properties of dyes lead to the difficulty in degrading. Among the various conventional methods for the removal of dyes from wastewater like coagulation, chemical precipitation, membrane extraction, complexation, solvent extraction, etc. [2], adsorption dominates due to its benefits such as high selectivity, easy operating, lower costs, and high efficiency in removing lower levels of dyes from aqueous solutions [3]. Various adsorbents, such as as-prepared metal oxides [4], silica based mesoporous materials [5], biochar [6], and cellulose based adsorbents [7] were investigated recently to overcome the shortages of utilizing activated carbon [8]. Particularly, adsorbents based on natural materials are gaining the increasing emphasis along with their availability in large scale, cost-effective, and facile chemical modification to enhance adsorption ability, resulting in an efficient solution for sewage treatment [9].

As the most abundant of naturally-occurring biopolymers, cellulose is an ideal biological material for the fabrication of new functional adsorbents for the removal of toxic dyes [10]. The hydroxyl groups on cellulose can be easily readily modified via various derivation reactions to introduce functional groups such as -COOH, -SO<sub>3</sub>H, and -NH<sub>2</sub> [11]. For the removal of dyes from wastewater, the functional-modified cellulose-based adsorbents has been extensively investigated recently due to the growing demand

of green-based and biodegradable products [12-14]. Such modifications improve the adsorptive and ion exchange capability of cellulose significantly, resulting in the fabrication of low density adsorbents which are inexpensive, renewable, and biodegradable. Moreover, the readiness of functional-modifying cellulose fibres allow them to induce adsorption/desorption processes in a controllable manner; whereas the conventional adsorption often proceeds irreversibly and uncontrollably. It would be ideally if the smart cellulose-based materials could be prepared along with an “on-off” switch which would control the adsorption and desorption. This has literally motivated our research interest presented in this work, i.e., manipulating the adsorption and desorption based on using the thermo- and pH- responsive adsorbents originating from cellulose fibres.

Recently, the application of cellulose-based materials with specific functional groups for the binding and removal of pollutants from aqueous solutions has been widely studied [15-16]. Nevertheless, the powder-shape adsorbents might make them difficult to utilize, filter, and separate effectively, resulting in their lower potential application in water clarification [17]. Beads and particles of other shapes are therefore necessary and have been studied as hot spot in researchers. Ram and Chauhan [18] developed new spherical nanocellulose-based functional adsorbents and these have been found to be rapid, efficient, and selective adsorbents to correct the environmental imbalances. Luo et al [19] synthesized the magnetic cellulose beads consisting of activated carbon. The as-prepared beads were used for the removal of dyes such as methylene blue (MB) and methyl orange (MO). Ma et al [20] have fabricated porous cellulose spheres (PCS) and then modified them with trisodium trimetaphosphate (STMP) to introduce phosphate

ester groups to enhance the adsorption capacity of spheres. Furthermore, unique cellulose-based hybrid beads were synthesized to remove cationic dyes [21] and heavy metal ions [22]. The adsorption mechanism has been especially investigated. Cellulose microfilaments have greater advantages compared with other types of cellulose fibers, due to better porous structure, adsorption capacity, and other applications. Microfilaments are ideal raw materials containing a variety of shapes and structures and are biocompatible and absorbable [23]. However, limited work has been published on combining dissolved cellulose fibers with cellulose microfilaments (CMF) as a semi-IPN type of adsorbent.

Recently, thermo- and pH- sensitive or called “smart” polymers have been well documented [24-26]. Among several thermal responsive polymers, poly (N-isopropyl acrylamide) (Poly-NIPAM) with the lower critical solution temperature (LCST) at 32 °C is the most commonly-used one. When the ambient temperature is below the LCST, the polymer chains swell in water, above the LCST, the polymer segments become more hydrophobic and become water-insoluble [27]. In recent decades, plenty of work [28-30] has been studied on Poly-NIPAM-based materials in the fields of biotechnology and pharmaceutical [31]. Furthermore, several studies on the graft modification of cellulose with Poly-NIPAM as the adsorbents for the removal of pollutant have been reported. Kobe et al prepared composite hydrogels using the modified cellulose nanofiber (CNF) as the multifunctional crosslinker and N-isopropylacrylamide (PNIPAM) as the monomer, respectively [32]. Chen et al investigated thermo-responsive poly (N-isopropylacrylamide-co-acrylic acid) (PNIPAM-co-AA) hydrogels as water-soluble

polymer in a polymer-enhanced ultrafiltration (PEUF) process, the fouling behavior could be controlled at different temperature and pH [33].

Apart from temperature, pH is also critical in the adsorption-desorption behaviors of adsorbents. Generally, pH affects the degree of ionization and the surface charge of materials, and thus the adsorption and desorption of probes could be controlled effectively by the changes in pH if the adsorbents possess the pH-responsive behavior. Typical pH-responsive polymers, poly (acrylic acid) (PAA) [34] and poly(4-vinylpyridine) (P4VP) [35] are more stable and can offer higher binding capacity compared to the low-molecular-weight types containing carboxyl or thiol. Researchers have been exploring materials with both pH- and thermos-responsive properties. Shi et al have synthesized thermo-responsive and conductive hybrid hydrogels. The conductive polymer hydrogels were crosslinked by phytic acid in PNIPAM matrix [36]. Xia et al studied the dual responsive (temperature and pH) silicon surface by grafting PNIPAA and PAA brushes, the contact angles (CAs) of the dual-responsive materials reversed when the pH and/or temperature changed [37]. Osypova et al [38] reported PAA-b-PNIPAM blocks copolymers to control the protein adsorption. However, the conventional polymerization contains several disadvantages such as the relatively low polymerization rate, high reaction temperatures, and extended polymerization times; therefore, it is necessary to design novel approaches to prepare responsive polymeric materials for the applications mentioned above. Microwave irradiation is synthetic tool which possesses several advantages such as decreased reaction time, increased the product yields, relatively fewer byproducts, and environmental friendly [39]. Microwave-assisted synthesis has been reported by some researchers in the field of

polymeric synthesis including step-growth polymerizations [40], free radical [41], and ring-opening polymerizations [42]. However, the reports on the microwave-assisted synthesis combined with cellulose-based adsorbents with both pH- and temperature-responsive properties are relatively sparse.

The interpenetrating polymer networks (IPN) or semi-interpenetrating polymer networks (semi-IPNs) have aroused increasing concern due to their multi-responsive properties, and the gel-like particles have great potential application in the areas of agrochemical and biomedical [43-45]. The semi-IPN copolymer hydrogels based on N-isopropylacrylamide (NIPAM) and itaconic acid (IA) monomers were fabricated by Kalagasydys et al [46] in the presence of a surfactant (polyethylene glycol) by a free radical polymerization method. Generally, the free radical polymerization of hydrophilic monomers in the presence of cross-linkers allows for the preparation of gel-like particles in water phase.

In this work, we aimed to explore a novel approach to prepare the cellulose/cellulose microfilaments composite spheres as an environmental-friendly adsorbent for the removal of dyes from aqueous solutions. The pH and thermal-responsive modification of as-prepared beads was carried out by microwave-assisted free radical polymerization. The cationic dyes, methylene blue (MB) and methyl violet (MV), were selected as the probes. Apart from developing an appropriate protocol for the synthesis of this dual-responsive semi interpenetrating network (semi-IPN) spheres, the morphology, thermal properties, and adsorption behaviors were also investigated to evaluate their potential application in other fields.

## **6.2 Experimental**

### **6.2.1 Materials**

Cellulose was filter paper (Qualitative P4, porosity: Medium-Fine; Flow Rate: Slow, Fisher Scientific). Cellulose microfilaments (CMF) was kindly provided by FPIinnovations Canada (Pointe Claire, QC, Canada), which was invented by FPIinnovations. The products were obtained via processing cellulose fibres mechanically. The resulting fibres in nano- or micro- range have the lengths from 50 to 800  $\mu\text{m}$  with the aspect ratios from 300 to 3000 and high surface area ( $> 80 \text{ m}^2/\text{g}$ ).  $\text{CaCO}_3$  nanoparticles (Product # 1951RH,  $\leq 30\text{nm}$ , 97.5%) was supplied by SkySpring Nanomatierials, Inc. Sodium hydroxide (solid), maleic anhydride (MA), urea, methylene blue, methyl violet, N-isopropylacrylamide (NIPAM, purchased from Sigma-Aldrich Chemical Co.), N, N'-methylenebisacrylamide (MBA), acrylic acid (AA), N, N, N, N-tetramethylethylene diamine (TEMED), and potassium persulfate (KPS) were all of analytical grade chemicals. Deionized water was used for all the experiments.

### **6.2.2 Experimental methods**

#### **6.2.2.1 Fabrication and modification of Cellulose/Cellulose microfilaments spheres (CCS)**

The cellulose-based spheres were prepared via a drop-wise precipitation of dissolved cellulose (as the matrix of composite adsorbents) mixed with CMF (as dispersed phase or reinforcements) in acidic aqueous solution. During the preparation, the cellulose (4g) was dissolved in the solution containing NaOH (7 wt %) /Urea (12 wt %) at  $-10 \text{ }^\circ\text{C}$  with

the aid of a high-speed shear homogenizer (Stanfen, Germany) to promote the dissolution of cellulose and generate the cellulose solution at 4% (wt). The CMF and nano-CaCO<sub>3</sub> (as a pore forming agent) were then added in different ratios after the cellulose was fully dissolved, followed by vigorous stirring of the mixture to produce a uniform suspension.

A typical procedure for making the spheres is described as follows: the mixtures were firstly added into HCl (1 mol/L) dropwise using a syringe with a constant stirring, followed by the washing process with distilled water to remove the water-soluble residues. The purified cellulose/cellulose microfilaments spheres (CCS) were then immersed into excessive acetone followed by washing several times, and the purified CCS were dried in a vacuum oven at 40 °C for 24 hours (Figure.6.1).

The fabrication of carbonylated CCS (MCCS) was conducted as follows: the CCS (2g) were immersed in the maleic anhydride solution (2g in 20mL acetone), and the solvent was evaporated in the fume hood before transferring into the vacuum oven, followed by the heating process at 100 °C for 3 hours. The as-resulted spheres were washed with excessive distilled water, ethanol, and finally acetone for several times, and then the purified MCCS were dried in the vacuum oven at 40 °C for 24 hours, such process had no organic solvent being used, resulting in an organic solvent-free approach.

#### **6.2.2.2 Microwave-assisted preparation of MCCS/poly (NIPAM-co-acrylic acid) semi-INP**

The CMF based-semi-IPN was prepared on MCCS by the concurrent crosslinking and free radical copolymerization of NIPAM and AA using potassium persulfate (KPS) as a

redox initiator and MBA as a cross-linker. A typical procedure for co-polymerization is described as follows: first, a 20-mL beaker equipped with a magnetic stirrer was loaded with NIPAM, acrylic acid, KPS, NMBA, TEMED (10  $\mu$ L), and distilled water to make a uniform solution. TEMED was added as an accelerator. The NIPAM monomer was added at an excess amount, and the concentrations of AA monomer were controlled at various ratios based on NIPAM. The MBA and KPS concentrations were 3 to 2 % based on the weight of NIPAM monomer. Then the MCCS were soaked in the mixed solution under gently stirring, and fully saturated by absorbing the mixed solution containing the monomers. Afterwards, the excess solution was removed and the saturated MCCS were transferred into the beaker containing paraffin oil and the emulsifier span-80. The saturated MCCS were dispersed in paraffin oil by vigorous shaking and the resulting solution was purged with nitrogen for 10 minutes. The beaker was then placed in the cavity of the microwave oven, and the temperature was controlled at 70 to 80 °C at a maximum 100 W irradiation dose. After 20 minutes polymerization, the MCCS were washed by excessive distilled water, ethanol, and acetone several times. The purified samples were placed in the vacuum oven for further drying at 40 °C for 24 hours. The corresponding samples were named as MPNAA-1, MPNAA-2, and MPNAA-3 in terms of the molar ratios of AA to NIPAM (1:2, 1:1, and 2:1) during the polymerizations. The schematic of the preparation is illustrated in Figure.6.1.

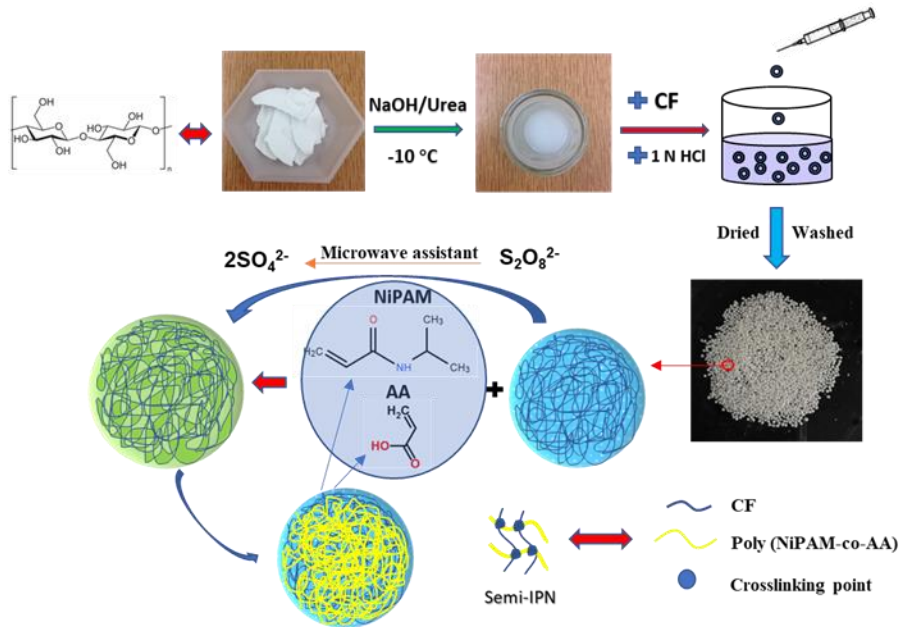


Figure.6.1 The Schematic of CCS and MPNAA Preparation

### 6.2.3 Characterization

The surface charge density of synthesized samples was determined via a colloid titration method using a titrator (PCD 03, Mutek, UK). The point of zero charge was detected and the charge density of samples could be calculated based on the volume of used PDADMAC and the mass of adsorbents.

Fourier transform infrared spectroscopy (FTIR) analyzed the dried samples. The spectra of the samples were recorded on a NEXUS 470 spectrophotometer (Nicolet Thermo Instruments, Canada) with a detector at 1 cm<sup>-1</sup> resolution from 500 to 4000 cm<sup>-1</sup> and 32 scans per sample.

Scanning electron microscopy (SEM, JEOL JSM-6400, Japan) was used for morphological characterization. Prior to observation, the surface of the samples was coated with a thin film of carbon using a sputter coater.

The thermal stability of the samples was measured using a Thermogravimetric Analyzer (TGA, Q600, TA Instruments, USA). Approximately 10 mg powder of the sample was used for the testing from 25 °C to 600 °C under N<sub>2</sub> atmosphere at a heating rate of 10 °C /min.

#### 6.2.4 Adsorption of cationic dyes

The batch mode adsorption studies were carried out to study the effect of shaking time, temperature, and pH on adsorption behavior. In this work, the stock solutions of 1000 mg L<sup>-1</sup> MB and MV were prepared and diluted further to obtain the tested solutions with different concentrations. The adsorbents (10mg) were immersed into 10 mL of dye aqueous solution of 20 mg/L at room temperature. All the experiments were carried out using the temperature-controlled shaker (SWB25, Thermo Electron Corporation, Germany) during the adsorption process at a fixed agitation speed at 150 rpm for all experiments. After predetermined period, the concentration of the dyes was measured using a UV-vis spectrophotometer (Genesys 10-s, Thermo Electron Corporation) [47]. The equilibrium adsorption capacity ( $Q_e$ , mg/g) and the fraction of removal ( $R$ , %) was calculated using the equations reported (Eq 6.1 and Eq 6.2) [48].

$$Q_e = (C_o - C_e)/m \times V \quad \text{Eq 6.1}$$

$$R = (C_o - C_e)/C_o \times 100 \quad \text{Eq 6.2}$$

where  $C_o$  and  $C_e$  (mg/l) are the initial and equilibrium concentrations (mg L<sup>-1</sup>) of the dyes in solution, respectively;  $V$  (L) is the volume and  $m$  (g) is the weight of adsorbents.

### 6.2.5 Desorption and regeneration

The dye-laden adsorbent was washed with deionized water, desorbed with 1 N HCl for 60 minutes at room temperature. The desorbed adsorbent was washed and dried, and the so-regenerated adsorbent was examined to determine its reusability.

Prior to the study of thermo-responsive properties, the desorption of the adsorbents was carried out by changing the temperature from 25 to 55 °C every 20 minutes at pH 3. The dye-loaded adsorbent was added into 10 mL of 0.001 mol/L HCl solution for desorption on the temperature-controlled shaker at 130 rpm. The desorption rate at each period was calculated.

### 6.2.6 Adsorption kinetics

The adsorption kinetic models can well predict the adsorption mechanism. In this work, four kinetic models were used to fit the adsorption data, including the pseudo-first-order, the pseudo-second-order [49], Elovich kinetic models [50] and intraparticle diffusion kinetic models [51]. The linear forms for the models are presented as follows (Eq 6.3, Eq 6.4, Eq 6.5, and Eq 6.6):

$$\ln(q_e - q) = \ln q_e - k_1 t \quad \text{Eq 6.3}$$

$$\frac{t}{q_t} = \frac{1}{k_2 q_e^2} + \frac{1}{q_e} t \quad \text{Eq 6.4}$$

$$q_t = \frac{1}{\beta} \ln \alpha \beta + \frac{1}{\beta} \ln t \quad \text{Eq 6.5}$$

$$q_t = k_{di} t^{1/2} + C_i \quad \text{Eq 6.6}$$

where  $q_t$  and  $q_e$  are the adsorption capacity at time  $t$  and at equilibrium ( $\text{mg g}^{-1}$ ), respectively.  $k_1$  is the pseudo-first-order equilibrium rate constant ( $\text{min}^{-1}$ ), and  $k_2$  is the pseudo-second-order equilibrium rate constant ( $\text{g mg}^{-1} \text{min}^{-1}$ ).  $\alpha$  and  $\beta$  are the initial

adsorption rate at zero coverage and the desorption constant related to the extent of surface coverage and activation energy for chemisorption in the Elovich model.  $k_{di}$  is the rate constant of intraparticle diffusion at the stage  $i$ ,  $C_i$  is the intercept at different stages and  $t$  is the adsorption time (minutes).

### 6.2.7 Adsorption isotherms

The experiments were carried out at the desired pH by agitating 10 mg of MPNAA-1, MPNAA-2, and MPNAA-3 in 10 mL of dye solution at different initial concentrations on a shaker at 130 rpm under controlled temperature of 25, 40 and 55°C, respectively. The concentrations of dye solution were measured after 3 hours' adsorption. Different isotherm models, including Langmuir, Freundlich, and Temkin models were used to calculate the adsorption results. The linear equations are as follows [52]:

The Langmuir model (Eq 6.7):

$$\frac{C_e}{Q_e} = \frac{1}{K_L Q_{max}} + \frac{C_e}{Q_{max}} \quad \text{Eq 6.7}$$

where  $Q_{max}$  ( $\text{mg g}^{-1}$ ) is the maximum adsorption capacity and  $K_L$  ( $\text{L mg}^{-1}$ ) is the Langmuir constant.  $C_e$  ( $\text{mg L}^{-1}$ ) and  $Q_e$  ( $\text{mg g}^{-1}$ ) are the concentration and adsorption capacity at the equilibrium, respectively.

A dimensionless constant  $R_L$  (Eq 6.8) reflects the essential characteristic of the Langmuir model by  $K_L$  [53]:

$$R_L = \frac{1}{1 + K_L C_0} \quad \text{Eq 6.8}$$

where  $C_0$  ( $\text{mg L}^{-1}$ ) is the initial concentrations of dyes,  $K_L$  is mentioned above. The different values of  $R_L$  represent the different types of isotherms:  $R_L > 1$ , unfavorable;  $R_L$

=1, linear;  $0 < R_L < 1$ , favorable;  $R_L = 0$ , irreversible. The value of  $R_L$  is smaller, the greater the affinity between the adsorbent and the adsorbate.

The Freundlich model (Eq 6.9):

$$\ln Q_e = \ln K_f + \frac{1}{n} \ln C_e \quad \text{Eq 6.9}$$

Where  $Q_e$  and  $C_e$  are noted previously.  $K_f$  is roughly an indicator of adsorption capacity and  $n$  is adsorption intensity.

The Temkin model (Eq 6.10):

$$Q_e = \frac{RT}{b_T} \ln A + \frac{RT}{b_T} \ln C_e \quad \text{Eq 6.10}$$

where  $A$  ( $\text{L mg}^{-1}$ ) and  $b_T$  ( $\text{J mol}^{-1}$ ) are the Temkin constants,  $T$  is the absolute temperature, and  $R$  is the universal gas constant  $8.314 \text{ J mol}^{-1}\text{K}^{-1}$ .

The competitive Langmuir model (Eq 6.11, Eq 6.12, and Eq 6.13) [54] is adopted for the binary system including MB and MV at different concentrations, which is given as follows:

$$Q_{e,i} = \frac{Q_{m,i} K_{L,i} C_{e,i}}{1 + \sum_{j=1}^N K_{L,j} C_{e,j}} \quad \text{Eq 6.11}$$

$$\frac{C_{e,1}}{Q_{e,1}} = \frac{1}{Q_{m,1} K_{L,1}} + \frac{1}{Q_{m,1}} C_{e,1} + \frac{K_{L,2}}{Q_{m,1} K_{L,1}} C_{e,2} \quad \text{Eq 6.12}$$

$$\frac{C_{e,2}}{Q_{e,2}} = \frac{1}{Q_{m,2} K_{L,2}} + \frac{1}{Q_{m,2}} C_{e,2} + \frac{K_{L,1}}{Q_{m,2} K_{L,2}} C_{e,1} \quad \text{Eq 6.13}$$

where  $Q_{e,1}$  and  $Q_{e,2}$  are the MB and MV adsorption capacity at equilibrium ( $\text{mg g}^{-1}$ ),  $C_{e,1}$  and  $C_{e,2}$  are the concentration of solution at equilibrium ( $\text{mg L}^{-1}$ ),  $Q_{m,1}$  and  $Q_{m,2}$  are the maximum adsorption capacity of MB and MV ( $\text{mg g}^{-1}$ ),  $K_{L,1}$  and  $K_{L,2}$  are the constant of Langmuir competitive model ( $\text{L mg}^{-1}$ ).

## 6.3 Results and discussion

### 6.3.1 FTIR spectra

The FTIR spectra of CCS, MCCS, and MPNAA-3 are presented in Figure.6.2 to reveal the changes of the cellulose spheres after the modification over microwaved-assisted polymerization. In the spectra of CCS, the characteristic peak at  $3440\text{ cm}^{-1}$  corresponded to the hydrogen bond O-H stretching vibration, whereas the C-H symmetric stretching vibration occurred at  $2902\text{ cm}^{-1}$ . The absorbance at  $1627\text{ cm}^{-1}$  was related with O-H bending of the absorption of combined water in the samples [55], and the band at  $1075\text{ cm}^{-1}$  was the C-O stretching vibration [56]. Compared with the spectra of CCS, the new peaks at  $1732$  and  $1639\text{ cm}^{-1}$ , were observed on MCCS, corresponding to carbonyl groups (C=O) and the vibration of vinyl groups (C=C), respectively [57]. Thus, the esterification between maleic anhydride and CCS was proved. In addition, in the FTIR spectrum of MPNAA-3, the existence of PNIPAM-co-AA chains was indicated by the appearance of peaks at  $1735\text{ cm}^{-1}$ ,  $1638\text{ cm}^{-1}$ , and  $1567\text{ cm}^{-1}$ , corresponding to the carboxyl groups of AA, C=O stretching for amide I, and N-H stretching of PNIPAM, respectively [58]. The band at  $1378\text{ cm}^{-1}$  could be assigned to  $-\text{CH}(\text{CH}_3)_2$  groups for PNIPAM [59]. These results proved that CMF/poly(NIPAM-co-AA) copolymers were synthesized successfully.

Moreover, the peak corresponded to -OH stretching shifted from  $3440\text{ cm}^{-1}$  to  $3395\text{ cm}^{-1}$  after the copolymerization, which could be attributed to extra carboxyl groups introduced after the copolymerization. In addition, the successful introduction of carboxyl groups on adsorbents could be verified via the colloidal titration method,

which gave the anionic charge density of  $1.523 \text{ mmol g}^{-1}$ , which is proportional to the number of carboxylic groups on CMF based-semi-IPN.

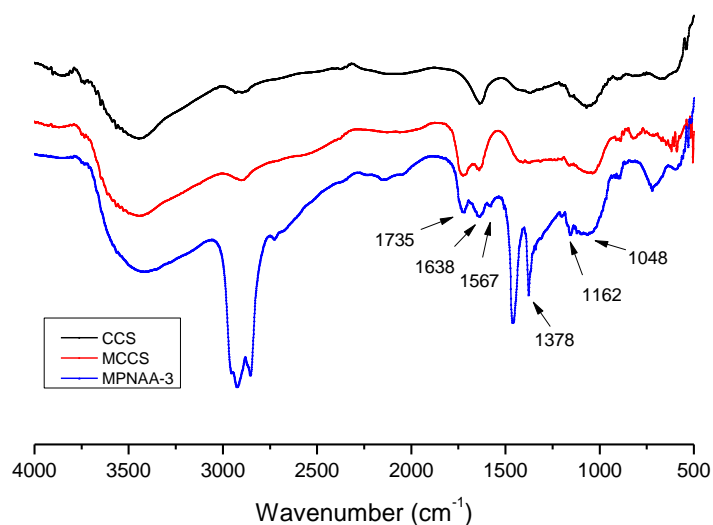


**Figure.6.2** The FTIR spectra of CCS, MCCS and MPNAA-3

### 6.3.2 Scanning electron microscope (SEM)

The morphologies of pure cellulose-based beads (CCS) and PNIPAM-co-AA grafted spheres (MPNAA-3) were observed using SEM (Figure.6.3). Figure.6.3a and Figure.6.3b indicated that the dissolved cellulose matrix reinforced with CMF formed an uneven porous structure with pores at various sizes in the spheres, demonstrating the role of nano- $\text{CaCO}_3$  in pore forming processes. Moreover, the individual CMF fibres as reinforcements appeared to be visible. Clearly, while the dissolved cellulose was precipitated under acidic condition, the nano- $\text{CaCO}_3$  reacted with HCl, releasing  $\text{CO}_2$  and resulting in porous structures on the spheres. In comparison with the morphology of

CCS (see Figure.6.3c), the spheres consisting of PNIPAM-co-AA-grafted cellulose (Figure.6.3d) appeared to be less porous or, due to the fact that the grafted copolymers might have filled up some pores or channels on the spheres.

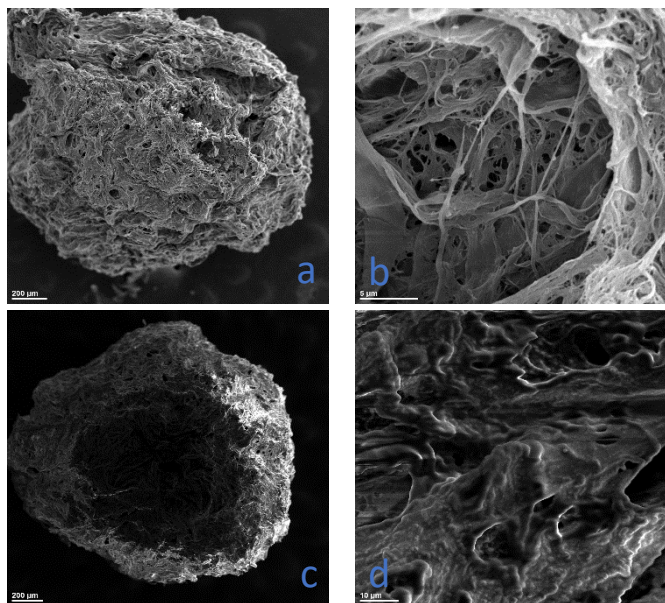
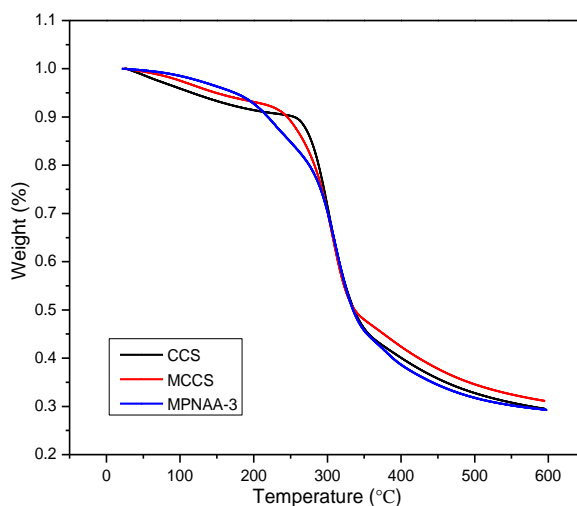


**Figure.6.3 SEM images of CCS (a, b) and MPNAA-3 (c, d).**

### 6.3.3 Thermal analysis

To reveal the thermal properties of cellulose/cellulose microfilaments beads (CCS), MCCS, and MPNAA-3, the TG and DTG curves are presented in Figure.6.4. In all three samples, a total mass loss of 80% over the temperature range between 25 °C and 600 °C was observed (see Figure.6.4a). Especially, the decomposition of MPNAA-3 occurred in four events, the first mass loss appeared at around 50-150 °C, probably due to the evaporation of a significant amount of water released from the samples. The second decomposition event occurred at around 227 °C and is attributed to the copolymer PNIPAM-co-AA staying in the channels of the spheres. The third mass loss happened at

temperatures higher than 311 °C, corresponding to the major thermal decomposition of cellulose and cellulose microfilaments. The fourth weight loss happened at 390 °C, due to the thermal degradation of PNIPAM-co-AA grafted cellulose and cellulose microfilaments. In addition, the results in Figure.6.4b indicated that the thermal decomposition for the maximum weight loss occurred at 311 °C for MPNAA-3, which was 5 °C and 10 °C higher than that of MCCS and CCS, respectively. Obviously, the PNIPAM-co-AA grafted spheres showed better thermal stability than CCS and MCCS.



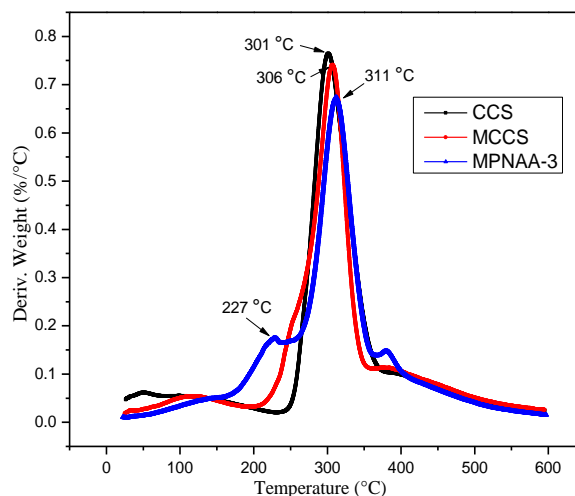


**Figure.6.4** The TGA and DTG curves of CCS, MCCS, and MPNAA-3.

### **6.3.4 Effect of pH on adsorption capacity**

The pH value of solution has been identified as an important influencing factor affecting the adsorption of cationic dyes. The removal of dyes as a function of pH was studied by varying the pH range from 3 to 11. The results are shown in Figure.6.5. As can be seen, the low adsorption capacities were observed at pH 5 or below for all three adsorbents, followed by a rapid increase in the fraction of removal with the further increase of the pH up to 9, and then leveled off when the pH of the solutions was further enhanced. Such changes are mainly due to the reduction of positive-charged groups on the adsorbents under alkaline conditions. Meanwhile, the negative-charged groups on the adsorbents could adsorb cationic dyes via electrostatic association, resulting in the effective adsorption of dyes at a higher pH. It should be noted that the existence of  $H^+$  in the solution played a critical role in the adsorption process. At  $pH < 7$ , a large number of

$H^+$  could compete with cationic dyes for the adsorption sites on the adsorbents, resulting in the occupation of adsorption sites and lowering the fraction of removal of dye. Thus pH 9 was the optimum pH value for dye adsorption.

In fact, polyacrylic acid shows the pH-sensitive conformation due to the  $pK_a$  value of 4.6. Thus, if  $pH < 4.6$ , most of the carboxylic groups on adsorbents remain in the protonated form (COOH), whereas the deprotonated form (COO<sup>-</sup>) [60] occurs if  $pH > 4.6$ . Consequently, the low fraction of removal at low pH was due to the electrostatic repulsion which occurred between the cationic dyes and the surface of MPNAA. This is also related to the increase in the charge density of cationic groups on the surface of adsorbent; and  $H^+$  ions compete with MB and MV for the adsorptive sites on the adsorbents significantly at  $pH < 4.6$ . As pH increased to alkaline, the surface of adsorbents was negatively-charged, resulting in the adsorption being driven by electrostatic attraction between positive-charged dyes and negative-charged adsorbents. In addition, the MPNAA-1, with fewer carboxylic groups, showed itself to be less sensitive to the pH compared to MPNAA-3.

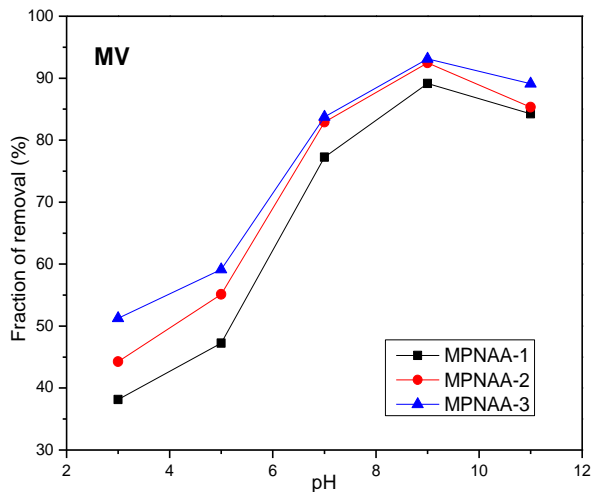
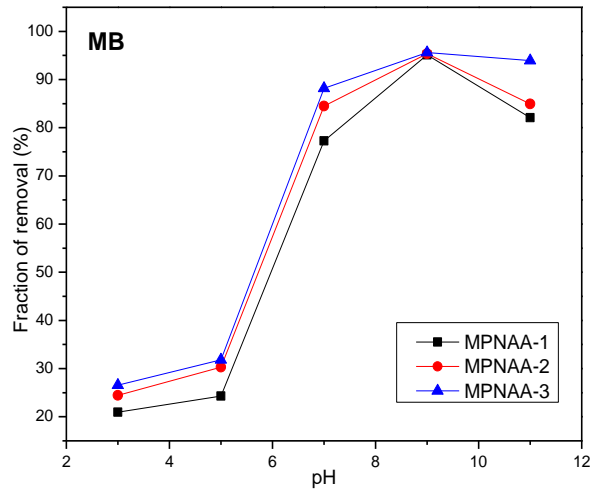


**Figure.6.5 Effect of pH on adsorption of dyes by MPNAA-1, MPNAA-2 and MPNAA-3.**

### **6.3.5 Effect of contact time on adsorption**

The effect of contact time is illustrated in Figure.6.6. The adsorption of MB was carried out under the following conditions: pH 9; 20 ppm of initial concentration of MB; temperature at 30 °C; and the adsorbent dosage at 1000 mg/L. The adsorption

equilibrium was reached at 100 minutes for MB, and such a process could be essentially divided to three continuous stages, as marked in the Figure. The first event, from 0 to 90 minutes, was governed by an external surface adsorption. The second event, from 90 to 180 minutes, was governed by an external surface adsorption. The second event, from 90 to 180 minutes, gradual adsorption process, was controlled by the intraparticle diffusion. The third step, from 180 minutes and after, was an equilibrium adsorption process, where the slow intraparticle diffusion was due to the relatively low concentration of MB. Moreover, the adsorption process of MB was imitated with different kinetic models and the adsorption mechanism of MB was studied systematically afterwards.

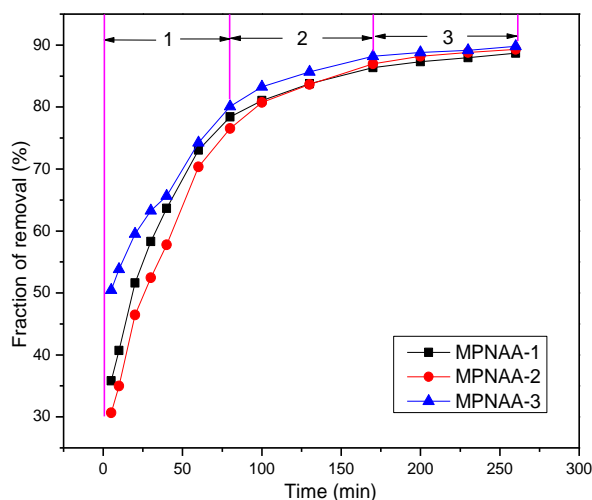


**Figure.6.6 Effect of contact time on adsorption**

### 6.3.6 Adsorption kinetics

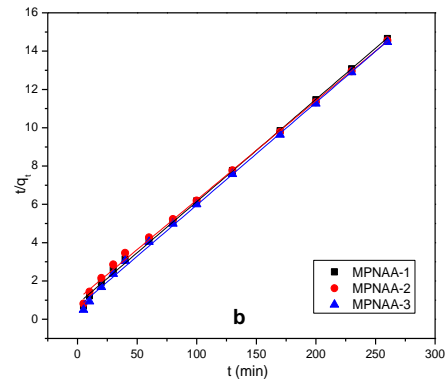
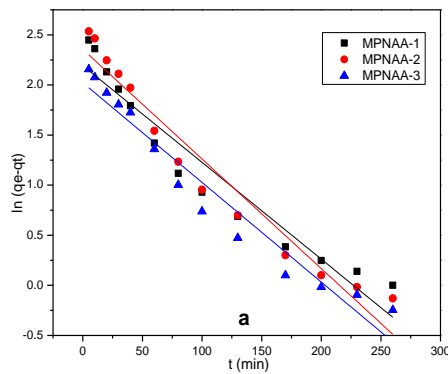
The adsorption kinetics can clearly describe the equilibrium capacity and elucidate the adsorption mechanism. In this work, four kinetic models were used, including Pseudo-first-order, Pseudo-second-order, Elovich model, and Intraparticle diffusion kinetic

models. The pseudo-second-order and the pseudo-first-order equations often model a surface-controlled adsorption process. Another adsorption kinetics model, named the Elovich equation, is well received for the surface-controlled adsorption onto energetically heterogeneous surface sites. Moreover, a simplified intraparticle diffusion model well describes the adsorption that is limited by diffusion within pores rather than by surface-related energy controls.

The results and parameters of each model are shown in Figure.6.7 and Table.6.1. The linear fittings of  $\ln (Q_e - Q_t)$  versus  $t$ ,  $t/Q_t$  versus  $t$ , and  $Q_t$  versus  $\ln t$  are presented in Figure.6.7. Clearly, the correlation coefficients  $R^2$  for the pseudo-second-order model were higher than those of the pseudo-first-order model and Elovich model. The pseudo-second-order model was more suitable to describe the adsorption kinetics of MB on MPNAA-1, MPNAA-2, and MPNAA-3. In this case, the adsorption rates of all the three adsorbents were controlled by chemical process [61]. The rate constant ( $k_2$ ) of MPNAA-3 was higher than those of MPNAA-1 and MPNAA-2, indicating a faster uptake of dyes onto the adsorbents. The faster adsorption rate might be related to the introduction of carboxylic groups in the adsorbents.

The kinetic profiles at different adsorption stages were further studied with the intraparticle diffusion kinetic model; and the results are presented in Figure.6.7 and Table.6.1. As shown in the figure, the adsorption process can be divided to three stages in terms of intraparticle model. The lines in the figure did not pass through the coordinate origin, indicating that the rate control step was the combination between the intraparticle diffusion and the boundary layer diffusion. To sum up, the first stage was controlled by the external surface adsorption or instantaneous adsorption; the second

stage was a gradual adsorption stage which attributed to the intraparticle diffusion; and the equilibrium adsorption was reached at the third stage. Table.6.1 indicates the adsorption rates for the three stages in the following order:  $K_{di,1} > K_{di,2} > K_{di,3}$ . In the beginning, the exterior surface of adsorbents adsorbed dyes, and in the first stage, the instantaneous diffusion period, approximately 75%, 74% and 77% of dyes were adsorbed by MPNAA-1, MPNAA-2, and MPNAA-3. The dyes entered the inner layers of adsorbents when the adsorption on the exterior surface saturated. However, the diffusion rate decreased with the diffusion of the dyes at the second stage. The final stage was the equilibrium period, during which the intraparticle diffusion rate levelled off and remained almost unchanged.



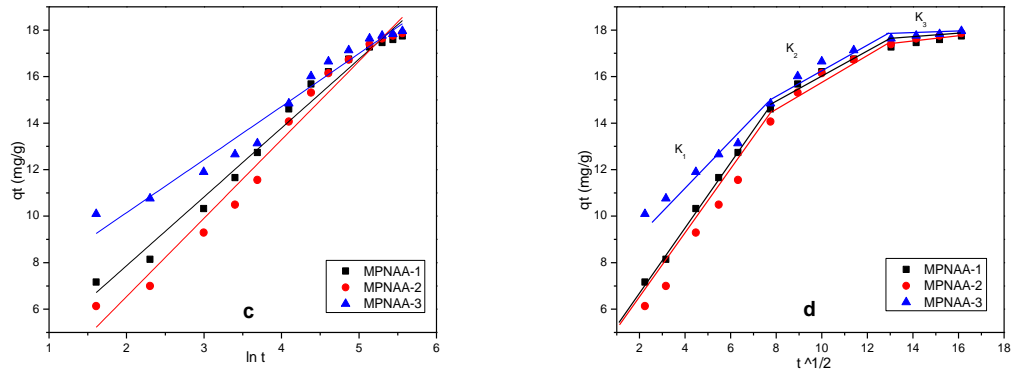


Figure.6.7 Adsorption kinetics of MB by MPNAA-1, MPNAA-2 and MPNAA-3. (a) The pseudo-first-order rate adsorption plot. (b) The pseudo-second-order rate adsorption plot. (c) The Elovich model plot. (d) The intra-particle diffusion model.

Table.6.1 Kinetics model constants and correlation coefficients ( $R^2$ )

Samples	$q_{e, exp.}$ (mg/g)	Pseudo-first-order			Pseudo-second-order		
		$q_{e1, cal}$ (mg/g)	$k_1 \times 10^2$	$R^2$	$q_{e2, cal}$ (mg/g)	$k_2 \times 10^3$	$R^2$
MPNAA-1	17.742	8.9	0.966	0.926	18.7	3.543	0.999
MPNAA-2	17.864	10.5	1.094	0.948	19.3	2.564	0.997
MPNAA-3	17.960	7.6	0.994	0.946	18.6	4.629	0.998
Elovich model		Intra-particle diffusion model					
$\alpha, \beta$	$R^2$	$K_{di,1}$ (mg/g h <sup>1/2</sup> )	$R^2$	$K_{di,2}$ (mg/g h <sup>1/2</sup> )	$R^2$	$K_{di,3}$ (mg/g h <sup>1/2</sup> )	$R^2$
5.712, 0.338	0.979	1.377	0.997	0.483	0.948	0.149	0.997
3.171, 0.297	0.975	1.441	0.994	0.608	0.948	0.151	0.968
2.393, 0.438	0.965	0.836	0.989	0.503	0.929	0.102	0.989

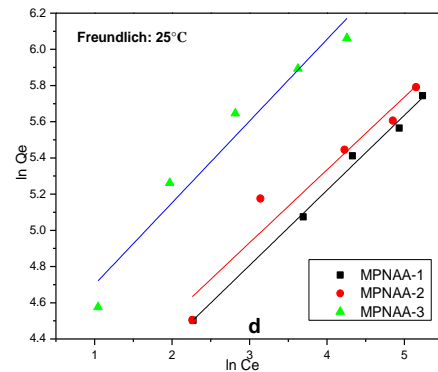
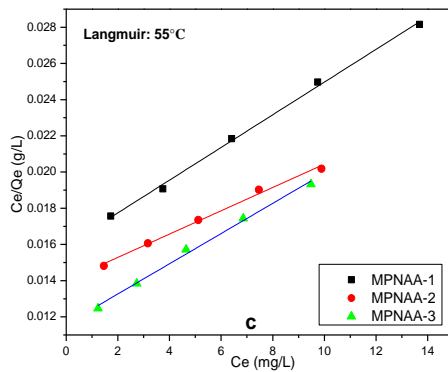
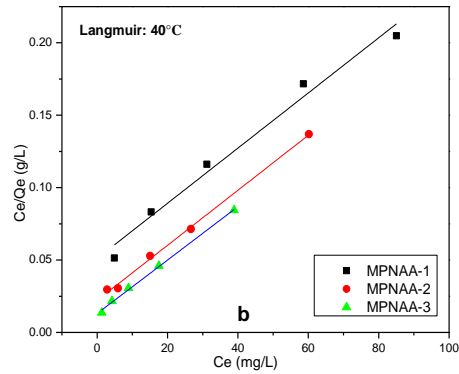
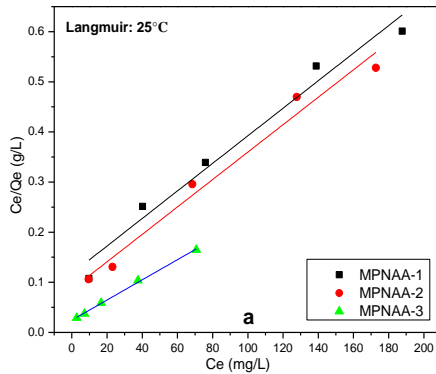
### 6.3.7 Adsorption isotherms

The adsorption isotherms and fitting results are shown in Figure.6.8 and Table.6.2. Obviously, the amount of the dye adsorbed by adsorbents increased with the increase of  $C_e$ , and finally reached a saturated value. Different isotherm models, Langmuir, Freundlich, and Temkin isotherms, were used in the study. The results indicated that the Langmuir plot of  $C_e/Q_e$  versus  $C_e$  revealed a better linear relationship with the relatively higher  $R^2$ , especially at higher temperatures (Figure.6.8b and Figure.6.8c, 313 and 328 K). On the contrary, the Freundlich isotherm and Temkin isotherm had lower  $R^2$ , showing a poorer fit at lower temperatures (Figure.6.8d-8e and Figure.6.8g-8h, 298 and 313 K). Therefore, a well-fit Langmuir isotherm could better describe the adsorption process. The adsorption of dyes occurred by a monolayer sorption on the surface of the adsorbents at a maximum adsorption ability of 602.41 mg/g. In addition, the adsorbent MPNAA-3 had higher  $R^2$  values in Langmuir isotherm and Temkin isotherm, suggesting that the adsorption of dyes on MPNAA-3 was a monolayer adsorption and could be affected by temperatures, which will be further proved in following studies.

At the temperature at 328 K, the adsorption behaviors could be more fit using Freundlich isotherm model, showing that the adsorption process of dyes was based on heterogeneous adsorptive energies on the adsorbent surface.  $K_F$  and  $n$  values in the Freundlich isotherm could be useful for the evaluation of the suitability of the adsorption. Greater  $K_F$  values with the increase of temperature indicates the higher adsorption capability, which corresponded with the trends showed in Figure.6.8. Generally, the value of the Freundlich empirical coefficient  $n$  in different ranges represents various results (2-10 means good, 1-2 means moderately difficult, and less

than 1 means poor adsorption characteristics, respectively) [62]. In Table.6.2,  $n$  is found to be around 2 for all the adsorbents, resulting in good adsorption capability towards cationic dyes. Moreover, the dimensionless constant  $R_L$  indicated that the adsorption towards dyes on all the adsorbents were favorable in this study.

The Temkin isotherm constant in Table.6.2 shows that the heat of adsorption ( $B_T$ ) of MPNAA-1, MPNAA-2, and MPNAA-3 decreases with the increase of temperatures, implying a possible exothermic process for the dyes adsorption onto the semi-IPN spheres [63].



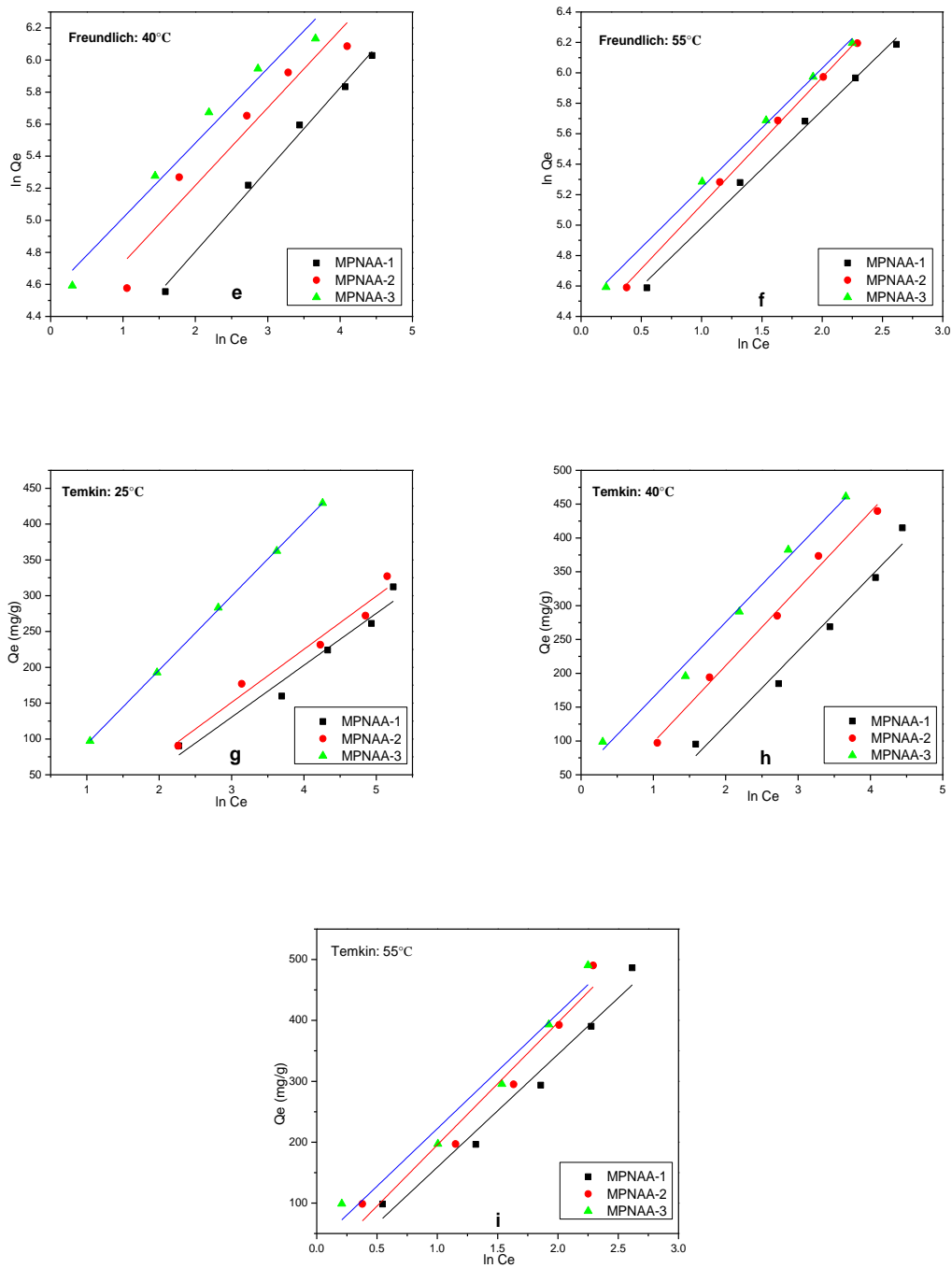


**Figure.6.8** The adsorption isotherms for the adsorption of MB by by MPNAA-1, MPNAA-2 and MPNAA-3. (a-c) Langmuir model, (d-f) Freundlich model and (g-i) Temkin model (adsorbent dosage 1000 mg/L, contact time 3 h, pH 9).

**Table.6.2 Isotherm model constants and correlation coefficients ( $R^2$ ) for the adsorption of MB.**

Samples	T (K)	Freundlich constants			Langmuir constants			Temkin constants			
		$K_F$	n	$R^2$	$Q_{max}$	$K_L \times 10^2$	$R^2$	$R_L$	A	$B_T$	$R^2$
MPNAA-1	298	35.236	2.411	0.992	363.6	2.343	0.966	0.078- 0.299	0.301	34.210	0.952
	313	43.995	1.958	0.992	526.3	3.718	0.978	0.051- 0.212	0.418	23.745	0.969
	328	67.491	1.297	0.993	555.5	5.661	0.998	0.034- 0.150	0.867	14.721	0.965
MPNAA-2	298	41.386	2.483	0.924	364.9	3.179	0.973	0.059- 0.239	0.383	33.412	0.963
	313	69.986	2.063	0.912	526.3	8.574	0.997	0.023- 0.104	0.870	22.909	0.991
	328	73.301	1.194	0.998	568.1	6.286	0.993	0.031- 0.137	0.974	13.575	0.949
MPNAA-3	298	70.098	2.216	0.939	497.5	8.214	0.998	0.024- 0.109	0.907	24.016	0.999
	313	94.478	2.143	0.962	540.5	14.18	0.997	0.014- 0.066	1.622	23.448	0.990
	328	86.450	1.273	0.997	602.4	7.155	0.994	0.027- 0.122	1.191	14.414	0.955

### 6.3.8 Adsorption in a binary system - Langmuir competitive model

The simulation results of Langmuir model and Langmuir competitive model are presented in Figure.6.9 and Table.6.3. Obviously, Figure.6.9 indicates that the Langmuir model could fit the adsorption very well in both single and binary systems. The Langmuir competitive model, however, could better describe the adsorption in binary system. In a single system, the  $R_L$  value for MB is lower than that of MV, resulting in

the lower  $Q_m$  of MB (497.5 mg/g) than MV (840.3 mg/g). In addition, the  $R_L$  value for MB is lower than that for MV, whereas the  $Q_m$  for MB is higher than MV in the Langmuir competitive model. The  $Q_m$  values for MB and MV were 197.2 mg/g and 677.2 mg/g in Table.6.3, respectively. Furthermore, the  $Q_m$  values were lower than those in single system, probably due to the competitive adsorption between MB and MV on the adsorbents. The Langmuir constant of MB was greater than that of MV in a single system, suggesting a stronger adsorption towards MB, whereas in the binary system, the adsorption towards MV was stronger than that towards MB.

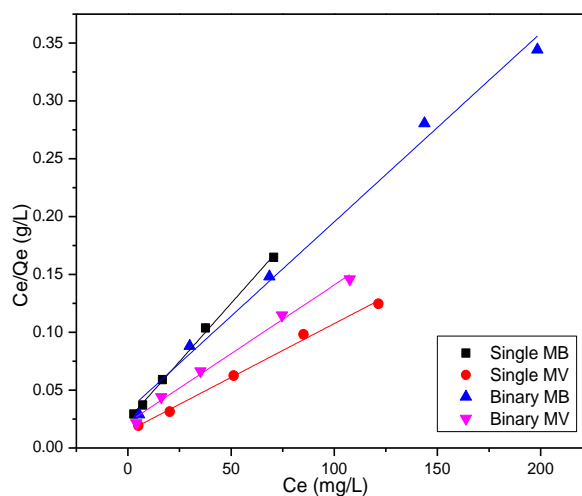


**Figure.6.9** The Langmuir isotherms for the adsorption of MB and MV from single and binary systems using MPNAA-3 at pH = 9 and T = 298K.

**Table.6.3 Adsorption isotherms parameters for dye adsorption in single and binary system**

Dye	Langmuir Model				Langmuir Competitive Model					
	$Q_{max}$	$K_L \times 10^2$	$R_L$	$R^2$	$Q_{m,1}$	$K_{L,1} \times 10$	$Q_{m,2}$	$K_{L,2} \times 10$	$R_L$	$R^2$
Single MB	497.5	8.214	0.024- 0.109	0.998						
Single MV	840.3	6.409	0.031- 0.135	0.994						
Binary MB	613.5	5.033	0.038- 0.166	0.989	197.2	1.565	--	1.994	0.012- 0.060	0.997
Binary MV	1075	5.385	0.036- 0.157	0.990	--	0.5649	677.2	0.5194	0.037- 0.161	0.996

### 6.3.9 The desorption and recycling of adsorbents

The recycling of adsorbent is critical for the application. The regeneration was carried out by immersing the dye-laden adsorbent into 1 N HCl solution for 60 minutes, and the desorption rate is presented along with the different cycle time in Figure.6.10a. The results in Figure.6.10a indicated that the desorption rate could decrease gradually as the cycle time was increased, which could be found that 87.12% of MB and 85.79% of MV were desorbed at the fifth recycle. In this case, the adsorbent revealed an excellent ability for the desorption of cationic dyes. During these processes, many positively-charged dyes exchanged with  $H^+$  which was offered by HCl in the solution.

The thermo-responsive properties of adsorbents could be reflected in the desorption process of dyes from MPNAA-1, MPNAA-2, and MPNAA-3. As indicated in Figure.6.10b, the desorption was a fast process for all the adsorbents (within 10 min at 25 °C). When the temperature was increased to 60 °C, the MB desorption rate for the dye-laden adsorbents also increased, while the desorption rate of dye dropped during the

next period at 25 °C. At each temperature variation period, the trend of desorption behavior remained unchanged, resulting in a strong evidence of the thermos-responsive properties on adsorbents. In addition, the desorption rate of MPNAA-2 was greater than that of MPNAA-3, showing that dye adsorbed onto MPNAA-3 was more stable due to the more amount of carboxyl groups on the adsorbent. Furthermore, adsorbent MPNAA-2 exhibited better thermal responsiveness, probably due to its lower carboxyl content than MPNAA-3 and greater polymer ratio than MPNAA-1.

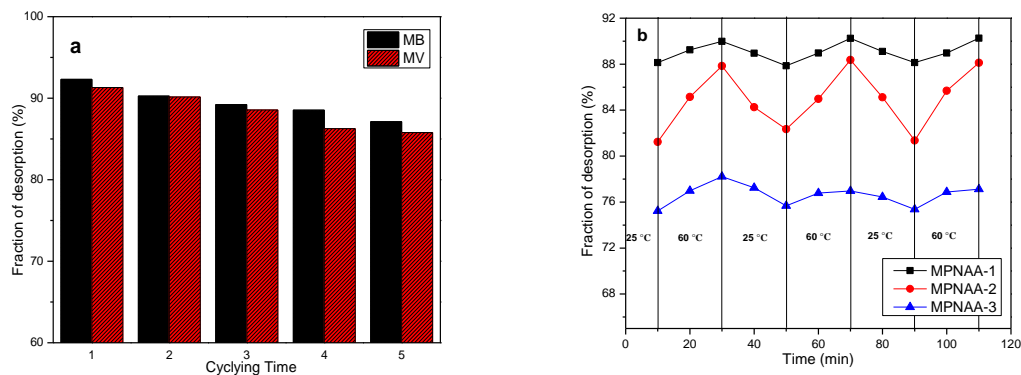


**Figure.6.10 Desorption behavior of dyes by MPNAA-3 (a) and swing desorption behavior by MPNAA-1, MPNAA-2 and MPNAA-3 with temperature variation.**

## 6.4 Conclusions

In summary, we successfully fabricated thermal- and pH- responsive semi-IPN cellulose microfilaments/ Poly (N-isopropylacrylamide-co-acrylic acid) spheres. The combination of cellulose microfilaments not only significantly enhanced the adsorption capacity efficiency but also simplified its utilization, filtration, and separation. The highly porous structure of semi-IPN spheres allowed the as-prepared adsorbents to have good stability

and dye adsorption capability. Also, the semi-IPN spheres were sensitive to the temperature. Moreover, the grafted carboxylic groups on both dissolved native cellulose and CMF and the porous structure of adsorbents created by pore forming agent were proved to be the key factors for the superior capacity of the adsorbents. The adsorption behaviors of adsorbents towards dyes (MB and MV) have been systematically studied in both single and binary systems. The maximum adsorption capacities of MB and MV were 497.5 and 840.3 mg g<sup>-1</sup> in a single system. The spheres exhibited a controllable adsorption and desorption process as pH- and temperature-responsive adsorbents. These results indicated that MPNAA could act as a new type of material for controlled dyes adsorption. Therefore, the dual-responsive semi-IPN spheres are expected to be a promising cost-effective and renewable adsorbent for efficient removal of cationic dyes. In addition, this synthesis technique uses natural porous spherical adsorbents as the carrier to prepare hybrid composite porous material, which could be extended to various systems to fabricate other functional porous materials.

## 6.5 References

- [1] Yoo, Y.; Martinez, C.; Youngblood, J. P. Synthesis and characterization of microencapsulated phase change materials with poly(urea-urethane) shells containing cellulose nanocrystals. *ACS Appl. Mater. Inter.*, 2017, 9, 31763-31776.
- [2] Panda, G. C.; Das, S. K.; Guha, A. K. Jute stick powder as a potential biomass for the removal of congo red and rhodamine B from their aqueous solution. *J. Hazard. Mater.*, 2009, 164, 374-379.
- [3] Garg, V. K.; Kumar, R.; Gupta, R. Removal of malachite green dye from aqueous solution by adsorption using agro-industry waste: A case study of *Prosopis cineraria*. *Dyes. Pigments.*, 2004, 62, 1-10.

- [4] Hua, M.; Zhang, S.; Pan, B.; Zhang, W.; Lv, L.; Zhang, Q. Heavy metal removal from water/ by nanosized metal oxides: A review. *J. Hazard. Mater.*, 2015, 211-212, 317-331.
- [5] Zhou, Q.; Lin, Y.; Shu, J.; Zhang, K.; Yu, Z.; Tang, D. Reduced graphene oxide-functionalized FeOOH for signal-on photoelectrochemical sensing of prostate-specific antigen with bioresponsive controlled release system. *Biosens. Bioelectron.*, 2017, 98, 15-21.
- [6] Lyu, H.; Gao, B.; He, F.; Zimmerman, A. R.; Ding, C.; Tang, J.; Crittenden, J. C. Experimental and modeling investigations of ball-milled biochar for the removal of aqueous methylene blue. *Chem. Eng. J.*, 2018, 335, 110-119.
- [7] Liu, S.; Xu, M.; Yu, T.; Han, D.; Peng, J.; Li, J.; Zhai, M. Radiation synthesis and performance of novel cellulose-based microsphere adsorbents for efficient removal of boron (III). *Carbohydr. Polym.*, 2017, 174, 273-281.
- [8] Bhatnagar, A.; Hogland, W.; Marques, M.; Sillanpaa, M. An overview of the modification methods of activated carbon for its water treatment applications. *Chem. Eng. J.*, 2013, 219, 499-511.
- [9] Kang, H.; Liu, R.; Huang, Y. Graft modification of cellulose: methods, properties and applications. *Polymer.*, 2015, 70, 1-16.
- [10] Chen, W.; Lu, W.; Yao, Y.; Xu, M. Highly efficient decomposition of organic dyes by aqueous-fiber phase transfer and in situ catalytic oxidation using fiber-supported cobalt phthalocyanine. *Environ. Sci. Technol.*, 2007, 41, 6240-6245.
- [11] O'Connell, D. W.; Birkinshaw C.; O'Dwyer, T. F. Heavy metal adsorbents prepared from the modification of cellulose: A review. *Bioresource Technol.*, 2008, 99, 6709-6724.
- [12] Soleimani, K.; Tehrani, A. D.; Adeli, M. Bioconjugated graphene oxide hydrogel as an effective adsorbent for cationic dyes removal. *Ecotox. Environ. Safe.*, 2018, 147, 34-42.
- [13] Salama, A. Preparation of CMC-g-P(SPMA) super adsorbent hydrogels: Exploring their capacity for MB removal from waste water. *Int. J. Biol. Macromol.*, 2018, 106, 940-946.
- [14] Benhalima, T.; Ferfera-Harrar, H.; Lerari, D. Optimization of carboxymethyl cellulose hydrogels beads generated by an anionic surfactant micelle templating for cationic dye uptake: Swelling, sorption and reusability studies. *Int. J. Biol. Macromol.*, 2017, 105, 1025-1042.

- [15] Alain, D.; Danie, L. D.; Michel, R. V. Cellulose Microfilaments from Potato Tuber Cells: Processing and Characterization of Starch-Cellulose Microfibril Composites. *J. Appl. Polym. Sci.*, 2000, 76, 2080-2092.
- [16] Wang, F.; Pan, Y.; Cai, P.; Guo, T.; Xiao, H. Single and binary adsorption of heavy metal ions from aqueous solutions using sugarcane cellulose-based adsorbent. *Bioresource Technol.*, 2017, 241, 482-490.
- [17] Jiang, X.; Wang, S.; Ge, L.; Lin, F.; Lu, Q.; Wang, T.; Huang, B.; Lu, B. Development of organic-inorganic hybrid beads from sepiolite and cellulose for effective adsorption of malachite green, *RSC Adv.*, 2017, 7, 38965-38972.
- [18] Ram, B.; Chauhan, G. S. New spherical nanocellulose and thiol-based adsorbent for rapid and selective removal of mercuric ions. *Chem. Eng. J.*, 2018, 331, 587-596.
- [19] Luo, X.; Zhang, L. High effective adsorption of organic dyes on magnetic cellulose beads entrapping activated carbon. *J. Hazard. Mater.*, 2009, 171, 340-347.
- [20] Ma, X.; Liu, C.; Anderson, D. P.; Chang, P. R. Porous cellulose spheres: Preparation, modification and adsorption properties. *Chemosphere.*, 2016, 165, 399-408.
- [21] Li, Y.; Xiao, H.; Chen, M.; Song, Z.; Zhao, Y. Absorbents based on maleic anhydride-modified cellulose fibers/diatomite for dye removal. *J. Mater. Sci.*, 2014, 49, 6696-6704.
- [22] Li, Y.; Chen, M. D.; Wan, X.; Zhang, L.; Wang, X.; Xiao, H. Solvent-free synthesis of the cellulose-based hybrid beads for adsorption of lead ions in aqueous solutions. *RSC Adv.*, 2017, 7, 53899-53906.
- [23] Wu, H.; Bremner, D. H.; Wang, H.; Wu, J.; Li, H.; Wu, J.; Niu, S.; Zhu, L. Fabrication and investigation of a biocompatible microfilament with high mechanical performance based on regenerated bacterial cellulose and bacterial cellulose. *Mater. Sci. Eng. C*, 2017, 79, 516-524.
- [24] Cao, F.; Yang, B. Supercooling suppression of microencapsulated phase change materials by optimizing shell composition and structure. *Adv. Mater.*, 2014, 113, 1512-1518.
- [25] Lee, Y. R.; Park, D.; Choi, S. K.; Kim, M.; Baek, H. S.; Nam, J.; Chung, C. B.; Osuji, C. O.; Kim, J. W. Smart Cellulose Nanofluids Produced by Tunable Hydrophobic Association of Polymer-Grafted Cellulose Nanocrystals. *ACS Appl. Mater. Inter.*, 2017, 9, 31095-31101.
- [26] Breger, J. C.; Yoon, C.; Xiao, R.; Kwag, H. R.; Wang, M. O.; Fisher, J. P.; Nguyen, T. D.; Gracias, D. H. Self-folding thermo-magnetically responsive soft microgrippers. *ACS Appl. Mater. Inter.*, 2017, 7, 3398-3405.

- [27] Plunkett, K. N.; Zhu, X.; Moore J. S.; Leckband, D. E. PNIPAM chain collapse depends on the molecular weight and grafting density. *Langmuir.*, 2006, 22, 4259-4266.
- [28] Leobandung, W.; Ichikawa, H.; Fukumori Y.; Peppas, N. A. Preparation of stable insulin-loaded nanospheres of poly (ethylene glycol) macromers and N-isopropyl acrylamide. *J. Control. Release.*, 2002, 80, 357-363.
- [29] Liu, P.; Luo, Q.; Guan Y.; Zhang, Y. Drug release kinetics from monolayer films of glucose-sensitive microgel. *Polymer.*, 2010, 51, 2668-2675.
- [30] Das, M.; Mardiyani, S.; Chan W. C.; Kumacheva, E. Biofunctionalized pH-Responsive Microgels for Cancer Cell Targeting: Rational Design. *Adv. Mater.*, 2006, 18, 80-83.
- [31] Ogawa, K.; Wang B.; Kokufuta, E. Enzyme-regulated microgel collapse for controlled membrane permeability. *Langmuir.*, 2001, 17, 4704-4707.
- [32] Kobe, R.; Yoshitani K.; Teramoto, Y. Fabrication of elastic composite hydrogels using surface-modified cellulose nanofiber as a multifunctional crosslinker, *J. Appl. Polym. Sci.*, 2016, 133, 42906.
- [33] Chen, J. J.; Ahmad, A. L.; Ooi, B. S. Thermo-responsive properties of poly (N-isopropylacrylamide-co-acrylic acid) hydrogel and its effect on copper ion removal and fouling of polymer-enhanced ultrafiltration. *J. Membrane. Sci.*, 2014, 469, 73-79.
- [34] Nalam, P. C.; Lee, H. S.; Bhatt, N.; Carpick, R. W.; Eckmann, D. M.; Composto, R. J.; Nanomechanics of pH-Responsive, Drug-Loaded, Bilayered Polymer Grafts. *ACS Appl. Mater. Inter.*, 2017, 9, 12936-12948.
- [35] Behbahani, M.; Bide, Y.; Bagheri, S.; Salarian, M.; Omid, F.; Nabid, M. R. A pH responsive nanogel composed of magnetite, silica and poly (4-vinylpyridine) for extraction of Cd (II), Cu (II), Ni (II) and Pb (II). *Microchim. Acta.*, 2016, 183, 111-121.
- [36] Shi, Y.; Ma, C.; Peng, L.; Yu, G. Conductive “smart” hybrid hydrogels with PNIPAM and nanostructured conductive polymers. *Adv. Funct. Mater.*, 2015, 25, 1219-1225.
- [37] Xia, F.; Feng, L.; Wang, S.; Sun, T.; Song, W.; Jiang, W.; Jiang, L. Dual-Responsive Surfaces That Switch between Superhydrophilicity and Superhydrophobicity. *Adv. Mater.*, 2006, 18, 432-436.
- [38] Osyrova, A.; Magnin, D.; Sibret, P.; Aqil, A.; Jérôme, C.; Dupont-Gillain, C.; Pradier, C. -M.; Demoustier-Champagne, S.; Landoulsi, J. Dual stimuli-responsive coating designed through layer-by-layer assembly of PAA-b-PNIPAM block copolymers for the control of protein adsorption. *Soft. Matter.*, 2015, 11, 8154-8164.

- [39] Wang, Y. M.; Zheng, S. X.; Chang, H. I.; Tsai, H. Y.; Liang, M. Microwave-assisted synthesis of thermo- and pH-responsive antitumor drug carrier through reversible addition-fragmentation chain transfer polymerization. *Express. Polym. Lett.*, 2017, 11, 293-307.
- [40] Komorowska, D. M.; Dimitrakis, G.; Bogdal, D.; Stankiewicz, A. I.; Stefanidis, G. D. A concise review on microwave-assisted polycondensation reactions and curing of polycondensation polymers with focus on the effect of process conditions. *Chem. Eng. J.*, 2015, 264, 633-644.
- [41] Zhang, C.; Liao, L.; Gong, S. Recent developments in microwave-assisted polymerization with a focus on ring opening polymerization. *Green. Chem.*, 2007, 9, 303-314.
- [42] Singla, P.; Mehta, R.; Berek, D.; Upadhyay, S. N. Ring opening polymerization of lactide in a monomode microwave using stannous octoate and dibutyltin dimethoxide catalysts. *J. Macromol. Sci. A.*, 2014, 51, 350-361.
- [43] Guo, B. L.; Gao, Q. Y. Preparation and properties of a pH/temperature-responsive carboxymethyl chitosan/poly (N-isopropylacrylamide) semi-IPN hydrogel for oral delivery of drugs. *Carbohydr. Res.*, 2007, 342, 2416-2422.
- [44] Zhang, G. Q.; Zha, L. S.; Zhou, M. H.; Ma, J. H.; Liang, B. R. Preparation and characterization of pH-and temperature-responsive semi-interpenetrating polymer network hydrogels based on linear sodium alginate and crosslinked poly (N-isopropylacrylamide). *J. Appl. Polym. Sci.*, 2005, 97, 1931-1940.
- [45] Zhao, Y.; Kang, J.; Tan, T. Salt-, pH-and temperature-responsive semi-interpenetrating polymer network hydrogel based on poly (aspartic acid) and poly (acrylic acid). *Polymer.*, 2006, 47, 7702-7710.
- [46] Kalagasidis, K. M.; Veličković, S. J.; Griffiths, P. C.; Filipović, J. Poly [(N-isopropylacrylamide)-co-(itaconic acid)] hydrogels with poly (ethylene glycol). *Polym. Int.*, 2010, 59, 256-262.
- [47] Dai, H. J.; Huang, H. H. Synthesis, characterization, and properties of pineapple peel cellulose-g-acrylic acid hydrogel loaded with kaolin and sepia ink. *Cellulose.*, 2017, 24, 69-84.
- [48] Wei, X.; Huang, T.; Yang, J.; Zhang, N.; Wang, Y.; Zhou, Z. Green synthesis of hybrid graphene oxide/microcrystalline cellulose aerogels and their use as superabsorbents. *J. Hazard. Mater.*, 2017, 335, 28-38.
- [49] Lin, Q.; Gao, M.; Chang, J.; Ma, H. Adsorption properties of crosslinking carboxymethyl cellulose grafting dimethyldiallylammonium chloride for cationic and anionic dyes. *Carbohydr. Polym.*, 2016, 151, 283-294.

- [50] Zhou, H.; Gao, B.; Zhou, Y.; Qiao, H.; Gao, W.; Qu, H.; Liu, S.; Zhang, Q.; Liu, X. Facile preparation of 3D GO/CNCs composite with adsorption performance towards [BMIM][Cl] from aqueous solution. *J. Hazard. Mater.*, 2017, 337, 27-33.
- [51] Teodoro, F. S.; Elias, M.M.C.; Ferreira, G.M.D.; Adarmeb, O. F.; Savedrac, R.M.L.; Siqueirac, M.F.; Silvad, L.H.M.; Gil, L. F.; Gurgel, L.V.A. Synthesis and application of a new carboxylated cellulose derivative. Part III: Removal of auramine-O and safranin-T from mono- and bi-component spiked aqueous solutions. *J. Colloid. Interf. Sci.*, 2018, 512, 575-590.
- [52] Ling, L. L.; Liu, W. J.; Zhang, S.; Jiang, H. Magnesium Oxide Embedded Nitrogen Self-Doped Biochar Composites: Fast and High-Efficiency Adsorption of Heavy Metals in an Aqueous Solution. *Environ. Sci. Technol.*, 2017, 51, 10081-10089.
- [53] Zhao, F.; Repo, E.; Yin, D.; Meng, Y.; Jafari, S.; Sillanpää, M. EDTA-Cross-Linked  $\beta$ -Cyclodextrin: An Environmentally Friendly Bifunctional Adsorbent for Simultaneous Adsorption of Metals and Cationic Dyes. *Environ. Sci. Technol.*, 2015, 51, 10570-10580.
- [54] Atar, N.; Olgun, A.; Wang, S.; Liu, S. Adsorption of anionic dyes on boron industry waste in single and binary solutions using batch and fixed-bed systems. *J. Chem. Eng. Data*, 2011, 56, 508-516.
- [55] Sun, R.; Fang, J.; Tomkinson, J.; Geng, Z.; Liu, J. Fractional isolation, physico-chemical characterization and homogeneous esterification of hemicelluloses from fast-growing poplar wood. *Carbohydr. Polym.*, 2001, 44, 29-39.
- [56] Lu, J.; Askeland, P.; Drzal, L. T. Surface modification of microfibrillated cellulose for epoxy composite applications. *Polymer.*, 2008, 49, 1285-1296.
- [57] Sanna, H.; Eveliina, R.; Mika, S. Removal of heavy metals from aqueous solutions by succinic anhydride modified mercerized nanocellulose. *Chem. Eng. J.*, 2013, 223, 40-47.
- [58] Ekici, S. Intelligent poly (N-isopropylacrylamide)-carboxymethyl cellulose full interpenetrating polymeric networks for protein adsorption studies. *J. Mater. Sci.*, 2011, 46, 2843-2850.
- [59] Li, G.; Yu, N.; Gao, Y.; Tao, Q.; Liu, X. Polymeric hollow spheres assembled from ALG-g-PNIPAM and  $\beta$ -cyclodextrin for controlled drug release. *Int. J. Biol. Macromol.*, 2016, 82, 381-386.
- [60] Bastakoti, B. P.; Guragain, S.; Nakashima, K.; Yamauchi, Y. Stimuli-Induced Core-Corona Inversion of Micelle of Poly (acrylic acid)-block-Poly (N-isopropylacrylamide) and Its Application in Drug Delivery. *Macromol. Chem. Phys.*, 2015, 216, 287-291.

[61] Pang, Y.; Zeng, G.; Tang, L.; Zhang, Y.; Liu, Y.; Lei, X.; Li, Z.; Zhang, J.; Liu, Z.; Xiong, Y. Preparation and application of stability enhanced magnetic nanoparticles for rapid removal of Cr(VI). *Chem. Eng. J.*, 2011, 175, 222-227.

[62] Yao, Y.; Bing, H.; Feifei, X.; Xiaofeng, C. Equilibrium and kinetic studies of methyl orange adsorption on multiwalled carbon nanotubes. *Chem. Eng. J.*, 2011, 170, 82-89.

[63] Sekar, M.; Sakthi, V.; Rengaraj, S. Kinetics and equilibrium adsorption study of lead(II) onto activated carbon prepared from coconut shell. *J. Colloid. Interf. Sci.*, 2004, 279, 307-313.

## **Chapter 7 Conclusion and Recommendation for Future Work**

The key objective of this dissertation targeted the development of cellulose-based green adsorbents for water clarification.

For the first generation of cellulose-based adsorbents, a hybrid adsorbent consisting of the maleic anhydride-modified cellulose beads combined with alkali-treated diatomite (MCDBs) was prepared. An appropriate amount of calcium carbonate was added during the formation of MCDBs to increase pore structure under an acidic condition and the excellent porous structure was achieved. The study on the application of as-prepared hybrid adsorbents also showed satisfying adsorption capabilities towards dyes and heavy metal ions with the competitive maximum adsorption capacities (over 100 mg/g for dyes and 45 mg/g for heavy metal ions). However, the properties, including porous structure and adsorption capabilities, were relatively low. In addition, the modification was also simple compared to other types of adsorbents reported elsewhere.

For the second generation of cellulose-based adsorbents, microfibrillated cellulose, an ideal material which would provide a variety of shapes and be biocompatible and absorbable, was selected as one of the raw materials for the preparation of cellulose-based spheres. MFC is superior due to its advantages in structure, performance, and application. This novel composite adsorbent was developed based on dissolved cellulose fibres (as matrix) reinforced with microfibrillated cellulose (MFC). Both cellulose fibres and microfibrillated cellulose were functional-modified using an organic solvent-free approach to introduce carboxyl groups onto cellulose and the surface of MFC, to further increase the adsorption capacity. Nano-sized  $\text{CaCO}_3$  was added as a pore forming agent

during the formation of dissolved cellulose/MFC (CMFC) composites. The results showed that the porous structure and adsorption capacities enhanced dramatically compared to the first generation-adsorbents. It was shown that excellent thermal properties were obtained while using MFC as the raw material. Moreover, the adsorption mechanism and the reusability were systematically studied.

Finally, to develop the multi-functional smart adsorbents to enhance both the adsorption capacities and the usability of cellulose-based adsorbents, the semi-IPN composite and microwave-assisted synthesis were introduced. Based on the results, the maximum adsorption capabilities of copolymer-grafted adsorbents were much higher than those of first and second generation-adsorbents. Moreover, the adsorption and desorption processes were controllable due to the pH- and thermal- sensitive properties.

The summary and comparison of all approaches are detailed as follows.

### **7.1 Summary of the maleic anhydride-modified cellulose hybrid beads (MCDBs)**

The first generation-adsorbent consists of the maleic anhydride-modified cellulose beads and alkali-treated diatomite (MCDBs). The pore size of the adsorbents was enhanced by introducing  $\text{CaCO}_3$  during the preparation. The dye adsorption capacity was dependent on various factors, such as pH, mixing time, temperature, and, most importantly, pH. The dye removal efficiency was high under alkaline condition ( $\text{pH} > 6$ ) as the adsorbent had a negative-charge, thus, increasing its affinity to the cationic dye ion. This cellulose fibre-based adsorbent was cost-effective and renewable. The dynamic and equilibrium data of adsorption fitted well with the Pseudo-second-model and the Langmuir isotherm equation, demonstrating that the adsorption process of dye is monolayer sorption and

dominated by the chemical adsorption. The corresponding results have been published on Journal of Materials Science. (Yuan Li, Mindong Chen, Huining Xiao, Zhaoping Song, Yi Zhao. Absorbents based on maleic anhydride-modified cellulose fibres/diatomite for dye removal. Journal of Materials Science (2014), 49: 6696-6704)

In addition, MCDBs was found to effectively adsorb  $\text{Pb}^{2+}$  from aqueous solutions. Further experiment data revealed that the adsorption process of  $\text{Pb}^{2+}$  on the MCDBs followed a pseudo-second-order kinetics and the equilibrium data can be well fitted with a Langmuir isotherm. The maximum adsorption capacities of adsorbent (Langmuir) was  $44 \text{ mg g}^{-1}$  from an initial concentration of  $800 \text{ mg L}^{-1}$  at pH 6 and at  $30 \text{ }^\circ\text{C}$ . The capacity of the adsorbents in  $\text{Pb}^{2+}$  removal remained unchanged after reusing three times. The MCDBs is a green-based, cost-effective, and renewable absorbent. It could be used to adsorb more heavy metal ions which are positive charged. The corresponding results have been published on RSC Advances. (Yuan Li, Mindong Chen, Xia Wan, Lu Zhang, Xu Wang, Huining Xiao. Solvent-free synthesis of the cellulose-based hybrid beads for adsorption of lead ions in aqueous solutions. RSC Advances (2017), 7: 53899-53906.)

## **7.2 Summary of dissolved cellulose fibre/microfibrillated cellulose beads**

The composite adsorbents consisting of dissolved cellulose fibres and microfibrillated cellulose were also extensively studied in this Thesis.

An easily operated and environmentally-friendly process was developed to prepare green and renewable composite adsorbents which consist of dissolved cellulose fibres as matrix and microfibrillated cellulose as reinforced microparticles. The combination of microfibrillated cellulose not only significantly enhanced the adsorption efficiency but

also simplified the operation, filtration, and separation. The grafted carboxyl groups on both dissolved cellulose fibres and MFC and a large specific surface area of CMFCs created by pore forming agent are believed to be the key factors for the superior capacity of the adsorbents. The maximum adsorption capacity of adsorbent (Langmuir) toward methylene blue dye was 303.03 mg g<sup>-1</sup>, which is higher than most bio-adsorbents reported elsewhere. Therefore, the MCMFCs are expected to be a promising cost-effective and renewable adsorbent for highly efficient removal of organic pollutants, thus minimizing the environmental concerns. The corresponding results are to be published on ACS Sustainable Chemistry & Engineering.

### **7.3 Summary of responsive semi-INP adsorbents**

In this work, two types of adsorbents were prepared by using microwave-assisted synthesis polymerization to develop the multi-functional smart adsorbents.

On one hand, temperature-responsive polymer-modified cellulose filaments/Poly (N-isopropylacrylamide) spheres (P-MCCBs) were successfully developed in the first part of the work. The cellulose filaments spheres were first prepared using a vacuum drying method in the presence of a pore forming agent (nano-sized CaCO<sub>3</sub>). Afterwards, NIPAM (N-isopropylacrylamide), a temperature-sensitive monomer was polymerized and grafted onto the cellulose filaments spheres through in situ free radical polymerization by using microwave-assisted polymerization. The spheres grafted with PNIPAM exhibited a controllable desorption rate at different temperatures (25 and 45 °C). The temperature effect on the dye and heavy metal adsorption rate was also observed. The adsorption kinetics followed the pseudo-second-order model, and the

desorption process could be fit by using Higuchi and Korsmeyer-Peppas models. These results indicated that porous P-MCCBs could act as a novel material for controllable adsorption and desorption processes of contaminants (Methylene Blue and  $Pb^{2+}$ ). (The corresponding results are to be submitted on Science of the Total Environment)

On the other hand, dual-responsive semi-INP cellulose microfilaments/ Poly (N-isopropylacrylamide-co-acrylic acid) spheres were fabricated by using microwave-assisted polymerization. Copolymer-modified cellulose microfilaments/Poly (N-isopropylacrylamide-co-acrylic acid) spheres showed an excellent pH- and temperature-properties, where a controllable adsorption and desorption process can be proved. Moreover, the adsorption kinetics followed the pseudo-second-order and exhibited a three-stage intraparticle diffusion model. Adsorption isotherms (at 298, 313, and 328 K) were fit using Langmuir, Freundlich, and Temkin models, which indicated that the MPNAA dominated the adsorption capacity towards MB and MV, with the maximum adsorption at 497.5 and 840.3  $mg\ g^{-1}$  in a single system. (The corresponding results have been submitted to ACS Applied Materials & Interfaces)

#### **7.4 Recommendations for future work**

Based on the conclusions above, there are some recommendations for the future work on this project.

First, further research is required to investigate the relationship between porous properties and the pore forming agents. Based on our work, some challenges remain in controlling the pore size distribution of adsorbents.

Second, according to the results demonstrated in this work, the application of diatomite and MFC could increase the properties of the adsorbents dramatically. However, the inner structure of the composites and the mechanism were not clearly studied. Based on these results, a balanced or combined approach should be further developed to study the requirements of using different types of fillers, thus to broaden the applications of cellulose-based materials.

Third, the most important recommendation is to study and reveal the mechanisms for both adsorption and desorption process. As long as the mechanisms were revealed, effective approaches could be possible to enhance the properties of the adsorbents.

Fourth, the industrial potential of adsorbents should be studied systematically, and the results could be extended to various systems to broaden their application.

## Curriculum Vitae

Candidate's full name: Yuan Li

Universities attended:

University of New Brunswick, 2015-2018

Ph.D. candidate, Department of Chemical Engineering

Nanjing University of Information Science and Technology, China

M.Sc., School of Environmental Science and Technology, 2011-2014

### Publications:

[1] Yuan Li, Mindong Chen, Huining Xiao, Zhaoping Song, Yi Zhao. Absorbents based on maleic anhydride-modified cellulose fibres/diatomite for dye removal. *Journal of Materials Science* (2014), 49: 6696-6704.

[2] Yuan Li, Mindong Chen, Xia Wan, Lu Zhang, Xu Wang, Huining Xiao. Solvent-free synthesis of the cellulose-based hybrid beads for adsorption of lead ions in aqueous solutions. *RSC Advances* (2017), 7: 53899-53906.

[3] Yuan Li, Huining Xiao, Yuanfeng Pan, Lidong Wang. Novel Composite Adsorbent Consisting of Dissolved Cellulose Fiber/ Microfibrillated Cellulose for Dye Removal from Aqueous Solution. *ACS Sustainable Chemistry & Engineering* (2018), 6: 6994-7002.

[4] Zhaoping Song, Huining Xiao, Yuan Li. Effects of renewable materials coatings on oil resistant properties of paper. *Nordic Pulp & Paper Research Journal* (2015), 30(2):344-349.

[5] Avik Khan, Yuan Li, Huining Xiao, Xuejun Zou. Rendering packaging paper antimicrobial with functional-modified starch: pilot paper machine trial at

FPIInnovations. Journal of Science & Technology for Forest Products and Processes (2016), 5: 11-16.

[6] Xu Wang, Peng Lu, Yuan Li, Huining Xiao, Xiangyang Liu. Antibacterial activities and mechanisms of fluorinated graphene and guanidine-modified graphene. RSC Advances (2016), 6: 8763-8772.

[7] Lu Zhang, Yuan Li, Hongcang Zhou. Preparation and characterization of DBU-loaded MCM-41 for adsorption of CO<sub>2</sub>. Energy (2018), 148: 414-423.

[8] Lu Zhang, Yuan Li, Hongcang Zhou, Mindong Chen. Performance of 1, 8-Diazabicyclo [5.4.0] undec- 7 -ene- Modified SBA-15 for Selective Adsorption of CO<sub>2</sub>. Energy & Fuels (2017), 31: 3062-3068.

[9] Yuan Li, Huining Xiao, Yuanfeng Pan, Min Zhang, Tianxiang Guo. Fabrication of dual-responsive semi-INP cellulose microfilaments/ Poly (N-isopropylacrylamide-co-acrylic acid) spheres for dye removal in single and binary systems. ACS Applied Materials & Interfaces (submitted).

[10] Yuan Li, Huining Xiao. Novel cellulose microfilaments based composite spheres: microwave-assisted synthesis, characterization, and application in water treatment. Science of the Total Environment (submitted).

#### **Conference Presentations:**

##### **Oral presentations:**

[1] Yuan Li, Huining Xiao. Preparation and characterization of cellulose fiber/inorganic porous filler hybrid adsorbents for water clarification. The annual conference of Graduate Research in University of New Brunswick, September 2016, Fredericton, NB, Canada.

[2] Yuan Li, Huining Xiao. Fabrication of dual-responsive semi-INP cellulose filaments/ Poly (N-isopropylacrylamide-co-acrylic acid) spheres for dye removal in single and binary system. Graduate Research seminar, January 2018, Fredericton, NB, Canada.

**Poster presentations:**

[1] Yuan Li, Huining Xiao. Green absorbents based on maleic anhydride-modified cellulose fibres for dye removal from aqueous solution. The annual conference of NSERC Green Wood Fibre Strategic Network (Canada), Paperweek Conference, November 2013, Montreal, Quebec, Canada.

[2] Yuan Li, Huining Xiao. Synthesis, modification, and adsorption properties of cellulose/cellulose filament spheres for dye removal. The Chemical Engineering Graduate Student Conference, November 2017, Fredericton, NB, Canada.